OJONUGWA ADUKWU

Optimisation of Gas-Lifted System Using Nonlinear Model Predictive Control

São Paulo
2023

OJONUGWA ADUKWU

Optimisation of Gas-Lifted System Using Nonlinear Model Predictive Control

Corrected Version

Doctoral thesis presented to the Escola Politécnica da Universidade de São Paulo to obtain the title of Doctor of Science

Area of Concentration:

Systems Engineering

Supervisor:

Professor Doctor Fuad Kassab Junior

São Paulo
2023

Este exemplar foi revisado e corrigido em relação à versão original, sob responsabilidade única do autor e com a anuência de seu orientador.

São Paulo, _____ de _____ de _____

Assinatura do autor: _____

Assinatura do orientador: _____

Catalogação-na-publicação

Adukwu, Ojonugwa
Optimisation of Gas-Lifted System Using Nonlinear Model Predictive Control / O. Adukwu -- versão corr. -- São Paulo, 2023.
183 p.

Tese (Doutorado) - Escola Politécnica da Universidade de São Paulo. Departamento de Engenharia de Telecomunicações e Controle.

1.Control Automatico 2.Controle Preditivo de Modelo Não-linear 3.Otimização 4.Sistema de Elevação a Gás 5.Modelagem I.Universidade de São Paulo. Escola Politécnica. Departamento de Engenharia de Telecomunicações e Controle II.t.

ACKNOWLEDGEMENT

Firstly, I thank my wife, Loveth Adukwu and my family, particularly my eldest brother, Sunday Adukwu, who had, have and will always support my academic pursuits. Without these wonderful people, it would have been extremely difficult if not impossible to pursue my academic dreams and reach my goals.

Many thanks also to all the personnel at *Escola Politénica da Universisade de São Paulo* and in particular at the *Engenharia de Telecomunicações e Controle* (PTC) and *Laboratorio de Simulações e Controle in B21 building*, for supporting my inquiries and technical issues.

I would especially like to thank my advisor Prof. Dr. Fuad Kassab Junior, who was always available for me at any time of need. Special thanks to Prof. Dr. Darci Odloak whose assistance and contribution to my research is of estimable value. He along with my supervisor guided me through all the research and development processes in this work.

I want to thank the Petroleum Technology Development Fund (PTDF) for supporting this work through the scholarship program of Oversea Scholars Scheme (OSS). Also special thanks to *Escola Politénica da Universisade de São Paulo* for granting me the opportunity to do my research here.

Finally, I would like to thank all my colleagues, with whom I partnered and worked together in research and classes. Among these are Amir Muhammed Saad, Guilherme Augusto Silva de Souza and Rafael Ribeiro Sencio. Special thanks to Jose Otavio Assumpcao Matias for his assistance with CasADi.

ABSTRACT

Gas-lifted system like every other artificial lift system is used when the natural energy for lifting crude oil from the reservoir into the downstream facilities becomes insufficient. This research focused on optimising crude oil recovery from gas-lifted oil well by using nonlinear model predictive control (NMPC). Two key approaches were used: (a) casing-heading instability reduction/elimination and (b) fault-tolerant control in the system. At first a developed nonlinear model predictive controller (NMPC) was presented. The controller was tested on continuous stirred tank reactor (CSTR) using IPOPT solver in CasADi and fmincon optimizer in MATLAB. Finite horizon NMPC was selected and used to optimise the gas-lifted system. The controller stabilised the undisturbed system improving production by 5.63% compared to the open-loop operation when the system is in casing-heading instability. For the two input case, the steady state production, aided by the high input target, reached 12.25kg/s which is far more than 9.57 kg/s for the one input case. This controller showed a 3.76% improvement over PI controller for the same purpose. Estimation performances of three nonlinear filters were compared and Extended Kalman filter was selected to provide the estimated states of the system which were used for fault-tolerant control of the gas-lifted system. Passive FTC, altering control bound and altering control cost were used to implement the FTC problems. Passive FTC provided more robustness but small output change. Reducing the upper control bound ensured stability but production could decline. Increasing the controller cost that prioritised the input target increased production but it was prone to casing-heading instability. While the FTC scheme could reduce the downtime, the casing-heading instability removal increases the average oil production rate hence optimising the gas-lifted system.

Keywords – Gas Lift, Model Predictive Control, Casing-Heading Instability, Fault-Tolerant Control, Optimisation.

RESUMO

O sistema de elevação a gás (*gas lift*, do inglês), como qualquer outro sistema de elevação artificial, é usado quando a energia natural para elevar o petróleo bruto do reservatório para as instalações a jusante se torna insuficiente. Esta pesquisa se concentrou na otimização da recuperação de petróleo bruto do poço de petróleo levantado a gás usando o controle preditivo de modelo não linear (NMPC, do inglês). Duas abordagens principais foram usadas: (a) redução/eliminação da instabilidade do cabeçote do revestimento e (b) controle tolerante a falhas no sistema. Inicialmente foi apresentado um NMPC desenvolvido. O controlador foi testado em reator de tanque agitado contínuo (CSTR), usando o *solver* de otimizações IPOPT no CasADi e o otimizador fmincon no MATLAB. O NMPC de horizonte finito foi selecionado e usado para otimizar o sistema gas-lifted. O controlador estabilizou o sistema não perturbado, melhorando a produção em 5,63% em comparação com a operação em malha aberta quando o sistema está em instabilidade de cabeçote de revestimento. A produção em estado estacionário, auxiliada pela alto alvo de entrada, atingiu 12,25 kg/s, muito mais do que 9,57 kg/s obtidos no caso de uma entrada. Este controlador apresentou uma melhoria de 3,76% em relação ao controlador PI (proporcional-integral) para o mesmo caso. O desempenho de estimativa de três filtros não lineares foram comparados e o filtro de Kalman estendido foi selecionado para estimar estados do sistema, que foram usados para controle tolerante a falhas (FTC, do inglês) do sistema de elevação a gás. FTC passivo, alterando limite de controle e alterando custo de controle foram usados para implementar os problemas de FTC. O FTC passivo forneceu mais robustez, mas pequena alteração na produção. Redução do limite superior de controle garantiu a estabilidade, mas a produção pode diminuir. Aumento do custo do controlador que priorizou o alvo de entrada aumentou a produção, mas estava propenso a instabilidade do cabeçote do revestimento. Enquanto o esquema FTC pudesse reduzir o tempo de inatividade, a remoção da instabilidade do cabeçote do revestimento aumenta a taxa média de produção de óleo, otimizando o sistema de elevação a gás.

palavras-chave –Elevação a gás, controle preditivo de modelo, instabilidade do cabeçote do revestimento, controle tolerante a falhas, otimização

LIST OF TABLES

LIST OF FIGURES

LIST OF NOTATIONS AND SYMBOLS

m_{ga} - mass of gas in annulus

m_{gt} - mass of gas in tubing

m_{ot} - mass of oil in tubing

P_s - pressure of separator

P_a - pressure of annulus

P_{wh} - pressure of wellhead

P_w - pressure of well

P_{bh} - Pressure of bottomhole

P_r - Pressure of reservoir

k_1 - Kenetic constant of first reaction

k_2 - Kenetic constant of second reaction

C_{A0} - inlet concentration of reactant A

C_{B0} - inlet concentration of reactant B

V - Volume

k - discrete sample time

t - time instant

T - continuous time horizon or interval

U_k - input sequence

u_{des} - desired input

u_k - input at k

x_k - state at k

x_0 - initial state k

P_1, P_2, P_3, P_4 - control problems

p - prediction horizon

m - control horizon

V_k - cost function at k

Q_x - state cost weight

Q_u - input cost weight

R_u - input moves cost weight

LIST OF ACRONYMS

CasADi: computer algebra system algorithmic differentiation

CSTR: continuous stirred tank reactor

DAE: differential/algebraic equation

DOS: dedicated observer scheme

EKF: extended Kalman filter

FDI: fault detection and isolation

FTC: fault-tolerant control

GLRT: generalised likelihood ratio test

GOR: gas oil ratio

GOS: general observer scheme

GRV: Gaussian random variable

IPOPT: interior point optimiser

KF: Kalman filter

LHP: left half plane

MPC: model predictive control

NLP: nonlinear programing

NMPC: nonlinear model predictive control

OCP: optimal control problem

ODE: ordinary differential equation

OLGA: oil and gas simulator

PF: particle filter

PI: proportional integral

PID: proportional integral derivative

RHP: right half plane

RMSE: root mean squared error

RTO: real time optimisation

SOS: simplified observer scheme

UKF: unscented Kalman filter

UT: unscented transform

CONTENTS

1 INTRODUCTION

1.1 Background

As production of hydrocarbon from beneath the earth surface increases, the natural energy for lifting it to the downstream facilities at the desired rate declines. At certain low production rate, it becomes necessary for artificial approach to be used to lift the hydrocarbons (KHAMEHCHI; MAHDIANI, 2017). Various artificial lift methods have been developed to maximise oil recovery while minimising total cost in delivering crude oil to the storage facilities. These artificial lift methods include sucker-rod pump, electrical submersible pump, gas-lifted system among others (FANCHI; CHRISTIANSEN, 2016), (BROWN, 1982). The most commonly used lift method in field with high gas-oil ratio with densely populated wells is the gas-lifted method (BROWN, 1982). This gas-lifted method accounts for over 70% of the artificial lift methods in Brazil (PLUCENIO et al., 2009).

Gas artificial lift method shown in Figure 1 involves pumping of lift gas into the annulus which then flows to the tubing. When the gas mixes with the oil in the tubing, the mixture density decreases making it possible for the available natural energy to lift the hydrocarbon again. Gas lift method is faced with many problems that affect its optimal operation. Instability in gas lift also known as severe slugging is a form of slugging flow that affects the average flow rate of produced oil. Removing this instability therefore increases flow rate and protects downstream equipment (JAHANSHAHI, 2013).

Increasing gas inflow into the annulus and decreasing outflow through the production choke, operating the injection valve at critical points that assures constant flow of gas through it and the use of control approach help to minimise this casing-heading instability (EIKREM et al., 2002). It is the control approach that forms one of the solutions to gas lift optimisation problem in this research as it is less conservative than the other two approaches.

Another obstacle to optimal operation of gas-lifted system is fault. Most faults in

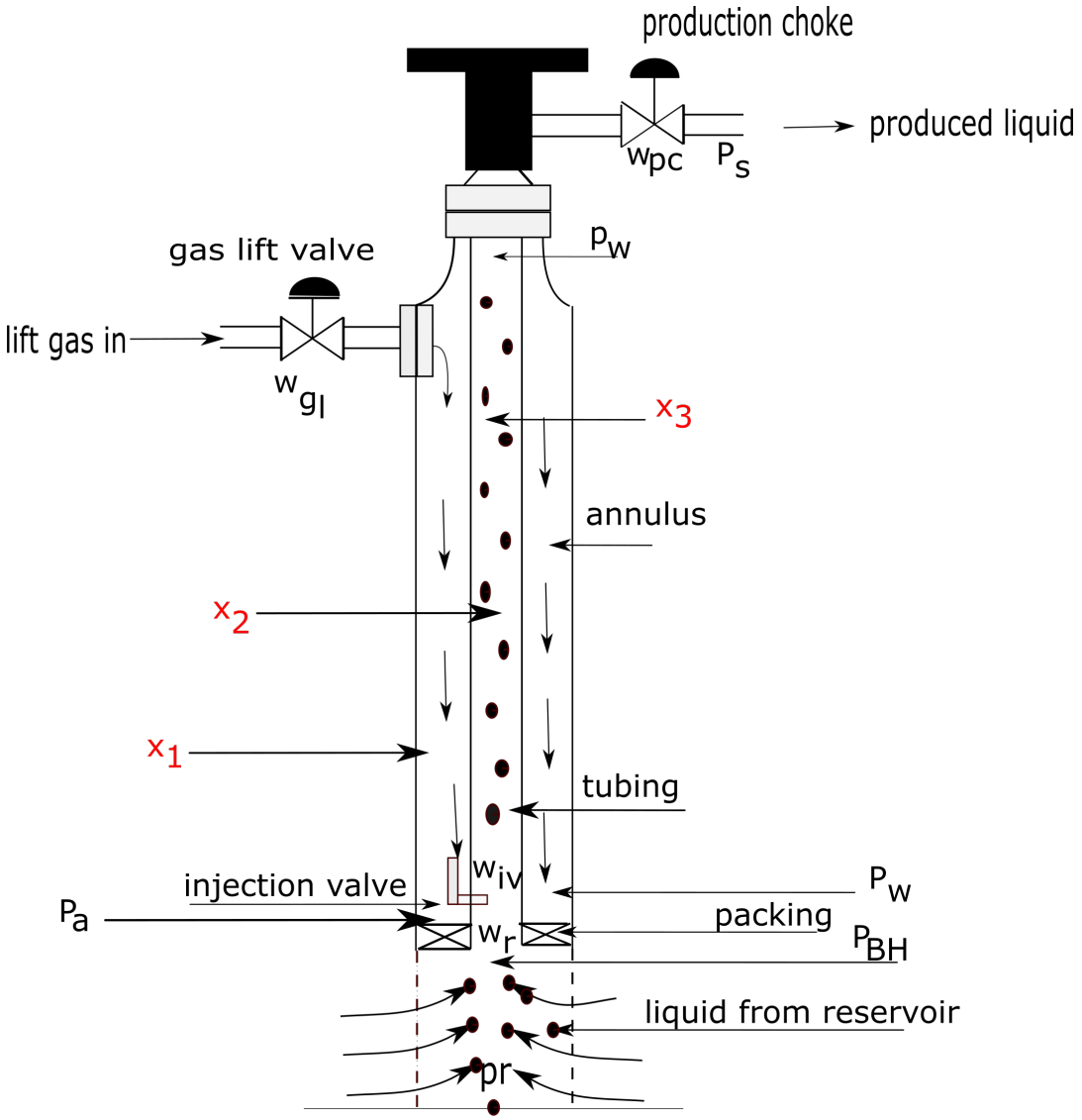

Figure 1: A single well gas-lifted system showing the states in red. These states are difficult for the sensors to measure accurately hence must be estimated by filters using the information from the sensors before being used for any control solution.

gas-lifted systems are not easily noticeable as the system will still continue to operate long after fault occurrence. The lift gas still flows into the annulus and mixes with tubing oil to lighten it for production to continue even in the presence of fault. When this happens reduced production that is not related to casing-heading instability occurs affecting the optimal operation of the gas-lifted system. These faults mostly results from instrumentation-related problems but some are due to valve faults. The fault effects show up in the abnormal values of the gas lift states and variables which measurements are usually not available or if available are usually not reliable. Estimating the states and the variable using filters, generating residual, evaluating residual and performing fault-tolerant control (FTC) helps to optimise the gas-lifted system.

Both casing-heading instability removal and fault-tolerant control can be implemented with nonlinear model predictive control (NMPC) with control zones. The zone control NMPC ensures the gas lift states are maintained in their zones that favour continuous unidirectional flow of gas from annulus into tubing while moving the inputs valves towards their optimal values. These two are interdependent as casing-heading instability can lead to fault in the system while fault can hinder control solution to casing-heading instability by either changing the controller internal model or reducing the input constraints. Removal of casing-heading instability and fault-tolerant operation of the gas-lifted system using MPC become necessary and form the main concern of this research.

We present here the motivation for this research, brief on gas-lifted systems and optimisation, the objective of the study and the research outlines.

1.2 Motivation

Flow assurance, a term coined by Petrobras as guarantee of flow (garantia do escoamento) is influenced by many factors such as hydrates, wax, asphatenes, scales, slugging flow, emulsion and corrosion (JAHANSHAHI, 2013). These in addition to faults either in the surface or downhole reduces flow rate of produced oil or increase cost of oil production. But slugging flow and faults constitute the major obstacle to flow assurance.

Poor flow assurance and in particular casing-heading instability reduces average oil production and it is not healthy for the downstream equipment (AAMO et al., 2005). For an adverse case of when the storage facilities are over-constrained, this oscillatory behavior can result in flaring as there may be less storage facilities to cope with peaks in production (KRISHNAMOORTHY; FOSS; SKOGESTAD, 2018). Consequently, casing-heading instability is not desired hence must be removed or minimized. One way to reduce this instability is pumping enough gas through the gas injection valve but this is faced with the constraints of limited gas supply from the compression station. Another solution is reducing the percentage opening of the production choke, but this will reduce average production as the optimal production computed by the upper optimization layer is far into the unstable region. A third solution is the control approach which monitors the two solutions above. Figure 1.2 shows oil production rate variation with choke opening and injected gas rate.

In Figure 2a, oil production increases with choke opening till casing-heading instability starts. This point occurs at low valve opening depending on the well characteristics,

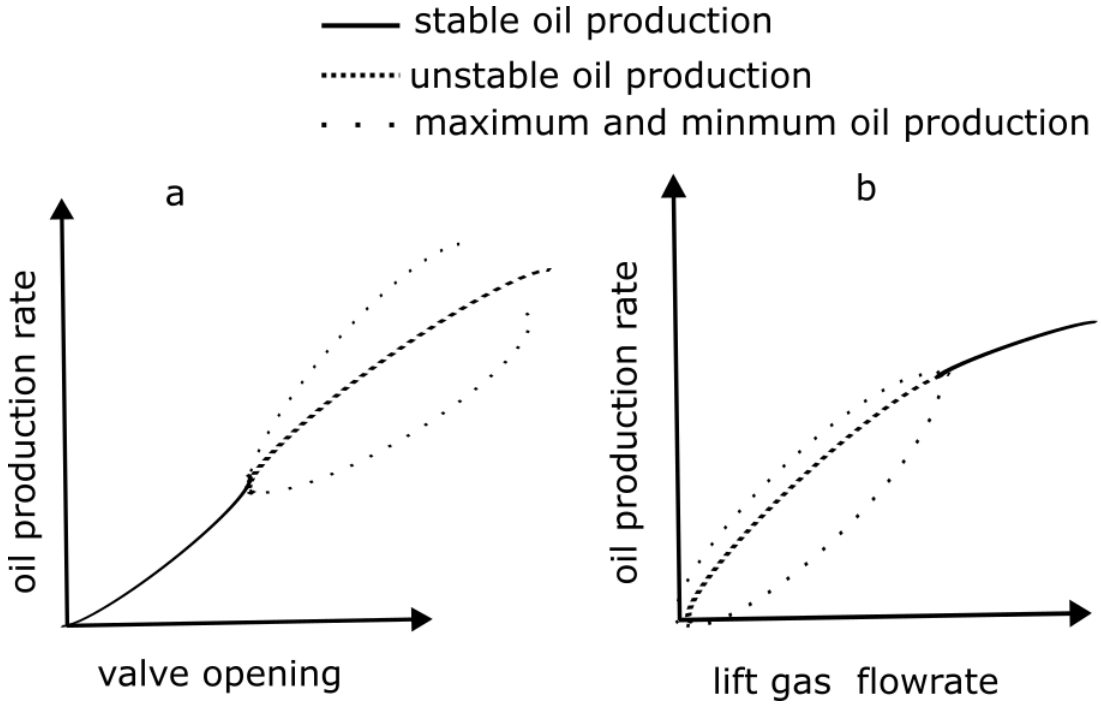

Figure 2: Oil production curve with: (a) percentage valve opening and (b) injection gas flow rate. To prevent oscillation, valve opening must be kept low while lift gas flow rate much be high enough.

in particular, the gas/oil ratio (GOR). Hence to prevent casing-heading instability, the percentage choke opening must be kept low. In Figure 2b, low gas flow rate corresponds to the unstable region hence to move the gas-lifted system out of unstable region, more gas has to be supplied to annulus. But this is limited by available gas supplied.

When gas injection rate into the annulus from the compressor station is kept constant while the percentage choke opening is used as input to control the oil production, optimal choke opening falls into the unstable region. Similarly, optimal flow through the gas lift valve falls into the unstable region when the choke is kept constant. Therefore an advanced control system that drives the input choke opening to the optimal input target as close as possible while avoiding or minimizing instability is necessary to optimize production. This in addition to monitoring the gas-lifted system for fault-tolerant control is the motivation of this work.

1.3 Gas Lift Optimisation Problem

Since the casing-heading instability results from periodic variation of annulus and tubing pressures and flow stops when annulus pressure is less than or equal to tubing pressure, decision of how to minimise this variation and/or keep the annulus pressure

above certain value while meeting the target for the valve opening is key to removing the instability. The pressure of the annulus is related to mass of gas in the annulus at a given time. Hence if a controller can be designed such that the control objective is to first drive the mass of gas in the annulus into a selected zone thereafter enforcing the input valve opening meets input target or moves as close as possible to the target, the gas-lifted system can be optimised.

Monitoring the gas-lifted system for early fault detection and fault-tolerant control ensures the controller can perform its function well hence optimising the system. Model predictive control (MPC) with input target and control zones has inherent fault accommodation capacity. As the gas-lifted system has the characteristic behaviour of hiding minor faults which affect optimal production rate, the MPC can combine the function of removing casing-heading instability with adjusting controller parameters and input constraints when fault is detected. This will not make the system operate at the desired optimal rate but production improves better when controller is used compared to ignoring the faults or suppressing casing-heading instability without the control means.

1.4 Objectives

The main aim of this thesis is the optimisation of gas-lifted system by casing-heading instability suppression and fault-tolerant control of the system. These are achieved using nonlinear model predictive control(NMPC).

The specific objectives of this research are:

(i) Controller presentation.

(ii) Gas lift casing-heading instability analysis and suppression.

(iii) Gas lift fault-tolerant control.

1.4.1 Controller Presentation

Present a nonlinear model predictive controller with input target and control zones and extend it to various cases of applications. Present different formulations of this NMPC with their advantages and shortcomings. Discuss the feasibility and convergence issues of the controller. Test the finite horizon formulation on simple ordinary differential equation (ODE) CSTR system.

1.4.2 Gas Lift Casing-Heading Instability

Present simplified model of gas-lifted system and derive the pressure profile in the annulus and tubing. Examine the phase portrait, bifurcation diagram, limit cycle and linearised behaviour at different operating points for the gas-lifted system. Simulate the casing-heading instability and apply the developed controller in removing the instability. Compare average production for open loop and closed loop. Examine the oil production using proportional-integral (PI) controller.

1.4.3 Gas Lift Fault-Tolerant Control

Compare estimation accuracy of extended Kalman filter (EKF), unscented Kalman filter (UKF) and particle filter (PF) on gas lift state estimation. Use EKF, to obtain state estimates for residual generation. Use the generalised likelihood ratio test (GLRT), as decision function for fault detection, dedicated observer scheme (DOS) for fault isolation and perform fault-tolerant control (FTC).

1.5 Thesis Outlines

The thesis outline is described in Figure 3 briefly. The gas-lifted system review leads to NMPC presentation and gas lift analysis. The analysis leads to state estimation using nonlinear filters. The NMPC uses the state estimation to stabilise casing-heading instability and also fault-tolerant control (FTC). The final result is the optimised gas-lifted system. The steps are explained further below:

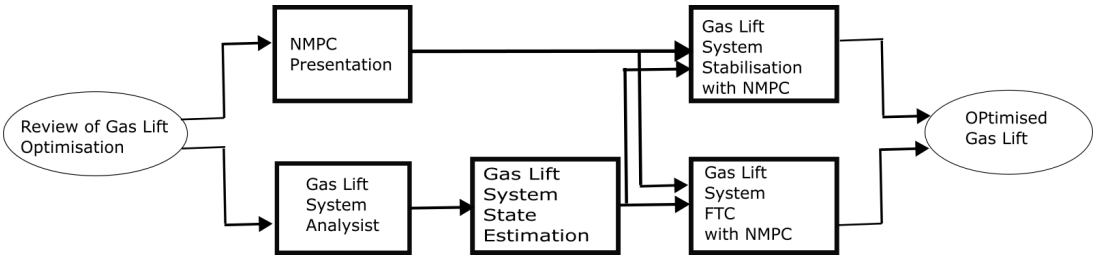

Figure 3: Thesis Outlines

Chapter one introduces the thesis giving background of the research area, the motivation for the research and the gas lift optimisation problem. It provides the objectives of the studies, the outline of the research and the contribution.

Chapter two reviews relevant literature on the casing-heading instability, optimisation

and MPC, fault-tolerant control and gas lift optimisation.

Chapter 3 discusses the developed NMPC. It discusses briefly multiple shooting and fmincon solvers used to solve the problem, then the various NMPC formulations are presented along with application to a simple CSTR for tracking and zone control with and without disturbances.

Chapter 4 discusses gas lift modelling and analysis. The pressure profile of the system showing the variation of pressure with height is derived as the pressure dictates the flow in the system. Gas lift behaviours are discussed here considering, bifurcation, limit cycle, phase portrait and the linearised behaviour at different operating points.

Chapter 5 discusses the use of FHNMPC in gas lift stabilisation. Gas lift models are solved using both ODE15s and Euler method. Then casing-heading instability is presented, the behaviour is presented for both field data and laboratory data. The simulation for various gas-lifted system conditions were done.

Chapter 6 compares the state estimation of gas-lifted system. (EKF), (UKF) and (PF) were used to estimate the states of gas-lifted system. Both residual visualisation and statistical approach were used to compare the estimation capacity of the filters.

Chapter 7 discusses fault-tolerant control in gas-lifted system. The (GLRT) was used for fault detection, (DOS) was used for fault isolation while various fault scenarios were examined.

Chapter 8 presents the conclusion and further works

1.6 List of Contributions

1.6.1 Main Contributions

1. Stabilisation of casing-heading instability with nonlinear model predictive control.
2. Direct nonlinear state estimation of gas-lifted system.
3. Fault-tolerant operation of gas-lifted system.

1.6.2 Conference Publications

1. Adukwu, O., Odloak, D., Kassab Junior, F. (2022). Optimization of CSTR Using Infinite Horizon Model Predictive Control with Setpoint Tracking and with Input Targets

and Control Zones. In 15th European Workshop on Advanced Control and Diagnosis (pp. 755-776). Springer, Cham.

2. Adukwu, O., Odloak, D., Kassab Junior, F. (2020, December). Stabilization of Artificial Gas Lift System Using Nonlinear Model Predictive Control with input Target and Control Zones. In 2020 IEEE Congreso Bienal de Argentina (ARGENCON) (pp. 1-7). IEEE.

1.6.3 Journal Publications

1. Adukwu, O.; Odloak, D., Saad, A. M.; Kassab Junior, F. (2022). State Estimation of Gas-Lifted Oil Well Using Nonlinear Filters. Sensors, 22(13), 4875. https://doi.org/10.3390/s22134875

2. Adukwu, O.; Odloak, D.; Kassab Junior, F. (2023). Optimisation of a Gas-Lifted System with Nonlinear Model Predictive Control. Energies, (16), 3082. https://doi.org/10.3390/en16073082

3. Adukwu, O.; Odloak, D.; Kassab Junior, F. (2023). Fault-Tolerant Control of Gas-Lifted Oil Well. IEEE Access, https://doi.org/10.1109/ACCESS.2023.3255645

4. Adukwu, O.; Odloak, D.; Kassab Junior, F. Gas-Lifted Systems: A hands-On Tutorial on Modelling and Analysis. Under Review.

1.7 Concluding Remarks

It is presented here the introduction to this research work. The background, the motivation, methodology applied, the research outlines and the contribution of the research work were presented.

2 REVIEW OF GAS LIFT OPTIMISATION

2.1 Background

The gas-lifted system is situated in an oil field with many other oil wells. Many factors affect the flow of the oil in the system as enumerated in chapter 1 but we limit the optimization to the case where there is only measurement and state noise, casing-heading instability and faults in the valve. In this chapter we review the gas-lifted system, the casing-heading instability behavior, the fault-tolerant control and optimisation of the system.

2.2 The Gas-Lifted System

Gas-lifted system is one of the artificial lift methods used in matured oil field. The natural lift pressure for the gas-lifted system is provided by the reservoir pressure (P_r). When this pressure is insufficient, oil production falls below desired flow rate. To describe this behaviour further, we first describe the oil field and an oil well.

2.2.1 The Oil Field and Oil Well

Figure 4 shows an oil field with many oil wells while Figure 1 (shown in the introduction) shows the gas-lifted well. The oil field shown in Figure 4 contains one or more oil wells connected to a platform which is connected to a separator through a common riser. The separator connects to the compressor station where the separated gas is compressed ready for supply to the gas-lifted well system through the annulus. The separated oil is sent to the storage facility for onward delivery to the pipelines. The gas-lifted oil well and its optimisation is the centre of the research.

The gas-lifted well shown in Figure 1 contains the annulus through which lift gas enters the system through the gas lift valve. The gas then enters the well (or tubing)

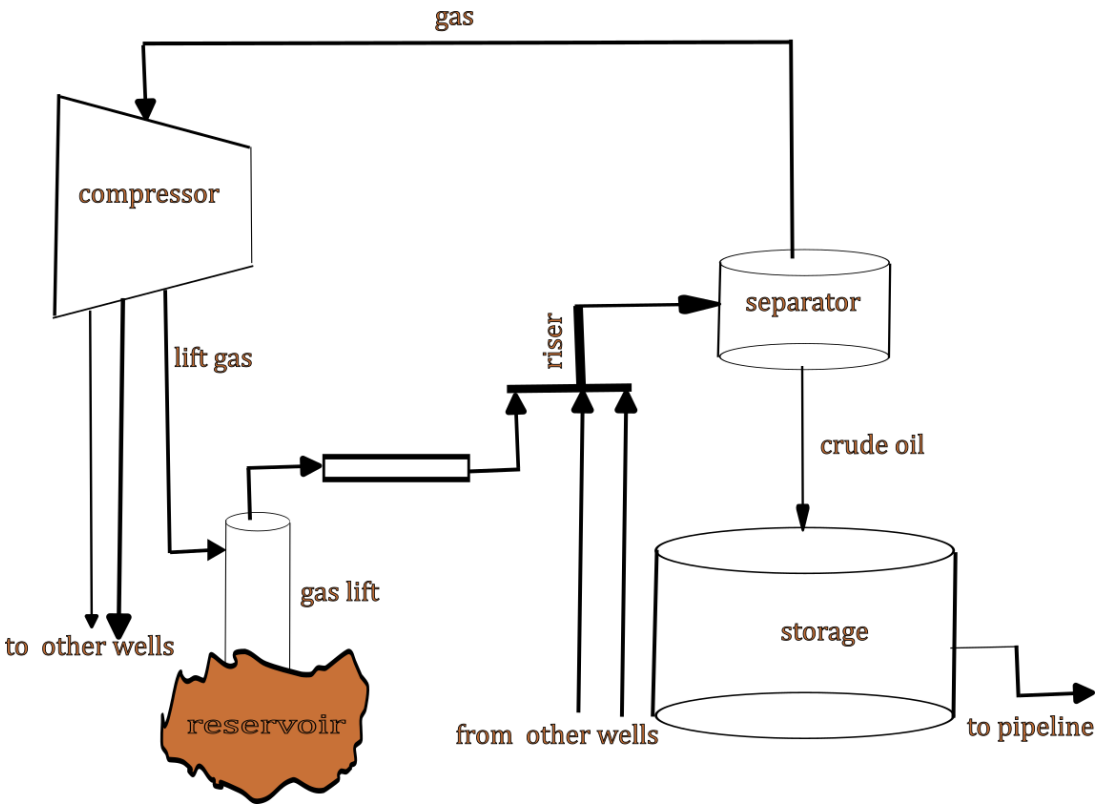

Figure 4: Oil field with many oil wells.

through the injection valve for mixing with the oil. The produced oil is delivered to the separator through the production choke. The states of the system are the mass of gas in the annulus (m_{ga}), the mass of gas in the tubing (m_{gt}) and mass of oil in tubing (m_{ot}). The key pressures are separator pressure (P_s), the annulus pressure (P_a), the well pressure (P_w), bottom hole pressure (P_{bh}) and the reservoir pressure (P_r). These are described further in chapter 4.

2.2.2 Casing-Heading Phenomenon

For there to be continuous unidirectional flow of gas from the annulus into the tubing, P_a must remain greater than P_w. The reservoir pressure (P_r) helps to reduce P_w to ensure continuous gas flow. But in the course of production, this is usually not possible as P_r declines leading to build up of oil in the tubing. Lift gas is then delivered to the annulus. The annulus pressure increases leading to increased pressure difference with the tubing. This makes lift gas to flow into the tubing to reduce the density of the tubing oil. Oil production increases, resulting in a further decrease in bottomhole pressure. More gas then flows into the tubing. The increased flow reduces the annulus pressure till the pressure difference is insufficient to permit gas flows into the tubing. Oil then

builds up in the tubing while gas builds up in the annulus until the annulus pressure becomes large enough to allow flow of gas into the tubing. A new cycle then starts. This leads to oscillatory behaviour of the gas-lifted states and variables. This oscillatory behaviour is called casing-heading instability. Further theoretical description of casing-heading instability can be found in (XU; GOLAN, 1989).

This oscillatory behavior of the gas-lifted system reduces the mean oil production and it is also not healthy for the downstream equipment. The behaviour could lead to a violation of the operational constraints of the gas-lifted system or environmental regulations hence it is not desired and must be removed. But depending on the percentage opening of the production choke, or the mass flow rate of injected gas, production of oil from the tubing through the choke could increase. Casing-heading instability can be minimized by many factors/approaches some of which are:

Natural factor such as high gas to oil ratio (GOR) which increases the mass of gas in the tubing hence reduces the density of tubing mixture.

Design consideration to increase the annulus volume to hold more gas at a time hence increase annulus pressure.

High injection gas flow rate which increases annulus pressure hence reduces the chances of casing-heading.

Demulsifier and other chemicals that improves flow assurance.

Control application like MPC among others.

The natural factors such as high gas-oil ratio (GOR) come as disturbance hence out of our control. Design approach is done based on predicted gas-lifted system behavior before operation. But the reservoir characteristics is fast changing during operation and the design might become ineffective in reducing casing-heading instability. Increase in injected gas flow rate is limited to the availability of gas from the compressor. In addition, production increases with supplied gas until an optimal point beyond which more gas supply reduces oil production as lift gas dominates the produced fluid. Demulsifier cost is prohibitively high and difficult to apply. Control therefore becomes the popular approach used to remove this instability due to its comparative cost advantage. We therefore discuss various control solution approach for minimising casing-heading instability and general optimisation of gas-lifted system.

2.2.3 Casing-Heading: Simple Feedback Control Solution

Early control solution to casing-heading instability includes the work of Blick and Boone (1986) where Laplace transform was used on the characteristic equations of flow from the well to determine if the particular well is stable or not. The unstable wells were then stabilized using simple feedback control employing simple proportional-integral-controller (PID) that varies the production choke diameter to control the flow rate of produced fluid. Asheim (1988) proposed two criteria for gas lift stability. In both cases (inflow response and pressure-depletion response), high flow rate of the lift gas is important in stabilizing the gas-lifted system (ASHEIM, 1988). Many control applications were based on this criteria.

Der Kinderen developed a control strategy called DanaCon for stabilizing the annulus pressure without manipulating the injection gas choke. This uses two PIDs in cascade control where the outer loop provides the setpoint for the casing-heading pressure while the inner loop determines the valve position (KINDEREN; DUNHAM; POULISSE, 1998). The combined effect is to keep the annulus pressure high to favour constant flow of lift gas from annulus into the tubing. Another feedback control application for the stabilization was performed by Bin and Golan (2003) using PI controller whose gains were selected by trail-and-error. The control structure used the production choke as input to regulate the bottomhole pressure to a value slightly higher than the steady state value obtained from simulation in OLGA (Oil and Gas) simulator. OLGA simulator also provided the period of oscillation which was used to determine the integration time of the PI controller. These controllers stabilized the gas-lifted system and improved production compared to open loop case.

Eikrem et al. (2002) used a PI controller to stabilize the unstable gas-lifted system where the production choke opening was the input while the downhole pressure and the annulus pressure were used as the controlled variables for the two control structures used. But this method works well when the downhole pressure measurement is very reliable which is not so in practice. Aamo et al. (AAMO et al., 2005) then developed a reduced order observer for estimating the states of the gas-lifted systems hence obtained the downhole pressure. The reduced order observer assumed the mass of gas in annulus is measured hence the masses of gas and oil in tubing were estimated and used for obtaining the downhole pressures. Using these estimates, a PI controller was designed in output feedback, to stabilize the system and the result validated using laboratory experiment.

Considering the states and variables as stochastic, Eikrem, Imsland and Foss (2004)

performed state estimation for obtaining the downhole pressure estimates using Kalman filter. A PI controller was then used to improve the oil production significantly. Scibilia, Hovd and Bitmead (2008) then extended the works of Eikrem, Imsland and Foss (2004) to case where the mass of gas in annulus is also estimated hence a full order observer was used to estimate the downhole pressure. Eikrem, Aamo and Foss (2008), also used PI controller to stabilize the oscillatory gas-lifted system using downhole pressure, casing head pressure and differential pressure as controlled variable with choke opening as manipulated variable for the three control structures.

A case were two inputs were used rather than the usual one input was considered in Rashid, Demirel and Couët (2011) where a nonlinear mixed integer optimization problem was solved to control casing-heading instability and optimize a gas-lifted network. Using both injected gas valve and the production choke as the control inputs, an offline mixed integer optimization problem was solved considering that the choke valve can be treated as discrete or continuous. A comparison of stabilization capacity of PID, LQR, LQG and cascade control is presented in (HANSEN, 2012) using simplified model of gas-lifted system. This also reveals that the bottomhole pressure is the best variable to use in stabilizing the gas-lifted system in casing-heading instability.

2.2.4 Casing-heading: Model-Based Control Solution

Most of the simple feedback controller discussed above used simple PI or PID controller to stabilize the gas-lifted system on the assumption that the models do not change rapidly. The gas-lifted system is highly dynamic hence over the entire operating range, the operating point could vary rapidly especially when in the casing-heading instability region and PID becomes suboptimal. One approach to still use a PI controller is discussed in (JAHANSHAHI, 2013) where a PI controller with gain adaptation was used. The issue with this approach is the determination of when to apply the gain change. Model-based approach has advantage here and it permits the controller to be used over wider operating range than the PID. An early model-based approach to gas lift stabilization is presented in Jansen et al. (1999) where nonlinear transient gas-lifted models were used to design a controller. Using the models, the gas lift variables like pressure, temperature and flow rates were predicted and the controller effort was to minimize the error between the externally provided operating point and the predicted values (JANSEN et al., 1999).

Advanced model-based control begins to gain traction in casing-heading instability in recent times. Garcia (2013) considered a more holistic approach to gas-lifted instability

removal or minimization. Control approach, choke opening and replacement of valves were considered for a third order model of the system. Jahanshahi, obtained a comprehensive solution to anti-slug flow in a pipeline-riser linear and nonlinear systems. Linear control solutions such as internal model controller (IMC), H-infinity and PI controllers were used to provide the robust solution to the system. Nonlinear approach such as gain-scheduled IMC, PI controller with gain adaptation, state feedback and output linearizing controller were used for the stability of the system. The simplified model of the gas-lifted system was also obtained through OLGA (Oil and Gas) software and verified experimentally (JAHANSHAHI, 2013). This model is very useful in gas-lifted system now.

A simplified third order model was used to stabilize gas-lifted system using nonlinear predictive generalized minimum variance control in (SHI et al., 2019). The robustness of this approach was proved by simulation where variations in valve characteristics and compressor pressure were used to induce disturbances. The approach removed instability of the system under these parameter variations.

2.3 Optimistion

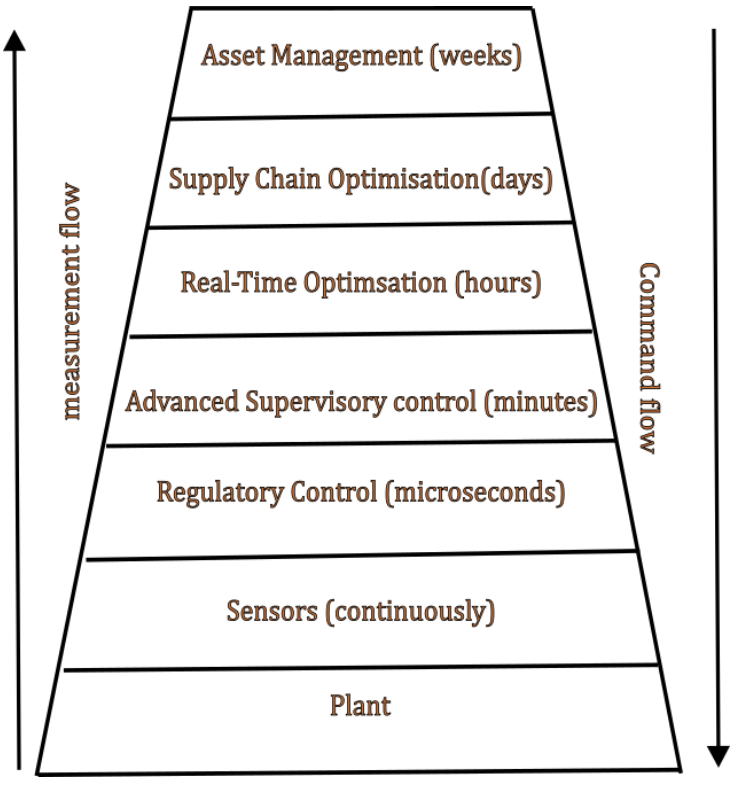

Figure 5: Optimisation hierarchy in gas-lifted system. While plant measurement flows from bottom to up, command flow flows from top to down.

Optimisation is at the heart of every decision process. In the upstream network,

optimization is performed at various stages in the optimisation hierarchy shown in Figure 5. Sitting on top of the hierarchy is the asset management that involves long term investment decisions such as decision on the lift system to be applied, the number of wells to be sited in a field. The decision period is usually weeks and months. The next phase, supply chain optimization deals with decision on inventory of parts and storage resources which are constraints in the optimization process. The period is usually days.

The real-time optimization is responsible for daily allocation of resources like lift gas distribution among various wells and set-points for the control layers with a period usually in hours. The supervisory control layer implements the setpoints provided by the RTO (real time optimsation) layer. The supervisory layer and regulation layer together form the control and automation layer (KRISHNAMOORTHY; FOSS; SKOGESTAD, 2016). The sensor works continuously. While command flows from top to down in Figure 5, plant measurements move in the reverse direction from plant to asset management. MPC is found in the control and automation layer and forms the center of this research.

At each level, the optimal solution lies at the intersection of the constraints. Gas lift RTO (real time optimsation) is usually done at steady using nonlinear model which changes due to the variation in gas lift parameters. These parameters are updated during parameter estimation at steady state based on measurements hence altering the model. The parameter update (parameter estimation) and optimization cycle causes delay in the execution of the optimization hence Krishnamoorthy, Foss and Skogestad (2018) proposed a means to update model dynamically while RTO (real time optimsation) still takes place at steady state hence avoiding the steady state wait time. A survey of gas lift optimization discussing various approach used and challenges is presented in (RASHID; BAILEY; COUËT, 2012).

2.4 Model Predictive Control (MPC)

Model Predictive control (MPC) like other advanced control use the complex relationships between controlled and manipulated variables in a quantitative way to define control actions (CAMPOS et al., 2013). MPC is an advanced control strategy that uses the model of the system to be controlled to predict the future trajectory of the states. MPC then solves an online optimal control problem (OCP) subject to input and state constraints to determine the open-loop input sequence that minimizes a given cost function. However, only the first element of the computed future control sequence is applied at a given sampling time (MARTIN; ODLOAK; KASSAB, 2013; MAYNE, 2014). At the

next sampling time, the horizon recedes and the OCP is solved again, usually using the shifted control sequence from the previous time step as the initial guess for the OCP. This procedure is used to approximate the infinite horizon optimal control problem hence it is not optimal in itself.

2.4.1 MPC Formulation

Usually linear MPC is considered since the MPC has the advantage that its performance is still acceptable even in the presence of up to 20% model inaccuracy (ROSSITER, 2017). But as most process systems are nonlinear and the demand for better product quality and health with safety regulations weighs in, the need for Nonlinear Model Predictive Control (NMPC) comes in. This is because unlike linear MPC, where change in operating condition reduces the performance of the optimisation as process linear model would have changed, NMPC can accommodate change in system operating point (MARTIN; ODLOAK; KASSAB, 2013).

NMPC unlike linear MPC uses nonlinear model of the process systems to predict the systems state trajectory hence compute the future input sequence required to meet the set objective. While this ensures that the natural dynamics of the system is better captured and the system can be operated more closely to the constraints boundary, it comes with its setbacks. The major problems affecting the application of NMPC are the computational demand in solving the optimisation problem, implying difficulty of obtaining an optimal solution. Also if the optimal solution is obtained, the chance that the optimal solution will be a global optimum and not a local minimum constitute the problems of NMPC (ALLGOWER; FINDEISEN; NAGY, 2004).

MPC finds useful application in multivariable systems where in most cases it is not desired that the output tracks a fixed setpoint for all the outputs. This is usually the case where there are more controlled output than there are available manipulated inputs. In such case, MPC is used in zone control and input target formulation where the function of the controller is to ensure that the outputs (or states) lie in the given zones while enforcing that the input meets the input target (CAPRON; ODLOAK, 2018). Linear MPC has found tremendous application in this area but the use of NMPC is just beginning to gain traction in zone control and input targets.

The use of finite horizon reduces the computation effort required in obtaining the solution of optimal control problem (OCP) but increases the risk of instability in the resulting NMPC. Consequently, infinite horizon NMPC is used to overcome the instability

fears. Since one of the constraints is the state evolution which is nonlinear, different approaches are used to obtain the prediction model for the NMPC. Common among these are the Euler approximation, single shooting, multiple shooting among other methods (SHARMA; GLEMMESTAD, 2012). Euler method is fast but allows approximation error to propagate down especially for a very large system. Single shooting discretises the input, reduces the original boundary value problem (BVP) to initial value problem (IVP) and solves for the best trajectory that makes the final value of the IVP as close as possible to the final value of the BVP. Multiple shooting approach divides the horizon into finite elements and integrates over each element then optimises the initial state values that give a desired final value. Consequently, the initial states therefore form part of the decision variables and the shooting gap is closed at the end of the horizon.

The key concepts of MPC are therefore summarised as (LEE, 2011; RAKOVIĆ; LEVINE, 2018):

System model: MPC requires the model of the system to be controlled to predict the system future trajectory.

Cost function: MPC solves online cost function to determine the optimal control input to the system. This cost function is obtained from multi-objective function which is reduced to a single cost function by summing the scaled objectives.

Receding Horizon: MPC control and prediction horizons remain constants but move forward (recede) every sample time.

2.4.2 MPC Objectives and Advantages

Model predictive control is aimed at achieving some objectives which might be difficult for other control methods to achieve. These key objectives of MPC are (QIN; BADGWELL, 2003):

Prevent violation of input and output constraints: MPC is aimed at preventing input and output constraint violations hence it includes constraints in its formulation.

Dynamic output optimisation: MPC drives the controlled variables to their steady state optimal values. This is the aim of all control methods too.

Dynamic input optimisation: MPC aims to drive the manipulated variables to their steady state optimal values.

Prevents excessive manipulated variables movement: MPC aims at prevent-

ing the excessive movement of manipulated variables by penalising input moves. For example the valve movement in the gas-lifted system may be limited to 2% change per sample time hence preventing aggressive valve movement.

MPC controls plant as much as possible when actuators and sensors fail: MPC is robust to faults.

These objectives are easily achieved due to MPC having the following advantages over other controllers (OCAMPO-MARTINEZ, 2007).

1. MPC concept is very easy.
2. MPC can be used to control virtually all types of process dynamics.
3. MPC is efficient for multivariable systems.
4. MPC has explicit use of constraints in its optimisation which helps to minimise the chance of controller output being different from plant input.
5. It has inherently, delay compensation.

2.5 Gas-Lifted System Fault-Tolerant Control

Another issue that affects flow assurance hence the optimal operation of gas-lifted well is fault in actuator, gas lift parameter, and sensor. While parametric fault has multiplicative effects on the system output and varies slowly, both sensor and actuator faults have additive effect on the system output and can lead to abrupt system breakdown. Also a fault in the gas-lifted system can be hidden and the system runs while produced oil flow rate is drastically reduced for the gas lift injection rate. This reduced production results from the fault affecting the gas lift parameters hence the model leading to a change in the optimal control constraints and the admissible inputs (BLANKE et al., 2006). Hence carrying out fault-tolerant control on the gas-lifted system improves oil production even though the system might not be operating at optimal level.

Willersrud et al. (2013b, 2015) used an observer to estimate the states and parameters of the drilling system. These parameters are nearly constant in the absence of drilling problems except in the presence of some disturbances. Then generalised likely ratio test (GLRT) function was used for the fault detection and diagnosis. Gilbertson, Hover and Colina (2010) comprehensively examined failure modes in injected gas valve and their sensitivity analysis. One conclusion of their work is that it revealed that the mass flow

rate of lift gas through the injection valve is highly sensitive to some parameters among which are temperature and pressure of the gas and pressure of the reservoir. Consequently, for a given temperature of gas, pressure and reservoir pressure the PDF of the flow rate can be examined for a healthy system and the threshold set. Exceeding this threshold can be triggered as fault.

Sotomayor and Odloak (2005) used observer-based approach for fault detection and diagnosis in two process plants. Both parametric and actuator/sensor faults were diagnosed by this approach. The full-order observer was used for sensor faults in FCC units and was able to detect the faults satisfactorily. The use of observer-based approach for fault detection employs different observer schemes for fault isolation based on ease of implementation on one hand and reliability on the other hand. Some of the observer schemes used for sensors fault isolation are discussed here briefly:

2.5.1 Simplified Observer Scheme (SOS)

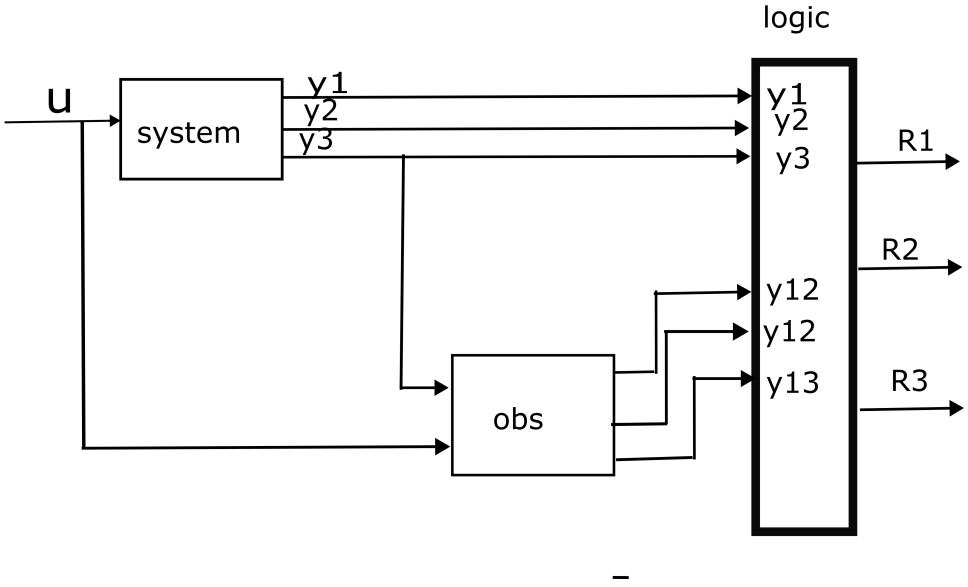

Figure 6: Simplified observer scheme for a three-output system. In this fault isolation scheme, there is only one observer which is fed with one output of the system while the observer outputs the estimates of the three variables.

The SOS shown in Figure 6 has one observer that might be full order or reduced order, takes input from one sensor at a time and outputs the estimated output of all the measurements. For isolation purpose, if all the sensor outputs are fault-free, the observer outputs are the same as the actual sensor outputs. Consequently, the residuals which are the difference between the observer outputs and sensors outputs will be zero for all the

measurements. If however one of the sensor outputs is faulty, the estimated outputs from observer depends on which sensor outputs is the input to the observer.

If the observer input is not the output of the faulty sensor, the estimated output will be the true outputs for all the measurements. Since the faulty sensor outputs the wrong measurement, its residual will not be zero while other residuals are zero hence the faulty sensor can be identified (isolated). If however, the input to the observer is from the faulty sensor, the estimated outputs are wrong estimates. The residuals for the measurements will be nonzero but the residual for the faulty system will be zero hence the faulty sensor can be identified (CLARK, 1978).

2.5.2 Dedicated Observer Scheme

The DOS is similar to the SOS diagram except that there is one observer for each output hence it has n observers for n measurements sensors. One observer takes input from one sensor and like SOS, outputs all the measurements. The observer that carries the faulty sensor output produces wrong estimates while those taking the no-fault sensor outputs provide the true estimates of the measurements. From the residual, the faulty sensor can be detected and isolated similar to SOS. The advantage of the DOS over SOS is the ability of the DOS to detect more than one fault at a time while the SOS enjoys the simplicity of the implementation (CLARK, 1979).

2.5.3 General Observer Scheme

The GOS is similar to the DOS in all respect except that all the observers take input from all the sensors except one. Like SOS and DOS, the GOS outputs the estimates for all the measurements. Since all the observers take inputs from all the sensors except one, one fault can be detected and isolated at a time hence the GOS cannot detect simultaneous fault like the DOS. The GOS enjoys more reliability as a fault in any sensor can more reliably be detected than DOS (FRANK, 1987).

2.6 Optimization of Gas-Lifted Well Using Nonlinear Model Predictive Control

We assume here that the steady state optimal solution to the gas-lifted system has been computed in the optimisation layer and we want to use controller to approach this

optimal values as close as possible. The gas-lifted system operation can take any of the following forms:

1. Nominal gas lift.
2. Gas lift with disturbance/noise.
3. Gas lift with disturbance/noise and casing-heading instability.
4. Gas lift with disturbance/noise, casing-heading and minor fault.
5. Gas lift with disturbance/noise casing-heading and major fault.

The complexity of optimisation increases down the ladder. In condition (1), the control effort is minimal. The gas-lifted system runs normally and possibility of meeting optimal solution is highest in this case. Condition (2) requires simple controller like PID in feedback control to run the gas-lifted system. The possibility of meeting optimal operation is influenced by the level of disturbance/noise. Condition (3) can be resolved by simple MPC and the optimal operation depends on degree of disturbance and amplitude of oscillation of the casing-heading instability. Condition (4) can be handled by MPC with fault-tolerant capability like nonlinear MPC with zone control and input target. The performance here is suboptimal. Condition (5) is difficult to achieve with control application.

MPC use in gas-lift optimisation is already a matured research area. Willersrud et al. (2013a) and Willersrud et al. (2011) used two approaches to optimise off-shore oil and gas production. These methods: the unreachable set-points and the soft constraint improved the optimal oil production compared to the two layer approach. Diehl et al. (2018) used multivariable approach but NMPC to optimize and stabilize a gas-lifted system. The control inputs were production choke and the gas lift valves. The methodology also provides for possibility of using slow and fast valves when appropriate, hence improving the life of the valves. These approaches were used on gas lift in condition (3).

We are considering condition (4) here where an MPC with input target and control zones are used to handle casing-heading instability and perform fault-tolerant control also. The control zone helps remove the casing-heading instability by permitting the setting of the state zones based on system needs and such that the annulus pressure remains higher than the tubing pressure aiding continuous flow of gas from the annulus into the tubing. The fault-tolerant control involves estimating the gas lift states using EKF, performing fault detection using GLRT and adjusting the controller parametrs or input constraints.

2.7 Concluding Remarks

This chapter briefly reviewed casing-heading instability, optimization and MPC then fault detection and diagnosis and the gas lift fault-tolerant control.

3 NONLINEAR MODEL PREDICTIVE CONTROL (NMPC)

3.1 Background

In this chapter, the NMPC used in this thesis is presented. Two simulation cases were considered here: (1) case where there are setpoint for the states (which can be considered as outputs) and (2) case in which there is no output setpoint but control zones. These two cases were used for optimizing Continuous stirred tank reactor (CSTR), a simple ordinary differential equation (ODE) system. For setpoint tracking, the controller ensured that the setpoints were met even after a change in setpoint. For the case where there is no setpoint for states, the controller enforced the states to be in the zones then computed input to meet a given target. For setpoint tracking, the controller used multiple shooting method for model evaluation while IPOPT solver was used for solution of the optimisation/control problem. The controller used Euler approximation for prediction model evaluation while fmincon solver was used for the solution of the optimisation problem in the case of zone control

The purpose of this chapter is to understand the controller to be used for casing-heading instability removal and fault-tolerant control with combined effect of optimising the gas-lifted system. To do this, we started with a simple ODE system which is the CSTR before extending it to the more complex gas-lifted system that is a differential algebraic (DAE) system in the following chapters. Simulation results showed that the controller can ensure that the states are kept within their zones while the input tracked the target. Also the setpoints are met for setpoint tracking.

3.2 Continuous Stirred Tank Reactor and Multiple Shooting

The controller was first applied to a simple ODE system. The CSTR is a common laboratory equipment for process experiments and it is described briefly. As the Euler method of evaluating an ODE or DAE is established, we explain below only the multiple shooting techniques briefly.

3.2.1 Continuous Stirred Tank Reactor(CSTR)

The CSTR is a commonly used reactor for chemical reaction experiments be it endothermic, exothermic or isothermal. It has different degree of sophistication depending on the type of reactions, the inputs, the states and the output desired. The dynamic behaviour of the CSTR depends on many factors such as residency time, bifurcation, limit cycle direction, stability among others (UPPAL; RAY; POORE, 1976).

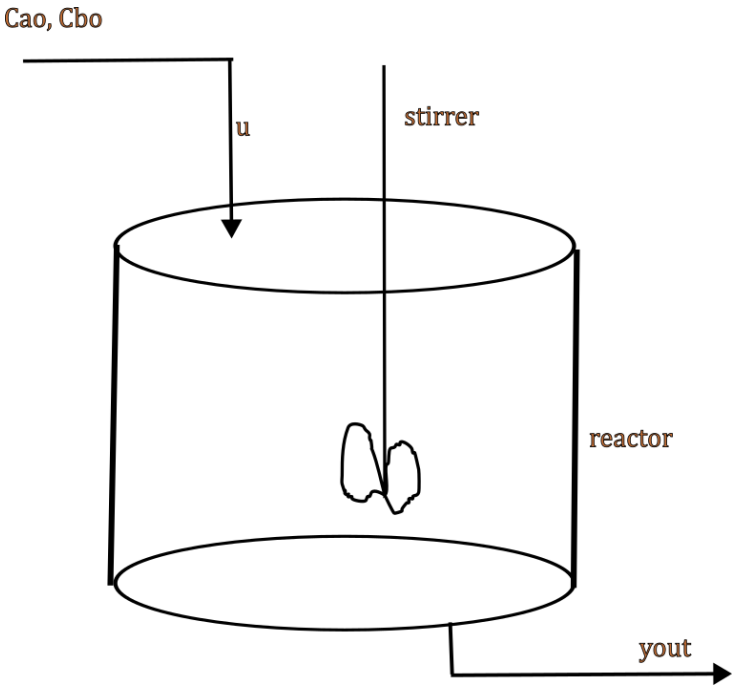

Figure 7: Schematic of a CSTR. The input is the inflow rate. The states are the concentrations of the reactants and the output is concentration of reactant B.

Figure 7 shows a schematic of CSTR. The objective in this study is to optimise the production of reactant B for a given isothermal reaction with two consecutive reactions given as A $\rightarrow$ B $\rightarrow$ C. Both reactions are first-order in the reactants. Concentration of C was not modelled here because the objective of this chapter is to properly examine the behaviour of A and B in general and optimise concentration of B in particular, to

see how the controller works before applying to a more complex gas-lifted system. This controller can also be used for the case where the concentration of C as well as the internal temperature of the CSTR is captured in the model and for higher order models of the CSTR.

The model for the simple CSTR is given in equations 3.1.

$$\frac{dx_1}{dt} = \frac{u(t)}{V}(C_{AO} - x_1(t)) - k_1 x_1(t) \tag{3.1a}$$

$$\frac{dx_2}{dt} = \frac{u(t)}{V}(C_{BO} - x_2(t)) + k_1 x_1(t) - k_2 x_2(t) \tag{3.1b}$$

Where x_1 and x_2 are molar concentration of A and B respectively, k_1 and k_2 are kinetic constants. V is the volume while u is the input and it is the inlet inflow. C_{A0} and C_{B0} are inlet concentrations of species A and B respectively.

3.2.2 Multiple Shooting

The solution of the differential equation which is one of the equality constraints in the OCP must be known either analytically or by numerical approach. With the difficulty in obtaining the solution analytically, numerical method like multiple shooting can be employed. Multiple shooting is used for solving boundary value problem. The key idea is to determine the set of initial states at each sample time that ensure the final state is the desired state. Euler method and other methods like Runge-Kutta for solving initial value problems are employed to obtain the systems states after the initial guess.

With this approach, the task of IPOPT is to find the optimal initial values of the states at each sample time that makes the terminal value equal the initial values of the next sample. This in addition to finding the optimal input that minimizes the cost function forms the function of IPOPT (MUNZIR; HALFIANI et al., 2012). Multiple shooting technique was used here instead of single shooting since we use a long prediction horizon where single shooting can become suboptimal.

In this chapter, multiple shooting method is used for solving the (ODE) for the IPOPT solver used for ensuring that the states track a given trajectory or input tracks when states are their zones. Thereafter, Euler method is used to integrate the ODE for fmincon solver.

3.3 NMPC Formulations

From Figure 5 the NMPC sits within the advanced supervisory control layer of the optimisation hierarchy. The supervisory layer steers the system to follow a given trajectory based on the setpoint provided by the upper layer. We present various formulations of the controller.

3.3.1 Infinite Horizon NMPC

Consider a nonlinear model of a system:

$$x_{k+1} = f(x_k, u_k) \tag{3.2a}$$

$$y_k = h(x_k) \tag{3.2b}$$

Where x and y are states and outputs respectively, while f and h are nonlinear functions of states and outputs respectively. The infinite horizon NMPC (IHNMPC) problem is given in (3.3), (3.4):

Problem P_1

$$\begin{aligned} \underset{U_k, x_{s,k}}{\text{minimize}} \quad & \\ & V_k = \sum_{j=0}^{\infty} ||(x(k+j|k) - x_{s,k})||^2_{Q_x} \\ & + ||(u(k+m-1|k) - u_{des})||^2_{Q_u} \\ & + \sum_{j=0}^{m-1} ||\Delta u(k+j|k)||^2_R \end{aligned} \tag{3.3}$$

Subject to

$$x_{min} \leq x_{s,k} \leq x_{max} \tag{3.4a}$$

$$u_{min} \leq u(k+j|k) \leq u_{max} \tag{3.4b}$$

$$\Delta u_{min} \leq \Delta u(k+j|k) \leq \Delta u_{max} \tag{3.4c}$$

$$x_{s,k} = f(x_{s,k}, u(k+m-1|k)) \tag{3.4d}$$

$$x_{k+1} = f(x_k, u_k) \tag{3.4e}$$

$$x(k) = x_k \tag{3.4f}$$

where the first, second and third terms in (3.3) are cost functions relating to state devi-

ation from artificial reference ($x_{s,k}$), deviation of last input in the control sequence from desired input (u_{des}) and input moves (Δu) respectively. Q_x, Q_u and R are penalties on states, input and input moves respectively. m is the control horizon. Equation (3.4a) provides the boundary condition for the artificial reference, (3.4b) is the boundary condition for the absolute input while (3.4c) is the constraint on input moves. At every sampling time (3.4d) computes the steady state using the last element in the control sequence. Constraint (3.4e) is the equality constraint that describes the state evolution of the nonlinear system while (3.4f) shows that the predicted states start from current measurement.

The optimal control sequence for an m length of control horizon is given by (3.5) while the control sequence for state prediction is given in (3.6).

$$U_k = \left[u(k|k)^T, u(k+1|k)^T, ..., u(k+m-2|k)^T, u(k+m-1|k)^T\right] \tag{3.5}$$

$$\begin{aligned} U_k = \Big[&u(k|k)^T, u(k+1|k)^T, ..., u(k+m-2|k)^T, \\ &u(k+m-1|k)^T, u(k+m-1|k)^T, ..., u(k+m-1|k)^T, ...\Big] \end{aligned} \tag{3.6}$$

Equation (3.6) implies that the input remains constant from the end of the control horizon m till the prediction horizon p which in this case is the infinite time. The cost function for this controller contains a term that penalises deviation of the input at the end of control horizon from the target input computed by the RTO (real time optimsation) layer. Hence after many sample times, when the desired input equals optimal input from the (real time optimsation), the second term in the cost function of (3.3) vanishes for an undisturbed, nominal system if the desired input is reachable.

The zones are usually selected based on system operating needs that put into consideration the constraints in the states. If the weights are properly selected to give priority to the first term in (3.3), the deviation from the steady state values dominates the cost function. This ensures that when the system states are in their zones, the control objective becomes forcing the input to track the input targets or getting close as much as possible.

3.3.1.1 Recursive Feasibility

Supposed there exists a solution to problem (3.3), (3.4) at k, the optimal input sequence obtained is as given in (3.5). At $k+1$, a feasible solution to the problem is given in (3.7) which is the previous solution, (3.5) shifted forward for one sampling time.

$$\begin{aligned} U_k = \Big[& u(k+1|k)^T, u(k+2|k)^T, ..., u(k+m-2|k)^T, \\ & u(k+m-1|k)^T, u(k+m-1|k)^T \Big] \end{aligned} \tag{3.7}$$

Consequently, (3.4b) and (3.4c) are met at $k+1$, since they are unchanged in (3.7). Then, constraint (3.4d) is met since $u(k+m-1|k)$ has not changed implying that (3.4a) is also met. Constraints (3.4e) and (3.4f) are met being state evaluation function and constraints that states must start from current measurement respectively, hence recursive feasibility is assured.

3.3.1.2 Convergence

Equation (3.8) is the cost function corresponding to input sequence (3.7) referring to shifted optimal input at $k+1$.

$$\begin{aligned} V_{k+1} = & \sum_{j=1}^{\infty} ||(x(k+j|k) - x_{s,k})||^2_{Q_x} \\ & + ||(u(k+m-1|k) - u_{des})||^2_{Q_u} \\ & + \sum_{j=1}^{m-1} ||\Delta u(k+j|k)||^2_R \end{aligned} \tag{3.8}$$

If V_k^{opt} is the optimal cost function corresponding to the input sequence (3.6), then (3.8) is equivalently:

$$\begin{aligned} V_{k+1} = & V_k^{opt} - (x(k|k) - x_{s,k})^T Q_x (x(k|k) - x_{s,k}) \\ & - \Delta u(k|k)^T R \Delta u(k|k) \end{aligned} \tag{3.9}$$

Then:

$$V_k^{opt} - V_{k+1} = (x(k|k) - x_{s,k})^T Q_x (x(k|k) - x_{s,k}) + \Delta u(k|k)^T R \Delta u(k|k) \tag{3.10}$$

The right hand side of (3.10) is positive or at least zero, being summation of quadratic terms weighted by positive-definite matrices Q_x and R. This is true only when the second term on the left hand side is smaller than the first term for a non-complex cost function (which is usually the case). The cost function is therefore decreasing or at worst non-increasing. It will decrease to zero if the input target is reachable. If the input target is unreachable it decreases to a value that is not zero but minimum showing the convergence of the controller.

The above formulation for problem (3.3) has the advantage that the controller can be optimal and guarantee of stability is assured due to the infinite horizon. However, applying numerical approach to its solution will be impossible due to difficulty in computing the infinite cost function.

3.3.2 Finite Horizon NMPC

To be able to apply numerical approach to the solution of this controller, we consider finite horizon NMPC given in problem P_2.

Problem P_2

$$\underset{U_k, x_{s,k}}{\text{minimize}}$$

$$\begin{aligned} V_k = & \sum_{j=0}^{P} ||(x(k+j|k) - x_{s,k})||_{Q_x}^2 \\ & + ||(u(k+m-1|k) - u_{des})||_{Q_u}^2 \\ & + \sum_{j=0}^{m-1} ||\Delta u(k+j|k)||_R^2 \end{aligned} \tag{3.11}$$

Subject to

$$x_{min} \leq x_{s,k} \leq x_{max} \tag{3.12a}$$

$$u_{min} \leq u(k+j|k) \leq u_{max} \tag{3.12b}$$

$$\Delta u_{min} \leq \Delta u(k+j|k) \leq \Delta u_{max} \tag{3.12c}$$

$$x_{s,k} = f(x_{s,k}, u(k+m-1|k)) \tag{3.12d}$$

$$x_{k+1} = f(x_k, u_k) \tag{3.12e}$$

$$x(k) = x_k \tag{3.12f}$$

3.3.2.1 Recursive Feasibility

The recursive feasibility follows the same argument as in problem P1 except that (3.7) now contains p elements where the last element is still u(k+m-1/k).

3.3.2.2 Convergence

Since the prediction horizon is not infinite, (3.10) is modified as follows:

$$\begin{aligned} V_k^{opt} - V_{k+1} = (x(k|k) - x_{s,k})^T Q_x (x(k|k) - x_{s,k}) \\ +\Delta u(k|k)^T R \Delta u(k|k) - (x(k+p+1|k) - x_{s,k})^T Q_x (x(k+p+1|k) - x_{s,k}) \end{aligned} \tag{3.13}$$

Equation (3.13) however is a sum and difference of quadratic terms hence for the controller to converge, the right hand term must be non-negative which implies:

$$\begin{aligned} &(x(k|k) - x_{s,k})^T Q_x (x(k|k) - x_{s,k}) + \Delta u(k|k)^T R \Delta u(k|k) \geq \\ &(x(k+p+1|k) - x_{s,k})^T Q_x (x(k+p+1|k) - x_{s,k}) \end{aligned} \tag{3.14}$$

Equation (3.14) gives the condition for the cost function to be non-increasing for the finite horizon control problem. The controller obtained from problem P_2 has a finite horizon hence can be practically implemented. This controller however might have a feasibility concern if (3.14) is not satisfied, hence the equation determines both feasibility and convergence. Also stability issue might arise from the finite horizon. To overcome the stability concern, terminal equality constraint is added to the controller.

3.3.3 Finite Horizon NMPC with Terminal Constraint

If terminal constraints is implemented, then the control problem (3.11), (3.12) becomes (3.15), (3.16).

Problem P_3

$$\underset{U_k, x_{s,k}}{\text{minimize}}$$

$$\begin{aligned} V_k = &\sum_{j=0}^{P-1} ||(x(k+j|k) - x_{s,k})||^2_{Q_x} \\ &+ ||(u(k+m-1|k) - u_{des})||^2_{Q_u} \\ &+ \sum_{j=0}^{m-1} ||\Delta u(k+j|k)||^2_R \end{aligned} \tag{3.15}$$

Subject to

$$x_{min} \leq x_{s,k} \leq x_{max} \tag{3.16a}$$

$$u_{min} \leq u(k+j|k) \leq u_{max} \tag{3.16b}$$

$$\Delta u_{min} \leq \Delta u(k+j|k) \leq \Delta u_{max} \tag{3.16c}$$

$$x_{s,k} = f(x_{s,k}, u(k+m-1|k)) \tag{3.16d}$$

$$x_{k+1|k} = f(x_k, u_k) \tag{3.16e}$$

$$x(k) = x_k \tag{3.16f}$$

$$x(k+p|k) - x_{s,k} = 0 \tag{3.16g}$$

Equation (3.16g) is the terminal constraint that forces the state deviation from desired steady state to be zero at p. The implication is that the first term in (3.15) is bounded. The implementation is also realisable because the first term in (3.15) is finite. The downside of this is the fear of instability resulting from the controller not being able to enforce constraint (3.16g). This can be minimised by making p very large.

3.3.3.1 Recursive Feasibility

This follows the same steps as in P_1.

3.3.3.2 Convergence

The end constraints enforces the stability of the controller.

In order to overcome this problem discussed in P3, slack variables are introduced to provide some degree of freedom for the states constraints to be extended temporarily. This controller results in problem P_4.

3.3.4 Finite Horizon NMPC with Terminal Equality Constraint and Guaranteed Feasibility

There could be an infeasibility and stability problem with the controller presented in section 3.2.3 if the controller parameters (in particular, the prediction horizon, p) are not properly selected. We present here in problem P_4, a controller that is stable irrespective of the selected controller parameters referred to as NMPC with guaranteed feasibility.

Problem P_4

$$\underset{U_k, x_{s,k}, \delta_k}{\text{minimize}}$$

$$\begin{aligned} V_k = & \sum_{j=0}^{P-1} ||(x(k+j|k) - x_{s,k}) - \delta_k||_{Q_x}^2 \\ & + ||(u(k+m-1|k) - u_{des})||_{Q_u}^2 \\ & + \sum_{j=0}^{m-1} ||\Delta u(k+j|k)||_R^2 + \delta_k||_S^2 \end{aligned} \tag{3.17}$$

Subject to

$$x_{min} \leq x_{s,k} \leq x_{max} \tag{3.18a}$$

$$u_{min} \leq u(k+j|k) \leq u_{max} \tag{3.18b}$$

$$\Delta u_{min} \leq \Delta u(k+j|k) \leq \Delta u_{max} \tag{3.18c}$$

$$x_{s,k} = f(x_{s,k}, u(k+m-1|k)) \tag{3.18d}$$

$$x_{k+1|k} = f(x_k, u_k) \tag{3.18e}$$

$$x(k) = x_k \tag{3.18f}$$

$$x(k+p|k) - x_{s,k} - \delta_k = 0 \tag{3.18g}$$

The controller provided in problem P_4 is feasible. This feasibility is due to the presence of slack (δ) which permits the states to temporarily violate the terminal constraints. The last term in (3.17) shows slack penalized in the cost function. This also changes (3.16g) to (3.18g) which contains the slack. The penalization of the slack implies that the slacks are optimised too.

3.3.4.1 Recursive Feasibility

This follows the same steps as in P_1.

3.3.4.2 Convergence

The end constraints enforces the stability of the controller while the slack permits the constraints to be artificially violated.

Problems P_4 is solved using the two approaches mentioned earlier. For both cases, multiple shooting approach is used with IPOPT solver while Euler approach is used with fmincon optimiser. The multiple shooting approach for converting the OCP to an NLP for obtaining the solutions numerically obtains the discrete nonlinear predictive model over a sampling period where the initial value of states are now part of the decision variables hence constraint (3.18e) can be written as:

$$x_{k+1|k} - f(x_k, u_k) = 0 \tag{3.19}$$

Note that when the objective is to enforce tracking, for the states, the artificial reference state becomes constant.

$$x_{s,k} = x_s \tag{3.20}$$

Where x_s is the desired state trajectory. This implies that the desired steady state is not computed at each sampling time but is known in this particular case. Also because of the difficulty in enforcing setpoint tracking and input target simultaneously, the second term in the cost function which is the term that implements input target is ignored or weakened by putting zero or very low weight. This will permit the controller to focus on enforcing only tracking.

For the zone control, the nonlinear constraint is integrated using Euler approximation. At each sample time, the artificial reference state is calculated. Then problems P_4 is solved to obtain the optimal control input over the given horizon. The first term of the computed control sequence is then applied to the system. The remaining input sequence with the last term repeated is used to form the initial guess for the next sampling time. This is repeated at each sampling time.

3.4 Simulation Results

In this section, simulation results are shown for the controller. This was tested on a simple ordinary differential equation (ODE) system, CSTR before selecting which for-

mulation to extend to a more complex differential algebraic equation (DAE) gas-lifted system. Table 1 shows the values of the parameters of the CSTR used in this simulation. The prediction model and the system model use the same paramters hence are the same.

Table 1: CSTR parameters, values and units

Parameters	Values	Unit
C_{A0}	0.900	$\frac{mol}{m^3}$
C_{B0}	0.100	$\frac{mol}{m^3}$
k_1	0.700	$\frac{mol}{m^3 min}$
k_2	0.035	$\frac{mol}{m^3 min}$
V	1.000	m^3

We started with the controller whose optimization uses multiple shooting techniques. The objective here is for the controller to ensure the states follow a given trajectory. We then simulated a case where we used Euler method to integrate the ODE and fmincon solver to ensure only zone control and input target.

3.4.1 Tracking Using Multiple Shooting without Disturbance

The model of the CSTR is given in (3.1). Table 2 shows the states and input bounds.

Table 2: Control parameters, initial states, state bounds and input bounds

States and inputs	Values	Unit
Q_x	diag(1 1)	–
Q_u	diag(0.0001)	–
R	diag(0.1)	–
x_{10}	0.509	$\frac{mol}{m^3}$
x_{20}	0.471	$\frac{mol}{m^3}$
x_{1max}	0.700	$\frac{mol}{m^3}$
x_{1min}	0.350	$\frac{mol}{m^3}$
x_{2max}	0.750	$\frac{mol}{m^3}$
x_{2min}	0.150	$\frac{mol}{m^3}$
u_{max}	2.00	$\frac{mol}{m^3}$
u_{min}	0.00	$\frac{mol}{m^3}$

Table 3: Steady states and desired input

parameters	initial Values	final Values	Unit
x_{1s}	0.4	0.55	$\frac{mol}{m^3}$
x_{2s}	0.5	0.4	$\frac{mol}{m^3}$
u_{des}	0.65	0.85	$\frac{mol}{m^3}$

The sampling time is T=0.2 min and the simulation interval is 200 samples (40 minutes). The system starts from initial states of x_{10}=0.509 and x_{20}=0.471. The initial input target is u_{des}=0.65 and changes to u_{des}=0.85 at the 100th control interval. While the state are x_{1s}=0.4 and x_{2s}=0.5 then changes to x_{1s}=0.55 and x_{2s}=0.4 at the 100th control interval. This is shown in tables (2) and (3). To ensure tracking, Qu, the penalty on the desired input deviation from final input in the input sequence is weakened or made zero as shown above. Consequently, the control effort is on driving the states to the set points than enforcing input target.

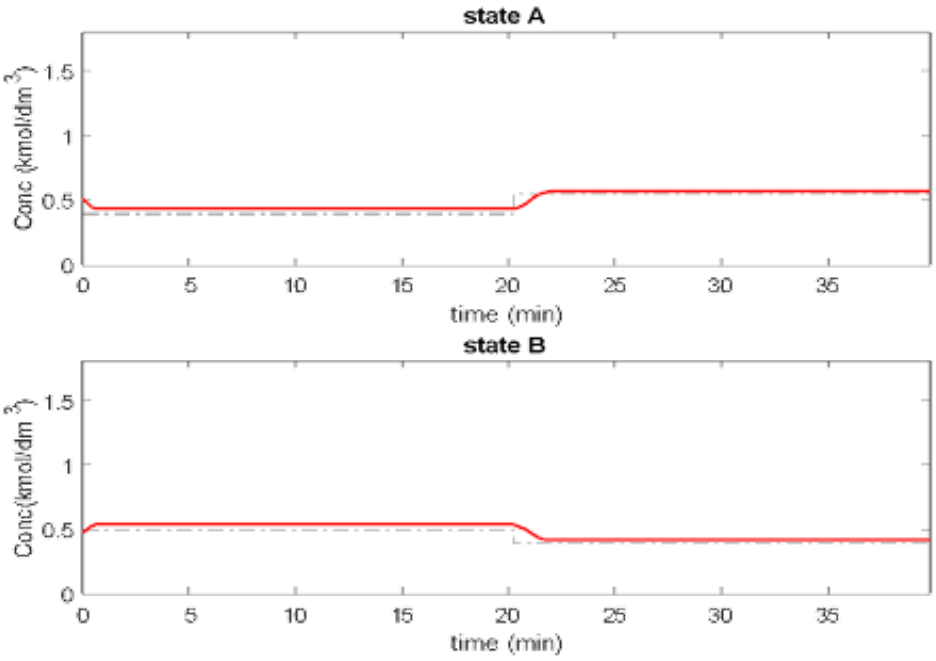

Figure 8: Optimal states by IPOPT: u_{des} within bound, both state costs penalised

Figure 8 shows the states while Figure 9 shows the input for the case where the states are reachable and Figure 10 shows the corresponding cost function. From Figure 8, the state trajectory (red solid) does not track the setpoint (dashdotted) accurately for both states. The input target (solid red) also is not tracked as seen in Figure 9. The state setpoint is more accurately tracked where the input target is less accurately tracked. This

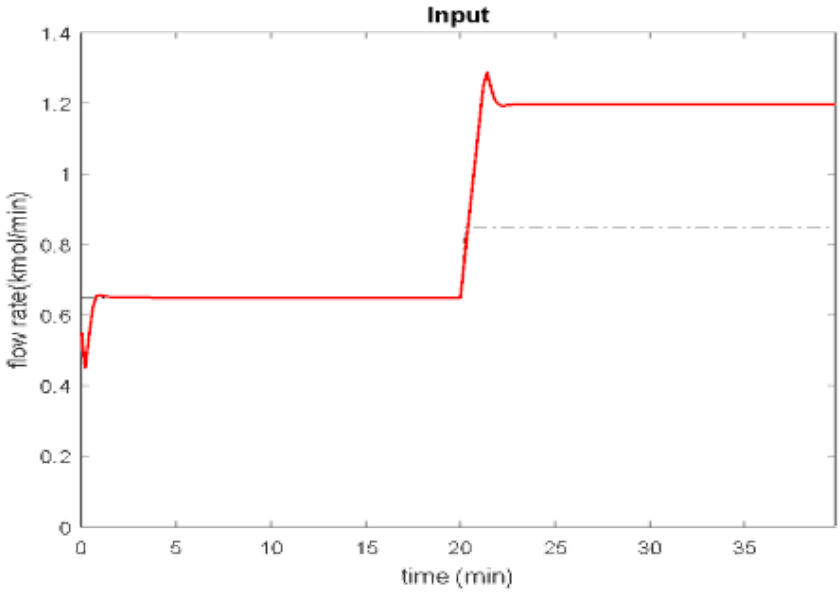

Figure 9: Optimal input by IPOPT: u_{des} within bound, both state costs penalised

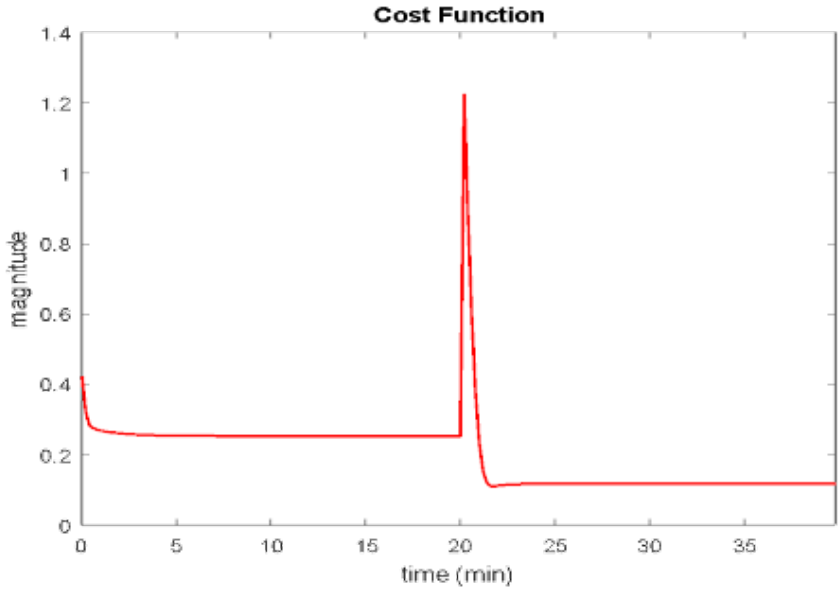

Figure 10: Cost with IPOPT: u_{des} within bound, both state costs penalised

is due to the fact that only one input is driving two states to their setpoints hence it is difficult to meet the state and the input target simultaneously. Consequently, input target is sacrificed for state setpoint tracking. Also note that the weakening of the weight on the input target cost term means more priority on state setpoint tracking than meeting input target. Consequently, the input is more deviated from the target than the state is from the state .

Figure 10 shows that the cost function decreases strictly but it is not zero due to setpoint not being met. The strict decrease of cost function is interrupted only at the

point that the setpoint changed. The cost function decreases afterwards. The offset despite not being zero, is very small. Note that with proper selection of setpoints, Figure 10 can still give a zero cost function as long as the input target is reachable.

To ensure tracking for states, states penalties were chosen such that only one state was considered at a time and the other made zero. This was done by making the corresponding penalty for the state to be zero. Figure 11 shows when only state A was considered and state B penalty was made zero while Figure 12 shows the input. Figure 13 shows the corresponding cost function. This simulation follows table 4 that includes the control parameters.

Table 4: Control parameters, steady states and desired input

parameters	initial Values	final Values	Unit
Q_x	diag(1 0)	diag(1 0)	–
Q_u	diag(0.0001)	diag(0.0001)	–
R	diag(0.1)	diag(0.1)	–
x_{1s}	0.4	0.55	$\frac{mol}{m^3}$
x_{2s}	0.5	0.4	$\frac{mol}{m^3}$
u_{des}	0.65	0.85	$\frac{mol}{m^3}$

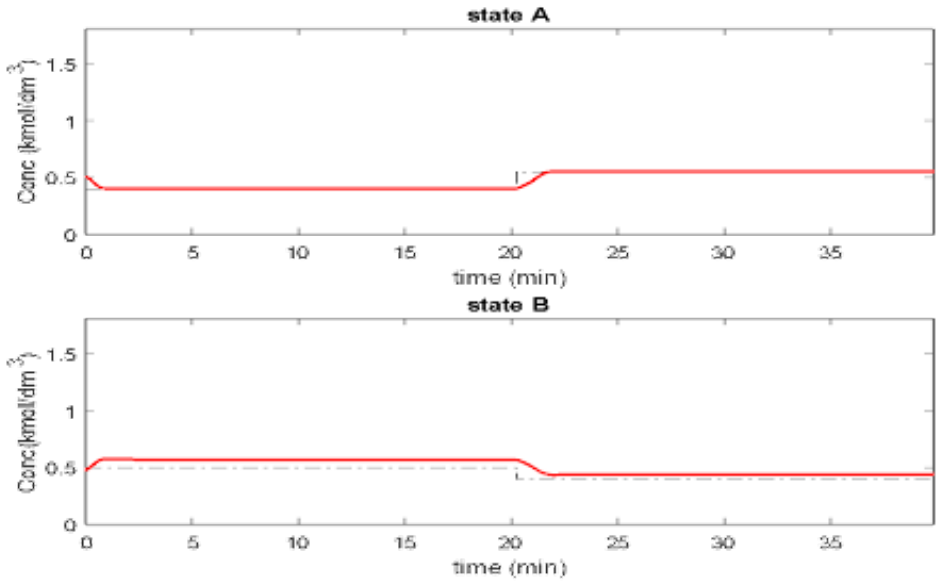

Figure 11: Optimal states by IPOPT: u_{des} within bound, state A costs penalised

With penalty for state B made zero, only the setpoint for state B is not met accurately as state A setpoint is met as Figure 11 shows. Similar result was obtained when the penalty

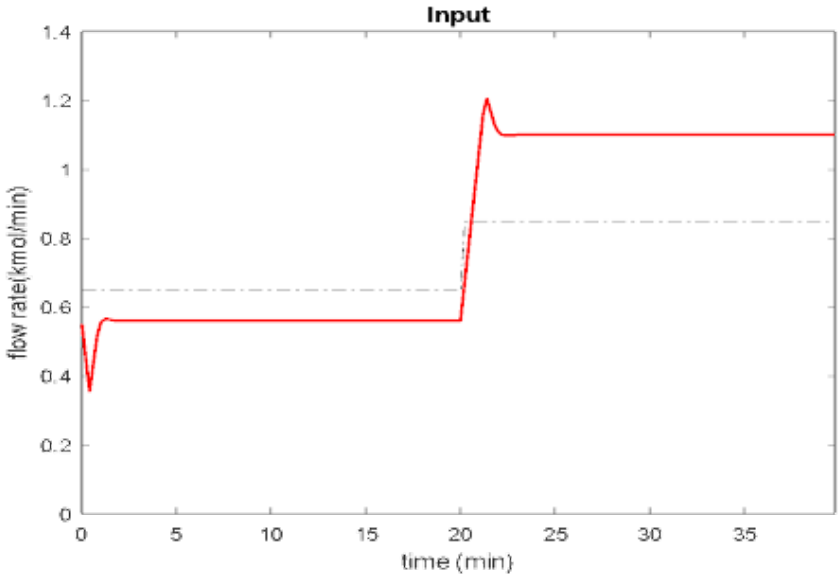

Figure 12: Optimal input by IPOPT: u_{des} within bound, state A costs penalised

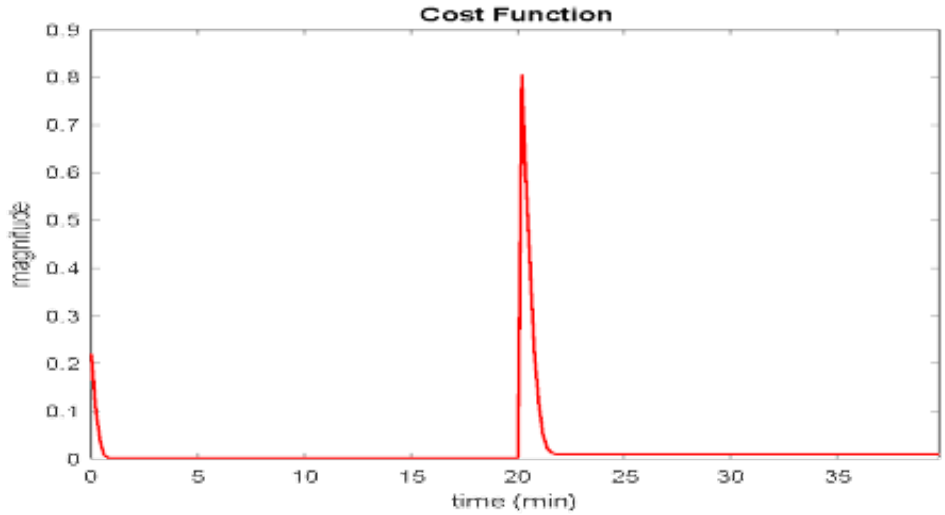

Figure 13: Cost with IPOPT: u_{des} within bound, state A costs penalised

for state A was made zero while state B was penalised. The input target in Figure 12 is again not met indicating that the input target is sacrificed to ensure that state A is met. The offset in the input target is bigger after the setpoint change than before the change. Consequently, the cost function in Figure 13 decreases to close zero before and after the change in setpoint and desired input but the offset is bigger after the change in setpoint. This offset is mainly contributed by the term in the cost function corresponding to the input deviation from input target.

Table 5: Out of bound steady states and desired input

parameters	initial Values	final Values	Unit
Q_x	diag(0 1)	diag(0 1)	–
Q_u	diag(0.0001)	diag(0.0001)	–
R	diag(0.1)	diag(0.1)	–
x_{1s}	0.4	0.75	$\frac{mol}{m^3}$
x_{2s}	0.5	0.14	$\frac{mol}{m^3}$
u_{des}	0.65	0.85	$\frac{mol}{m^3}$

We considered another case where the setpoint for the states after the 100th sample was out of state bound. The first 100 samples were still in the state bounds but the next 100 were changed to $x_{1s} = 0.75$ and $x_{2s} = 0.14$ which are outside state bounds. This simulation conditions are shown in table 5. Figure 14 shows the states for case where the setpoint for the states values are out of state bound after the 100th sample. The penalty for state A was made zero in this case. Similar result was got when penalty for B was made zero like the result shown in Figure 14.

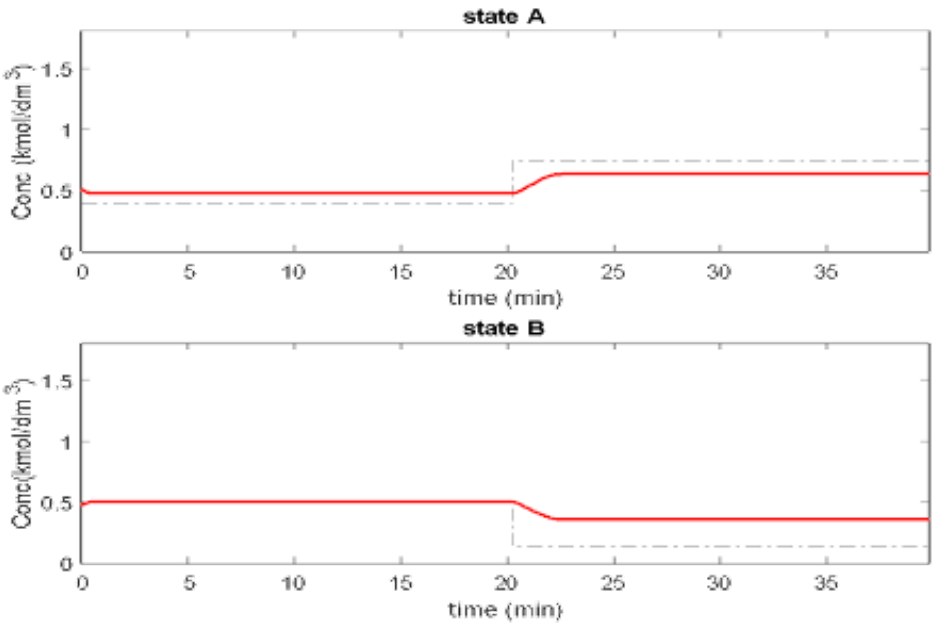

Figure 14: Optimal states by IPOPT: u_{des} within bound, state B costs penalised

State B in Figure 14 tracks accurately till the setpoint changes to out of state bound when it no longer tracks. State A does not track setpoint throughout as the penalty was made zero. This is due to available control action not being able to enforce tracking for state B despite the weight on state A being relaxed or made zero.

The preceding simulation results show that for setpoint tracking, it is required that the penalty on one of the states be made zero for the other state to track very well. This is because of the presence of only one input controlling the system to track the two states. In zone control, it is much easier for state zones to be respected for both states with one input as shown in the next section.

3.4.2 Zone Control Using Euler Method without Disturbance

We then considered a case where there were no setpoints for the states since our objective was to keep the states in their zones but the input must meet the targets if the states were in their zones. This time 'fmincon' was used for the optimization problem. No setpoint was used but an artificial reference was computed based on (3.4d). The simulation parameter follows table 2.

Figure 15 shows the states and Figure 16 shows the input for the case where the states were within state bound with input targets within the input bound while Figure 17 shows the corresponding cost function. The sample time is 1 minute and we simulated over 200 minutes. In Figure 15, the zones are represented by the green dashed lines while the states are represented by the blue solid lines. The figure shows that the controller can keep the states in their zones. Since there is no setpoint for the states, the input can then meet the input target while the states are driven inside their respective zones.

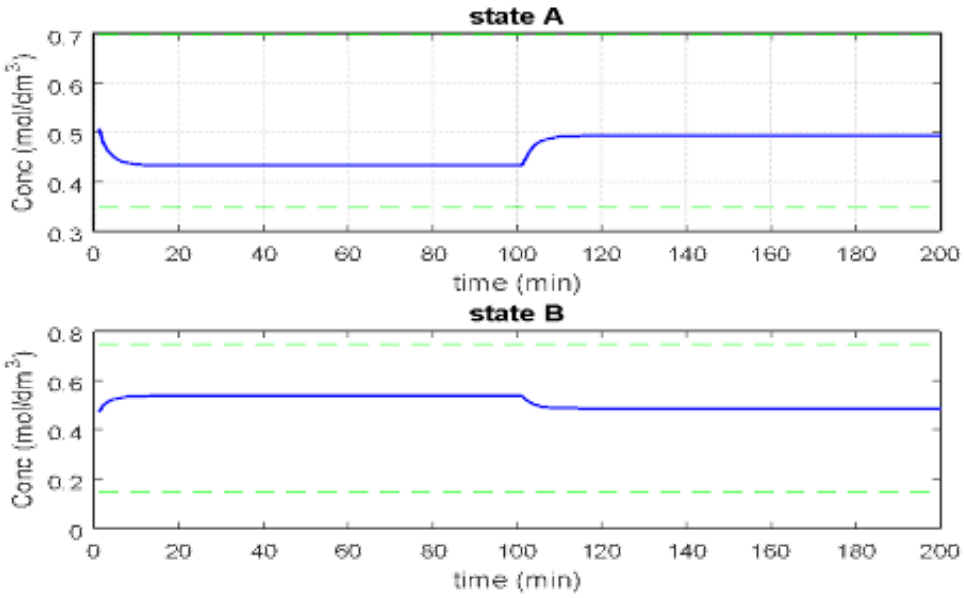

Figure 15: Optimal states by fmincon: u_{des} within bound

The input shown in Figure 16 (red solid line) meets the 0.65 (blue dotted line) value

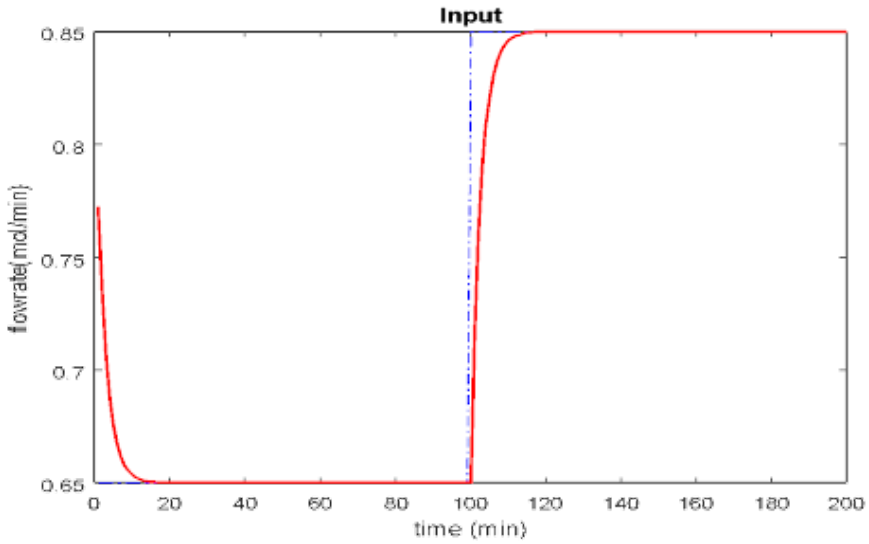

Figure 16: Optimal input by fmincon: u_{des} within bound

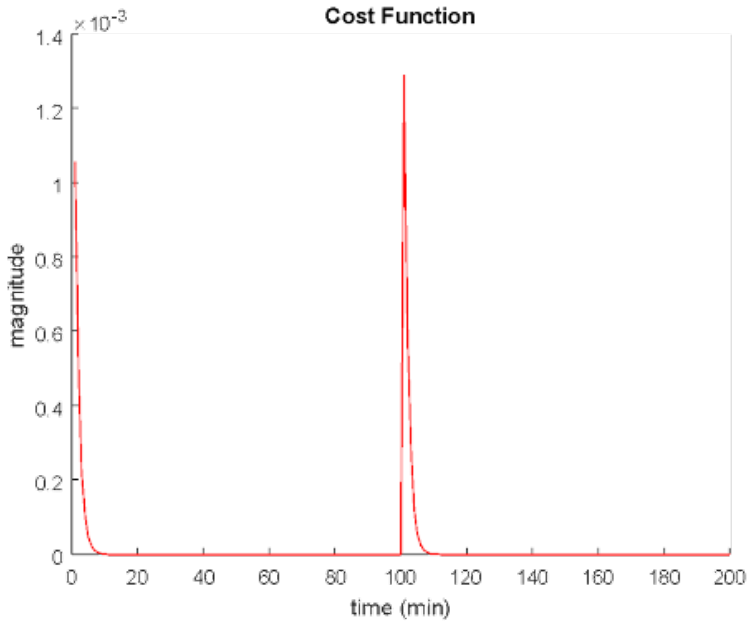

Figure 17: Cost function with fmincon: u_{des} within bound

before the 100th sample and meets the 0.85 thereafter. Figure 17 shows the cost function decreasing monotonically to zero before the change in input target comes in where the cost function rises slightly. The cost function returns to zero monotonically thereafter.

We considered another case here where the control input target was set outside the bound. We considered when the input target was 2.5. Recall that maximum input is 2.0. Figure 18 shows that the control zones (green dashed lines) can still be achieved with desired input out of bound. Notice that the input target (blue dotted line) is not met by the input (red solid line) since the input saturates as shown in Figure 19. This is

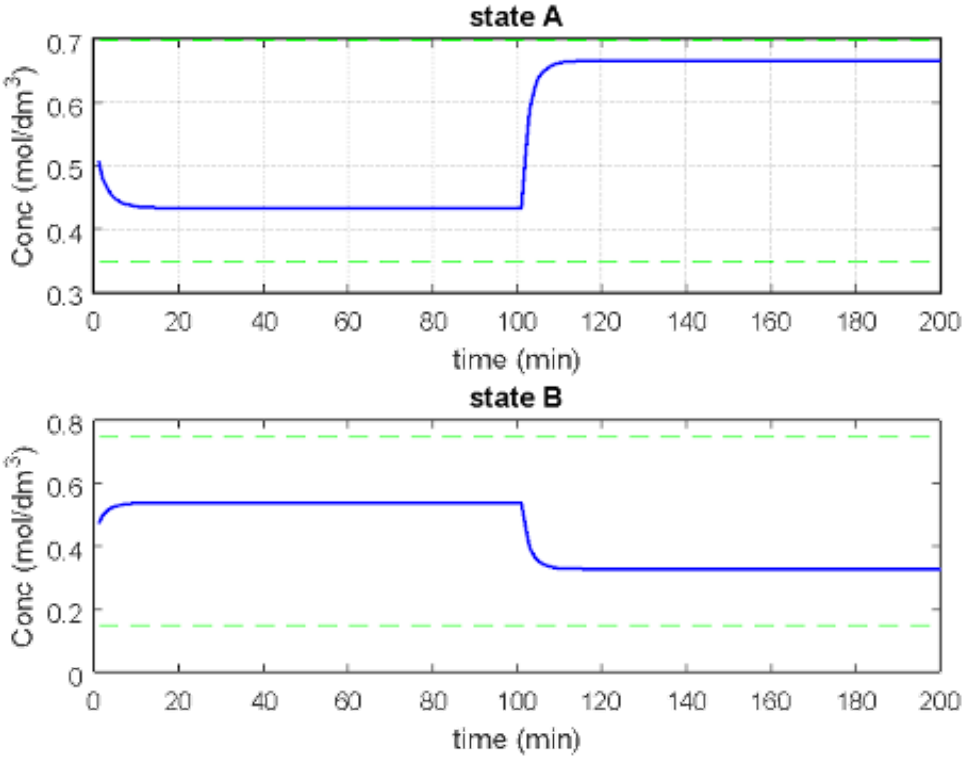

Figure 18: Optimal states by fmincon: u_{des}=2.5, out of bound

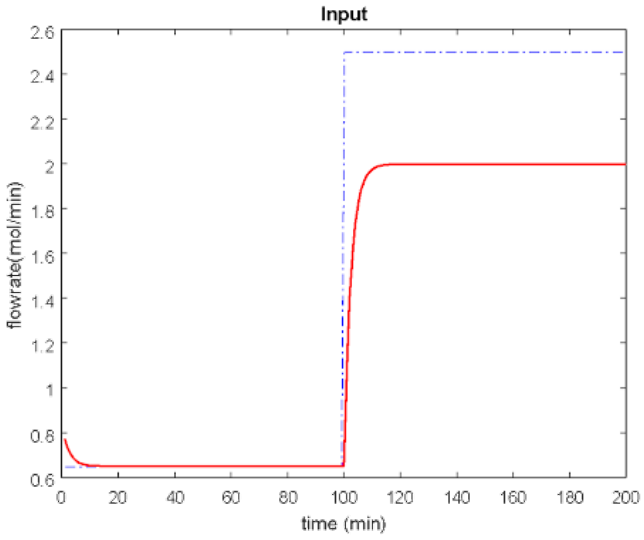

Figure 19: Optimal input by fmincon: u_{des}=2.5, out of bound

one advantage of the zone control strategy which gives freedom to the controller to first concentrate on ensuring states are in their zones before enforcing input target.

If the zones are made narrower, it becomes more difficult to ensure that states are in their zones or enforce input target for desired input out of bound. Figure 20 shows the cost function having a nonzero value when the desired input is out of bound. This means

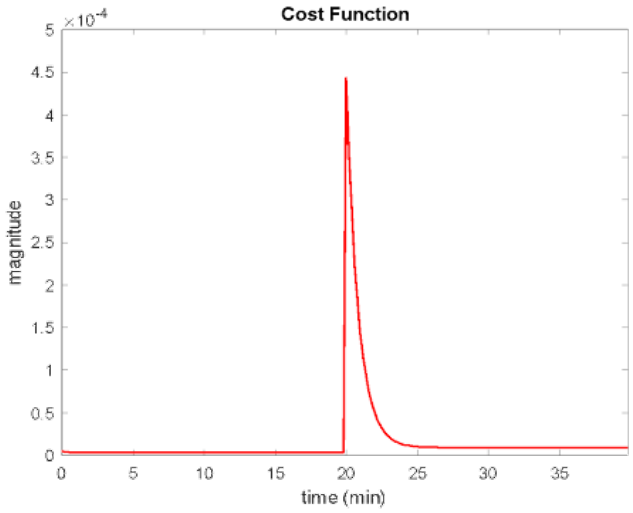

Figure 20: Cost function with fmincon: u_{des}=2.5, out of bound

that the cost function leaves an offset for an unreachable input target.

3.4.3 Zone Control with Disturbance

We then considered a case where the CSTR was subjected to disturbance for a period of 10 samples between 150th and 160th sample time. Figure 21 shows the state going out of the control zones when disturbance comes in. The controller is able to return the system inside the zone after the disturbance dies off. The input target is again meet in Figure 22. The controller tried to first bring the system states into the zone before enforcing the input target.

3.5 Concluding Remarks

Various formulations of nonlinear MPC were presented here. The recursive feasibility and convergence were discussed. The controllers were used here for zone control/input target and for tracking. The simulation results showed that the controller can enforce zone control when the desired input target did not violate control constraints. The controller can bring the system states to their zones when the control zone is violated due to disturbance. The controller also tracked but only when the penalty on the second state was weakened that the first state tracked accurately for a two state one input system.

This was done to test the performance of the developed controller on simple ODE system first before applying to complex/DAE systems. This is because as said in Allgower, Findeisen and Nagy (2004), a major case against the use of NMPC is that the solution

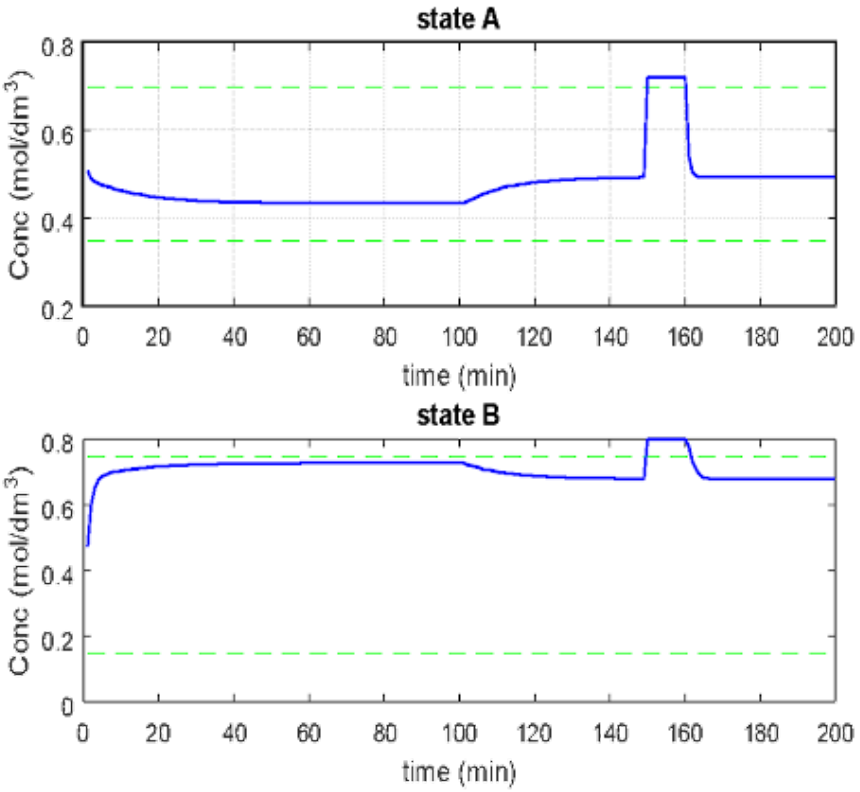

Figure 21: Disturbed optimal states by fmincon: u_{des} within bound

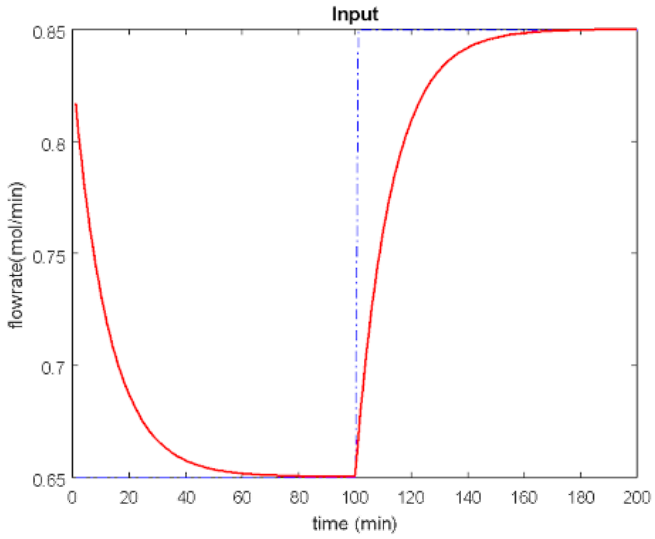

Figure 22: Disturbed optimal input by fmincon: u_{des} within bound

of the open-loop OCP can be difficult or impossible for large system and the gas-lifted system is a complex differential algebraic equation system.

4 GAS-LIFTED SYSTEMS MODELS AND ANALYSIS

4.1 Background

The controller presented in chapter three was used on a simple (ODE) system. It is intended to use the controller for stabilizing the gas-lifted system, a (DAE) system. The analysis of the system is important before the control application in Chapter (5).

In this chapter, we examine the gas-lifted system. We present and describe the simplified model for the system for ease of controller design. The pressure is the main source of driving force per unit cross sectional area for the system. This pressure is usually specified at fixed values in the system. Examining the pressure at different points is essential in the analyses of the gas-lifted system. We therefore derived the pressure profile in the annulus and in the tubing. This reveals pressure variation with height.

To gain insight into the nonlinear behavior, we first examined the system by linearizing it around selected operating points where the system behavior appears to be more complicated. Then local linear stability was examined from the eigenvalues of the linearized model and also the phase portrait around these equilibrium points. Thereafter limit cycle was considered for the system in the oscillatory region. Finally, the linear behaviour of the system at various operating points was compared with the nonlinear counterpart to justify the use of nonlinear model predictive control instead of the established linear MPC.

4.2 The Gas-Lifted System

The gas-lifted system shown in Figure (1) is one of the artificial lift methods employed when the natural energy for lifting hydrocarbons from the reservoir into the production platforms becomes insufficient. The states of the system are the mass of gas in the annulus, the mass of gas in tubing and the mass of oil in tubing indicated as x_1, x_2 and x_3

respectively. The key features of the system are the two volumes which are the annulus (that holds x_1) and tubing (that holds x_2 and x_3). The reservoir pressure (P_r) provides the natural pressure for lifting the crude up to the storage tank. Lift gas enters through the gas lift valve and out through the production choke while the injection valve connects the annulus and the tubing.

4.2.1 Gas-Lifted System Models

Gas-lifted system represented by partial differential equations such as in (ALIEV; DZHAMALBEKOV; IL'YASOV, 2011) describes the system closely but are more complex to handle. The more complex models are, the more difficult to use, hence trade-offs are usually made between model accuracy and ease of use for control application. In this research, we used a slight modification of the model presented in (JAHANSHAHI, 2013) which were verified in OLGA (Oil and Gas) software to be very close to the real system. This model is similar to that presented in (EIKREM; AAMO; FOSS, 2008). A highly nonlinear third order model is also presented in (SHI et al., 2019). Basically, the models used in gas-lifted system are not unique but depend on the underlying assumptions made. These models are presented below while the derivation and alternative models are given in appendix A.0.1:

The mass (differential equations):

$$\frac{dx_1}{dt} = w_{gl} - w_{iv} \tag{4.1}$$

$$\frac{dx_2}{dt} = w_{iv} + w_{rg} - w_{pg} \tag{4.2}$$

$$\frac{dx_3}{dt} = w_{ro} - w_{po} \tag{4.3}$$

The flow rate:

$$w_{iv} = C_{iv}\sqrt{max(0, \rho_a(P_a - P_w))} \tag{4.4}$$

$$w_{pc} = C_{pc}\sqrt{max(0, \rho_t(P_{wh} - P_s))}f(u) \tag{4.5}$$

$$w_{ro} = C_{iv}\sqrt{max(0, \rho_0(P_r - P_{bh}))} \tag{4.6}$$

$$w_{pg} = \left(\frac{x_2}{x_2 + x_3}\right) w_{pc} \tag{4.7}$$

$$w_{po} = \left(\frac{x_3}{x_2 + x_3}\right) w_{pc} \tag{4.8}$$

$$w_{rg} = GORw_{ro} \tag{4.9}$$

The pressure:

$$P_a = \left(\frac{T_a R}{V_a M_w} + \frac{g L_a}{V_a} \right) x_1 \tag{4.10}$$

$$P_{wh} = \frac{T_t R}{M_w} \left(\frac{x_2}{V_t - \frac{x_3}{\rho_0}} \right) x_2 \tag{4.11}$$

$$P_w = P_{wh} + \frac{(x_2 + x_3) g}{A_t} \tag{4.12}$$

$$P_{bh} = P_w + \rho_0 g H_{bh} \tag{4.13}$$

The density:

$$\rho_a = \frac{M_w}{T_a R} P_a \tag{4.14}$$

$$\rho_a = \frac{x_2 + x_3}{V_t} \tag{4.15}$$

$$f(u) = 50^{u-1} \tag{4.16}$$

The input is applied through the valve characteristic equation ($f(u)$) which are usually taken as u. Here we defined it in (4.16) according to (GARCIA, 2013). This input u itself is the valve opening in fraction or percentage.

Table 6 lists the symbols, definitions and units of the variables used in the models while Table 7 lists the constants, definitions, units and values used in this chapter. The max in the flow rate equations ensures that the upstream pressure is bigger than the downstream pressure else a flow rate of zero is produced to ensure a non-negative flow rate. V_a and V_t are annulus and tubing volumes respectively and are calculated from their respective areas and lengths.

4.2.2 Gas-Lifted System Input and Controlled Variables

The input here is the percentage valve opening that controls the flow rate of produced fluid through the production choke. In other cases, the flow rate of lift gas into the annulus is also considered as input but we fix it here with a regulatory controller. The controlled variable is usually the downhole pressure. However, for the zone control used here, the controlled variables are the gas-lifted states. The states as stated earlier are the masses presented in Equations (4.1)–(4.3).

Table 6: Lists of symbols, definitions and units of the variables used in the models.

Variable	Definition	Unit
w_{gl}	Gas flow rate into the annulus	kg/s
w_{iv}	Gas flow rate from annulus into tubing	kg/s
w_{rg}	Gas flow rate from reservoir into tubing	kg/s
w_{pg}	Gas flow rate through the choke	kg/s
w_{ro}	Oil flow rate from reservoir into tubing	kg/s
w_{po}	Oil flow rate through the choke	kg/s
w_{pc}	Mixture flow rate through the choke	kg/s
P_a	Annulus pressure	N/m^2
P_{wh}	Wellhead pressure	N/m^2
P_w	Tubing pressure	N/m^2
P_{bh}	Bottomhole pressure	N/m^2
ρ_a	Annulus gas density	kg/m^3
ρ_t	Tubing mixture density	kg/m^3

Table 7: List of the constants, definitions, units and values.

Parameter	Definition	Unit	Value
H_a	Height of annulus	m	1500
D_a	Diameter of annulus	m	0.189
H_t	Height of tubing	m	1500
D_t	Diameter of tubing	m	0.121
H_{bh}	Height of bottomhole	m	500
D_{bh}	Diameter of bottomhole	m	0.121
C_r	Reservoir valve coefficient	m^2	2.6×10^{-4}
C_{iv}	Injection valve coefficient	m^2	10^{-4}
C_{pc}	Choke valve coefficient	m^2	2×10^{-3}
ρ_0	Reservoir oil density	kg/m^3	1000
GOR	Gas/oil ratio	-	0.01
P_r	Reservoir pressure	N/m^2	15×10^6
P_s	Separator pressure	N/m^2	2×10^6
T_a	Annulus temperature	K	301
T_w	Tubing temperature	K	305
M_w	Molar mass of gas	kg	0.028
R	Gas constant	J/KM	8.314

4.3 Pressure Profile

The pressure controls the flow rate in the gas-lifted system and the practical system has many injection valves at set positions. Pressures are defined both at the annulus and well side of the injection valves at these locations hence the need to derive pressure variation with height. The pressure variation with height in the annulus (pressure profile) can be obtained as follows:

From the ideal gas law, the pressure at the annulus top is given as:

$$P = \frac{\rho RT}{M} \tag{4.17}$$

From the pressure formula $P = \rho gh$ the momentum balance is:

$$\frac{dP}{dh} = -\rho g \tag{4.18}$$

Substituting for ρ from (4.17) into into (4.18)

$$\frac{dP}{dh} = -\frac{gM}{RT}P \tag{4.19}$$

Separating the variables

$$\frac{dP}{P} = -\frac{gM}{RT}dh \tag{4.20}$$

Solving (4.20) from h_0 to h gives:

$$\ln P = -\frac{gM}{RT}h\Big|_{h_0}^{h} \tag{4.21}$$

And

$$P(h) = P(h_0)\exp^{-\frac{gM}{RT}(h-h_0)} \tag{4.22}$$

We solve for $P(h_0)$, the initial condition corresponding to pressure at the bottom of the annulus where h_o is the height at the bottom of the annulus assuming the mass of gas in the annulus is known. We note that total mass is the integral of the density over the entire volume.

$$m = \int_v \rho dv \tag{4.23}$$

Substituting for ρ from (4.17) and noting that $dv = Adh$, (4.23) becomes:

$$m = \int_{h_0}^{h} \frac{P(h)M}{RT}Adh = \frac{M}{RT}A\int_{h_0}^{h} P(h)dh \tag{4.24}$$

Solving (4.24) after substituting for P(h) from (4.22) gives:

$$m = \frac{A}{g} P(h_0) \left(1 - exp^{-\frac{gM}{RT}(h-h_0)} \right) \tag{4.25}$$

Hence the initial pressure is:

$$P(h_0) = \frac{mg}{A} \left(\frac{1}{1 - exp^{-\frac{gM}{RT}(h-h_0)}} \right) \tag{4.26}$$

Putting (4.26) into (4.22) the pressure profile becomes:

$$P(h) = \frac{mg}{A} \left(\frac{1}{exp^{\frac{gM}{RT}(h-h_0)} - 1} \right) \tag{4.27}$$

If we take h_0=0 and $h = L_a$, the pressure at the top of the annulus is obtained from (4.27) and the pressure at the bottom of the annulus is obtained from (4.26) as:

$$P_{at} = \frac{mg}{A} \left(\frac{1}{exp^{\frac{gM}{RT}L_a} - 1} \right) \tag{4.28}$$

$$P_a = \frac{mg}{A} \left(\frac{1}{1 - exp^{-\frac{gM}{RT}L_a}} \right) \tag{4.29}$$

Deriving the pressure profile in the tubing is slightly similar to annulus despite this is the case of two-phase fluid. The volume of the tubing now contains the two fluid hence (4.17) becomes:

$$P(1 - \frac{x_3}{v\rho_o}) = \frac{\rho RT}{M} \tag{4.30}$$

where ρ_o is the density of oil.

Following similar procedure as above, the pressure of gas at the top of the tubing (P_{at}) and injection valve location (P_{ab}) are obtained from (4.28) and (4.29) respectively.

$$P_{at} = \frac{mg}{A} \left(\frac{1}{exp^{\frac{gM}{RT}(1-\frac{x_3}{v\rho_o})L_a} - 1} \right) \tag{4.31}$$

$$P_{ab} = \frac{mg}{A} \left(\frac{1}{1 - exp^{-\frac{gM}{RT}(1-\frac{x_3}{v\rho_o})L_a}} \right) \tag{4.32}$$

Table 8: Comparing pressures from gas lift models and pressure profile.

Method	P_{at}**(bar)**	P_a**(bar)**	P_{wh}**(bar)**	P_w**(bar)**
Gas-lift models	76.5	89.4	32.1	85.8
Pressure profile	70.3	83.1	30.0	82.7
Percentage difference (%)	8.10	7.05	6.54	3.27

The equivalent of (4.11) and (4.12) obtained from the pressure profile are:

$$P_{wh} = \frac{mg}{A}\left(\frac{1}{exp^{\frac{gM}{RT}(1-\frac{x_3}{v\rho_o})L_a} - 1}\right) \tag{4.33}$$

$$P_w = \frac{(x_2 + x_3)g}{A_t} + \frac{mg}{A}\left(\frac{1}{1 - exp^{-\frac{gM}{RT}(1-\frac{x_3}{v\rho_o})L_a}}\right) \tag{4.34}$$

We compare in table (8), the pressures at the bottom and top of annulus and well using the pressure profile and the equations in section 4.2.1. These are obtained at steady state using table (7). From table (8), the percentage difference between using the verified models and extracting the pressures from the pressure profile is highest in P_{at} and smallest in P_w. Despite this relatively low differences, the models in section 4.2.1 are preferred to the results from the pressure profile for the following reasons:

(1) The pressure from the pressure profile is more nonlinear and difficult to handle than the pressure from the verified gas lift models. This will be obvious when attempt is made to linearise the model.

(2) The annulus pressure using the pressure profile is 83.1 bar while the well pressure is 82.7 bar. These values are very close compared to the corresponding 89.4 bar and 85.8 bar respectively for the verified gas lift model. Since pressure difference between these two pressures are required for gas flow from annulus to tubing, using the pressure from pressure profile could aid casing-heading instability even if the system is not within this region.

4.4 System Analysis

We start by examining the behavior of the gas-lifted system around an operating point. This is because linear analysis in most cases is enough to understand most system and adapt it for a given application. Understanding this linear behavior of the system will give insight into the behavior of the nonlinear gas-lifted system. The study of the

behavior of the system around the fixed points will help in the proceeding chapters.

4.4.1 Equilibrium Points of a Nonlinear System.

The equilibrium point of a nonlinear system is the point at which the system dynamics dies off. Consequently, the behavior of the system appears to better be studied around this point than any other point since it is more complicated around this region as the phase portrait will reveal. Obtaining the equilibrium (critical points) for the gas-lifted system in terms of fixed parameters, states and input is difficult analytically. We therefore present below the critical points as functions of states and the algebraic variables of the system. The critical points correspond to when:

$$\frac{dm_{ga}}{dt} = \frac{dm_{gt}}{dt} = \frac{dm_{ot}}{dt} = 0 \tag{4.35}$$

implying that:

$$w_{gl} = w_{rg} \tag{4.36a}$$

$$w_{iv} = w_{pg} - w_{rg} \tag{4.36b}$$

$$w_{ro} = w_{po} \tag{4.36c}$$

From (4.4) and (4.14) and taking note that the steady state for x_1 corresponds to when $w_{gl} = w_{iv}$ according to (4.36a), we have:

$$\rho_a = \left(\frac{w_{iv}}{C_{iv}\sqrt{max(0,(P_a - P_w))}} \right)^2 \tag{4.37}$$

$$P_a = \frac{RT_a}{M_w}\rho_a \tag{4.38}$$

Putting (4.37) into (4.38) we have:

$$P_a = \frac{RT_a}{M_w}\left(\frac{w_{iv}}{C_{iv}\sqrt{max(0,(P_a - P_w))}} \right)^2 \tag{4.39}$$

From (4.10) we obtain x_1=m_{ga} as:

$$x_1 = \left(\frac{RT_a}{V_a M_w} + \frac{gL_a}{V_a} \right)^{-1} P_a \tag{4.40}$$

The steady state for x_1 based on (4.39) and (4.40) is:

$$x_{1ss} = \left(\frac{RT_a}{V_a M_w} + \frac{gL_a}{V_a}\right)^{-1} \frac{RT_a}{M_w} \left(\frac{w_{iv}}{C_{iv}\sqrt{max(0,(P_a - P_w))}}\right)^2 \tag{4.41}$$

Which simplifies to:

$$x_{1ss} = \left(\frac{w_{iv}}{C_{iv}}\right)^2 \frac{RT_a V_a}{RT_a + M_w g L_a} \left(max(0,(P_a - P_w))\right)^{-1} \tag{4.42}$$

Similarly, the critical points x_{2ss} and x_{3ss} can be got as follows:

From (4.15), we obtain x_2 as:

$$x_2 = \rho_m V_t - x_3 \tag{4.43}$$

substituting for x_3 and simplifying:

$$x_{2ss} = \left(\frac{w_{gl} + w_{rg}}{w_{gl} + w_{rg} + w_{pc} + w_{pg}}\right) \rho_m V_t \tag{4.44}$$

From (4.7) and noting that at steady state $w_{gl} = w_{iv}$:

$$x_{3ss} = \left(\frac{w_{pc} - w_{pg}}{w_{wgl} - w_{rp}}\right) x_{2ss} \tag{4.45}$$

Equation (4.44) is then substituted in (4.45).

Similarly, obtaining the critical input in terms of parameters and states is practically impossible analytically hence we obtain that also in terms of parameters and algebraic variables. From (4.5) we note that input is introduced as a function of u. This function is defined according to the user. Consequently, we solve for $f(u)$ in generic term.

$$f(u_{ss}) = \frac{w_{pc}}{C_{pc}\sqrt{max(0, \rho_m(P_{wh} - P_s))}} \tag{4.46}$$

Equations (4.42), (4.44) and (4.45) give the critical points for the states while (4.46) gives the input. It is noticed that none of the 4 equations is expressed in terms of constant parameters and/or states/inputs. The closest to obtaining that is (4.42) where only the annulus pressure and the well pressure at the injection point are not constant. Consequently, to use the equations, the steady state values of these algebraic variables must be known. Note also that other methods abound depending on the choice of algebraic

variables in the final steady state equation. Also the equilibrium point can be found directly without using the (4.42), (4.44) and (4.45) as long as (4.36) is obeyed.

The natural equilibrium for the gas-lifted system corresponds to when the derivatives of the states have zero values and the derivative of the input is zero too for the case where the function in (4.16) is u. Consequently, the equilibrium points here are induced equilibrium points which are obtained for the purpose of the application. We choose these equilibria based on the desired values of the input and find the corresponding steady state values. It is these steady states values that we linearize our system for the subsequent analysis.

4.4.2 Linearisation Around the Equilibrium Point

The relationship between the three states of the gas-lifted system is nonlinear as the 3-D representation in figure 23 shows. Figure 23 also shows that there exists small correlation between the states with the only noticeable one being that at point C, the three states have their bigest values simultaneously. Point A also shows both x_1 and x_2 having high values but x_3 being small. At Point B only x_2 has large value while the rest have small values. The system can be linearized around any of the points from A to C when we consider states based on the application but in our case here, we use the input to determine the corresponding steady states and linearize the system.

Suppose the operating point obtained in subsection 4.4.1 is denoted as $x_0 = [x_{10}\ x_{20}\ x_{30}]$ we show a planer representation of Figure 23 in Figure 24. Linearization is done by obtaining the linear equivalent of the nonlinear system around this equilibrium point. This is done by taking the Taylor series expansion around the operating point while ignoring higher order terms. Since the value of the function is zero at the equilibrium point, the zeroth order is ignored too as its value is zero. Consequently, only the first order is selected.

We obtain the Jacobians evaluated at the equilibrium point to get Matrixes A, B, C and D such that the state space representation of the linearized system is represented by the deviation variable given as:

$$\dot{\Delta x} = A\Delta x + B\Delta u \tag{4.47a}$$

$$\Delta y = C\Delta x + D\Delta u \tag{4.47b}$$

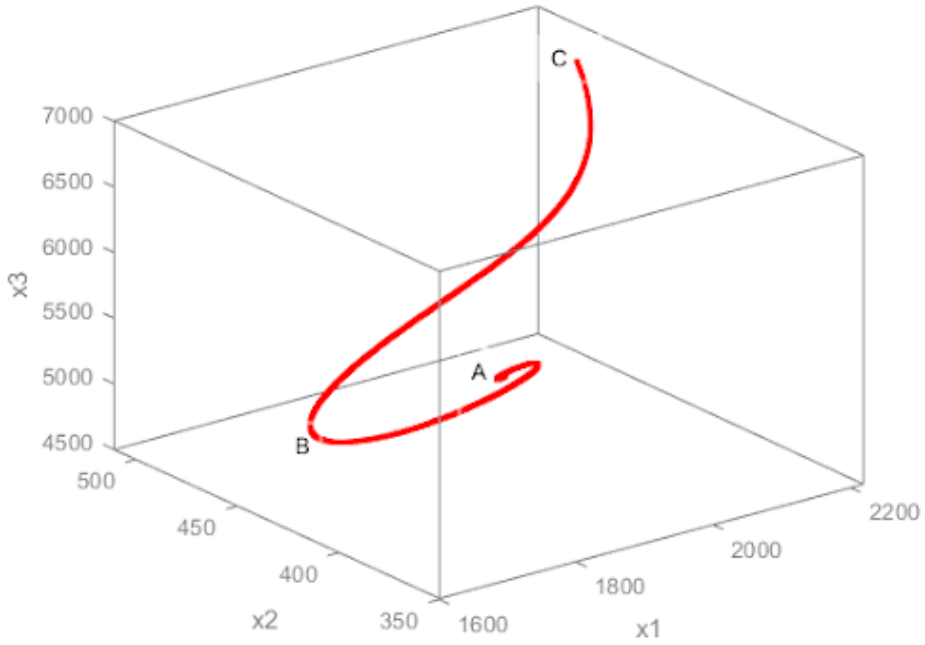

Figure 23: 3-D relationship between the three states of the gas-lifted system when the system is in steady state.

Where the new state variables based on the perturbation from the equilibrium point is Δx, the new input Δu and the new output Δy defined as:

$$\Delta x = x - x_0 \tag{4.48a}$$

$$\Delta y = y - y_0 \tag{4.48b}$$

$$\Delta u = u - u_0 \tag{4.48c}$$

Matrix A is the state Matrix, B is the input matrix, C is the output matrix and D is the feed forward matrix. These matrices are obtained as follows but first we redefine equations (4.1), (4.2) and (4.3).

$$f_1 = w_{gl} - w_{iv} \tag{4.49a}$$

$$f_2 = w_{iv} + w_{rg} + w_{pg} \tag{4.49b}$$

$$f_3 = w_{ro} + w_{po} \tag{4.49c}$$

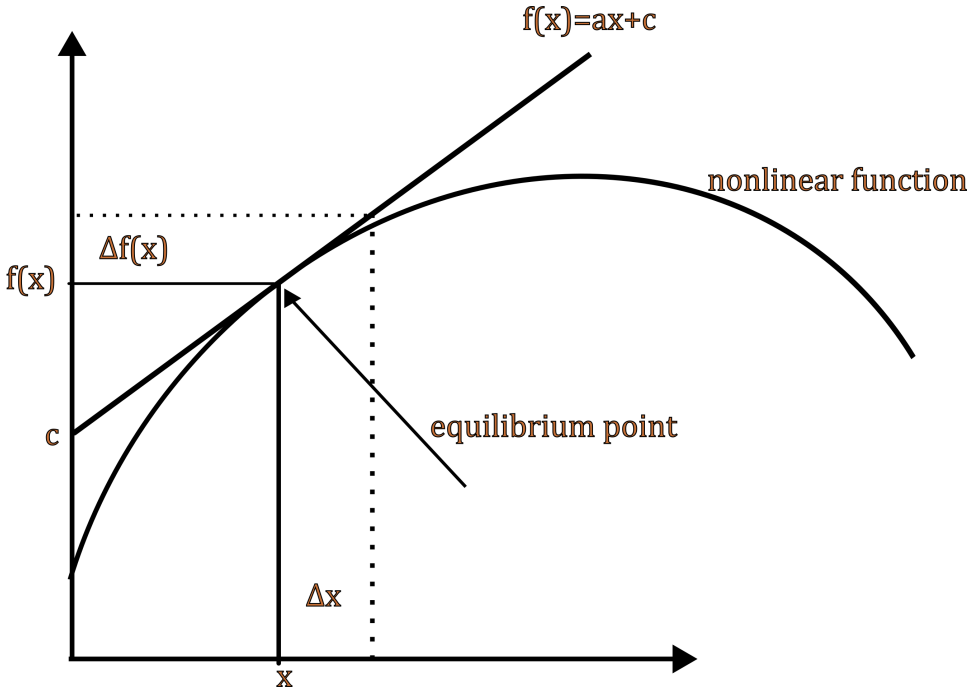

Figure 24: Linearisation around an equilibrium point

$$A = \begin{bmatrix} \frac{\partial f_1}{\partial x_1} & \frac{\partial f_1}{\partial x_2} & \frac{\partial f_1}{\partial x_3} \\ \frac{\partial f_2}{\partial x_1} & \frac{\partial f_2}{\partial x_2} & \frac{\partial f_2}{\partial x_3} \\ \frac{\partial f_3}{\partial x_1} & \frac{\partial f_3}{\partial x_2} & \frac{\partial f_3}{\partial x_3} \end{bmatrix} \qquad B = \begin{bmatrix} \frac{\partial f_1}{\partial u} \\ \frac{\partial f_2}{\partial u} \\ \frac{\partial f_3}{\partial u} \end{bmatrix} \tag{4.50a}$$

(4.50b)

$$C = \begin{bmatrix} \frac{\partial y}{\partial x_1} & \frac{\partial y}{\partial x_2} & \frac{\partial y}{\partial x_3} \end{bmatrix} \qquad D = \begin{bmatrix} \frac{\partial y}{\partial u} \end{bmatrix} \tag{4.50c}$$

Where y is given in (4.8) as the flow rate of the produced oil. Obtaining the elements of the above matrixes is not straightforward due to the gas-lifted system being a DAE system. The procedure for obtaining this is given in details in appendix (B), simplifying as far as necessary. Note that $m_{ga} = x_1$, $m_{gt} = x_2$, $m_{ot} = x_3$ in the algebraic variables and $A_a L_a$ and $A_w L_w$ are replaced by V_a and V_t respectively.

The gas-lifted system ass linearised around the operating point corresponding to the the input $u = 0.6$. The result from calculating the linear matrices was compared to that obtained from Simulink model using Linear Analysis tool in MATLAB. The resulting state space matrices are given in equations (4.51) and (4.52) for calculated and for Linear Analysis respectively.

$$A_{cal} = \begin{bmatrix} -0.0037 & 0.0073 & 0.0010 \\ 0.0037 & -0.011 & -0.0011 \\ 0 & -0.0567 & -0.0060 \end{bmatrix}, B_{cal} = \begin{bmatrix} 0 \\ -2.697 \\ -34.91 \end{bmatrix}$$

$$C_{cal} = \begin{bmatrix} 0 & 0.0230 & 0.0017 \end{bmatrix}, D_{cal} = \begin{bmatrix} 34.91 \end{bmatrix} \tag{4.51}$$

$$A_{sim} = \begin{bmatrix} -0.00369 & 0.0073 & 0.000985 \\ 0.00369 & -0.01098 & -0.001041 \\ 0 & -0.0575 & -0.005993 \end{bmatrix}, B_{sim} = \begin{bmatrix} 0 \\ -2.716 \\ -36.91 \end{bmatrix}$$

$$C_{sim} = \begin{bmatrix} 0 & 0.02264 & 0.00173 \end{bmatrix}, D_{sim} = \begin{bmatrix} 34.20 \end{bmatrix} \tag{4.52}$$

The corresponding elements in the matrixes in (4.51) and (4.52) are nearly equal except element b3 that differs by some margin. But since the sign is the same and the difference is about 5.7% while every other one has difference of less than 2% between the calculated and the result from the Linear Analysis tool, we assume the linearization was accurate enough. Figure 25 compares the unit step responses of calculated result with the Linear Analysis tool. The step response was applied to the deviation variables evaluated at $x_0 = [2155\ 444\ 5795]^T$ corresponding to $u = 0.6$.

The unit step response in Figure 25 shows the calculated states and the result from the Linear Analysis being almost identical. Even though the steady states converges to values far away from the equilibrium point, the result from both methods converge. But the state x_2 has negative values at some points despite the gas-lifted system is a positive system. This is the result of using unit step response at $u = 0.6$. Since the state space model is a deviation variable, the unit step input ($\Delta u = 1.0$) implies that the final input is $u = 1.6$. This is a big deviation from the equilibrium point making the approximation not accurate at steady state. Hence for the gas-lifted system, a unit step response takes the steady state far away from the equilibrium point which could result in states being negative.

We therefore simulated around the equilibrium point. We started from $x_0 = [2290\ 529\ 5480]^T$ corresponding to $u = 0.6$ and applied a deviation input $\Delta u = 0.1$. Figure 26 shows the step response. In this case, the calculated model and the model from Linear Analysis tool is seen to converge although on zooming the graph, there existed slight difference.

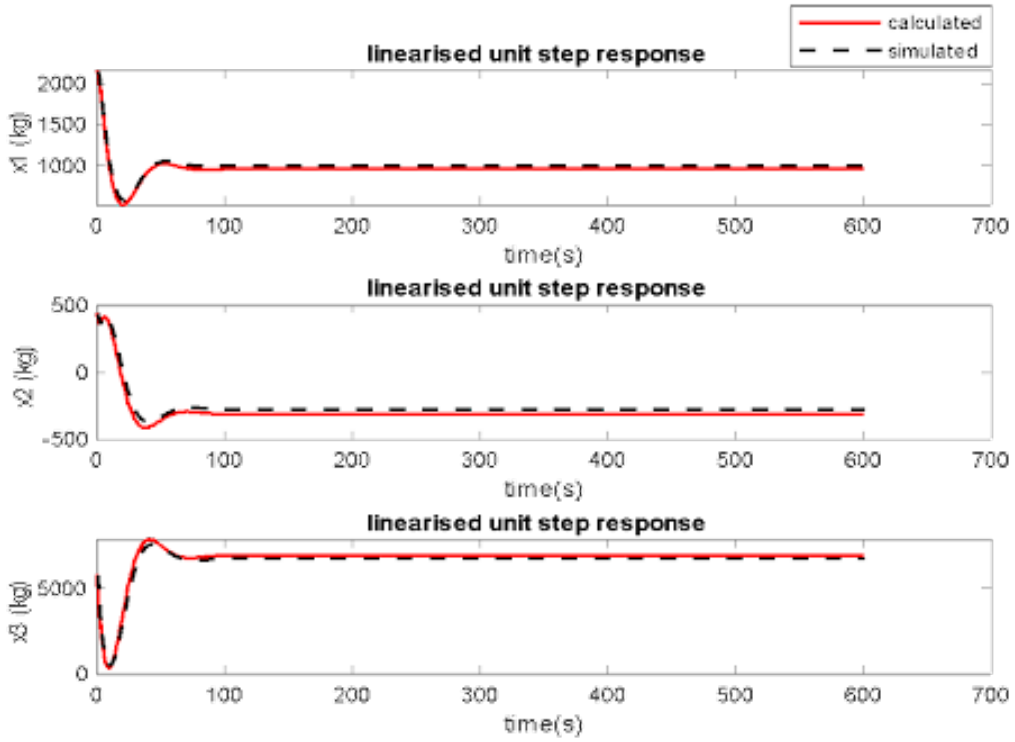

Figure 25: Unit step response for linearised system

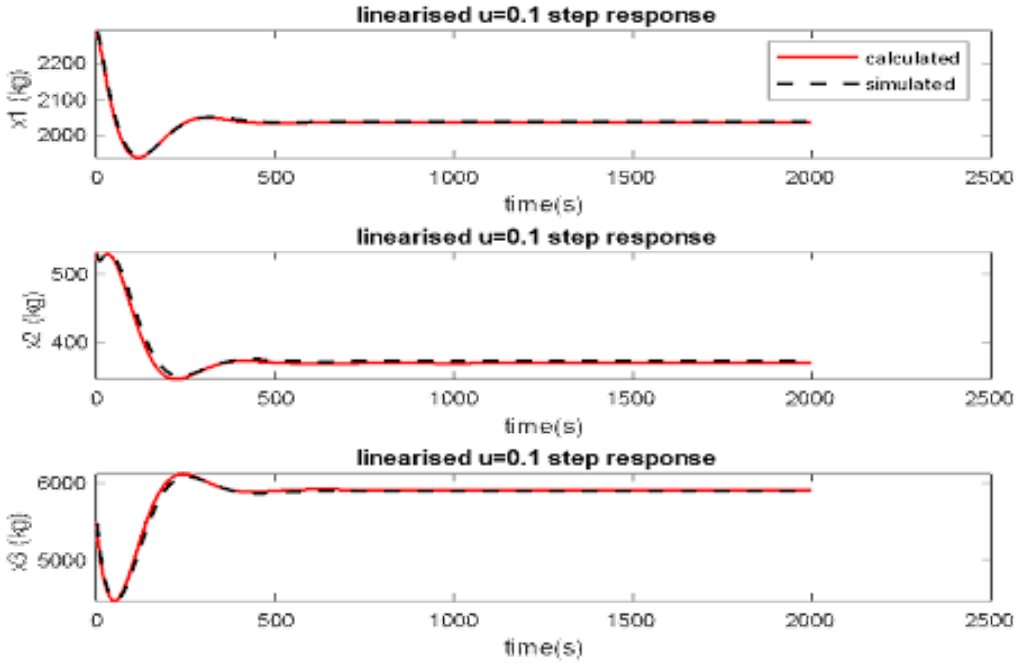

Figure 26: Step response of 0.1 for linearised system

This difference was more on state x_2 than the other states. With the deviation input very small, the system was evaluated in the region around the equilibrium point hence none of

the states was negative. The states also did not deviate much from the equilibrium point at steady state.

The Linear Analysis tool can therefore be used to obtain the linear model between any two points in the gas-lifted system from the nonlinear model built in Simulink. We then linearized the system around the equilibrium points corresponding to $u = 0$, $u = 0.6$ and $u = 0.95$. These correspond to the lowest value of the input, the value of input just before the system goes into oscillation and the value of u when the system is in the oscillatory state respectively.

We examined the behaviour of both linearised and nonlinear models at three operating points corresponding to $u = 0$ $u = 0.6$ and $u = 0.95$. In all three cases, we started from the same initial condition $x_0 = [2448\ 1360\ 1256]^T$ which corresponds to $u = 0$. This implies that deviation input according to (4.47) becomes $\Delta u = 0$, $\Delta u = 0.6$ and $\Delta u = 0.95$ respectively while the deviation initial states become $x_0 - x_0$, $x_{0.6} - x_0$ and $x_{0.95} - x_0$ respectively. Where x_i for $i = 0, 0.6$ and 0.95 are the equilibrium points for the various cases simulated. We compared the linearized with the corresponding nonlinear states. For the nonlinear states, the inputs are $u = 0$, $u = 0.6$ and $u = 0.95$ respectively. But like the linear, the initial condition is the same for the three cases.

Note from (4.8) that input $u = 0$ does not correspond to zero flow rate through the value as well as zero states and algebraic variables. This was because the input is applied through the valve characteristic function (4.16). We compared the Linear system (red solid) with the nonlinear one (black dashed) in Figures 27, 28 and 29 which are the equilibrium points corresponding to $u = 0$,$u = 0.60$ and $u = 0.95$

In Figure 27, the linear and nonlinear states converge to a very high degree. The difference of 4kg, 4kg and 30kg correspond to percentage difference of 0.16%, 0.29% and 2.38% respectively between the linearized and the nonlinear states. These are negligible except for x_3 hence it can be assumed that the linearized and the nonlinear states converged when the model was linearized at $u = 0$. Similarly, when linearized around $u = 0.6$, the linearized converged to nonlinear states except for state x_1 as shown in Figure 28.

When linearized around $u = 0.95$ which is the region of casing-heading instability, the linear states did not converge to the nonlinear states as Figure 29 shows. Despite being in instability region, the linearized states oscillatory behavior dampened out while the nonlinear states oscillations remained. This makes the states of the linearised and the nonlinear not to converge. It is this occurrence as well as the difference in behavior when the gas-lifted system is operated far away from the equilibrium points that makes the use

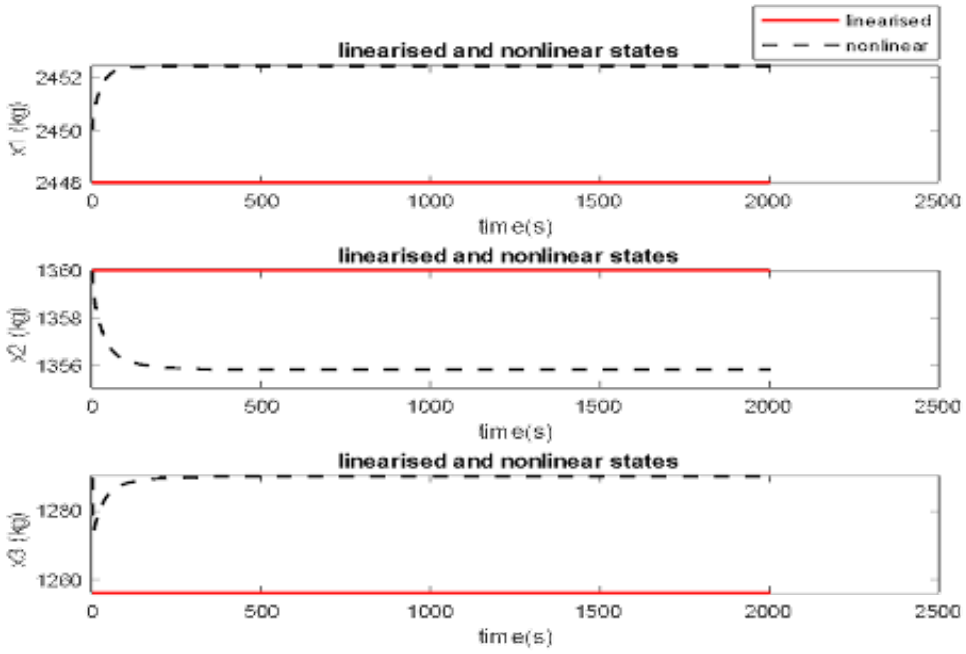

Figure 27: Nonlinear models and linearised models at u=0

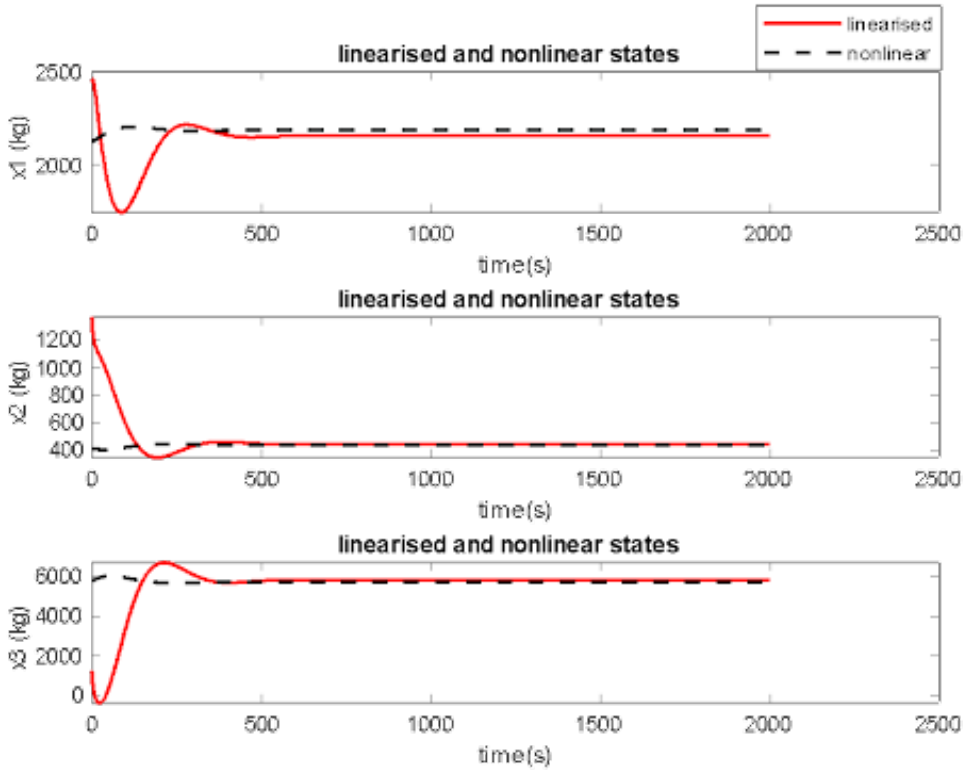

Figure 28: Nonlinear models and Linearized models at u=0.6

of nonlinear control approach a better option than the linear control for the system.

The steady states are mainly determined by the input values for the nonlinear model

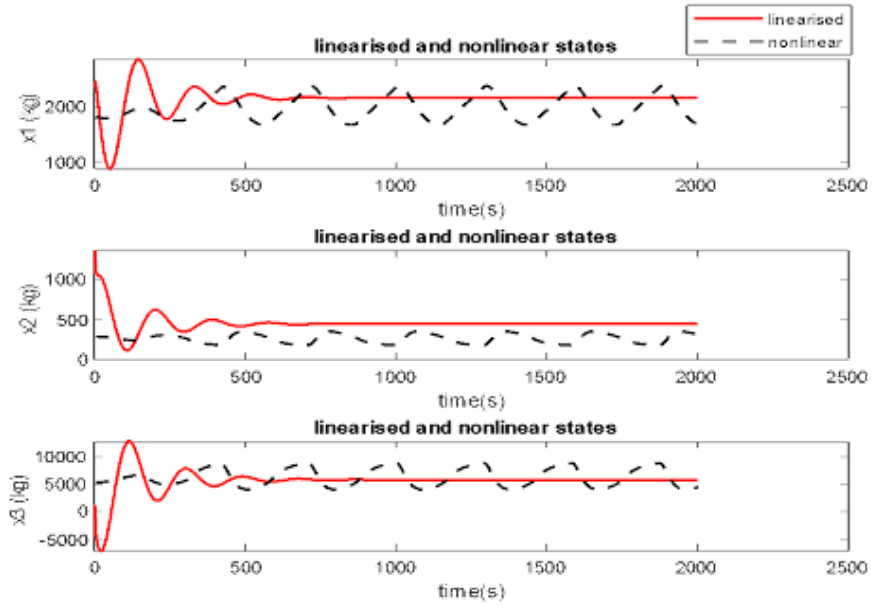

Figure 29: Nonlinear models and linearised models at u=0.95

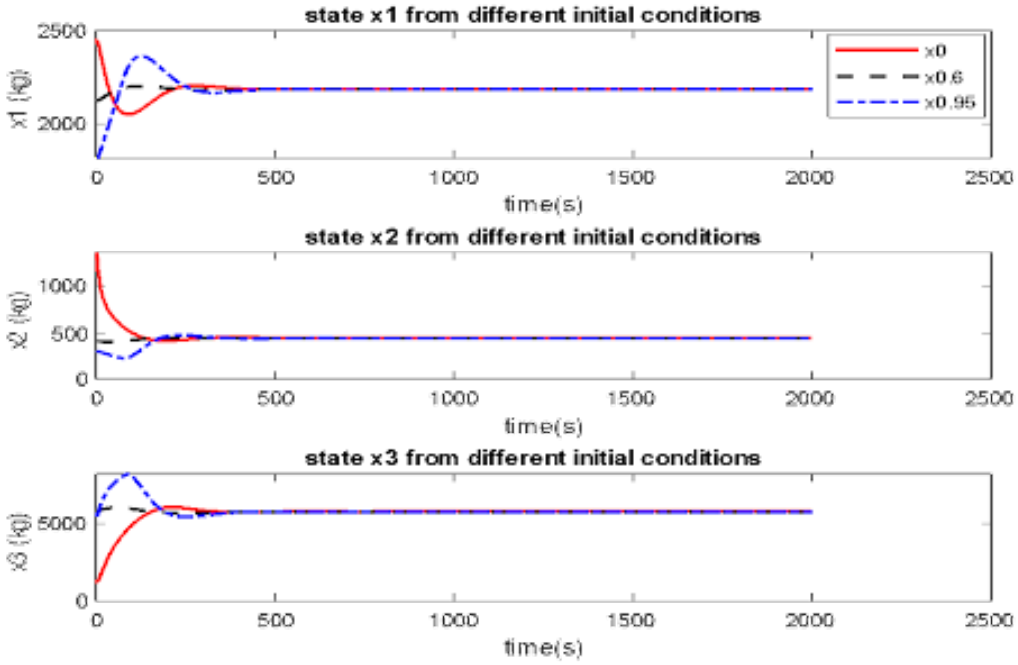

Figure 30: Nonlinear states for initial states corresponding to u=0, 0.6 and 0.95

for different initial conditions. This is not the case with the linearised models whose steady state differ from each other when they start from different initial conditions. Figure 30 shows the states for the nonlinear system under different initial conditions. The input for the nonlinear is 0.6 while the initial conditions correspond to the steady states for which $u = 0$, $u = 0.6$ and $u = 0.95$ respectively.

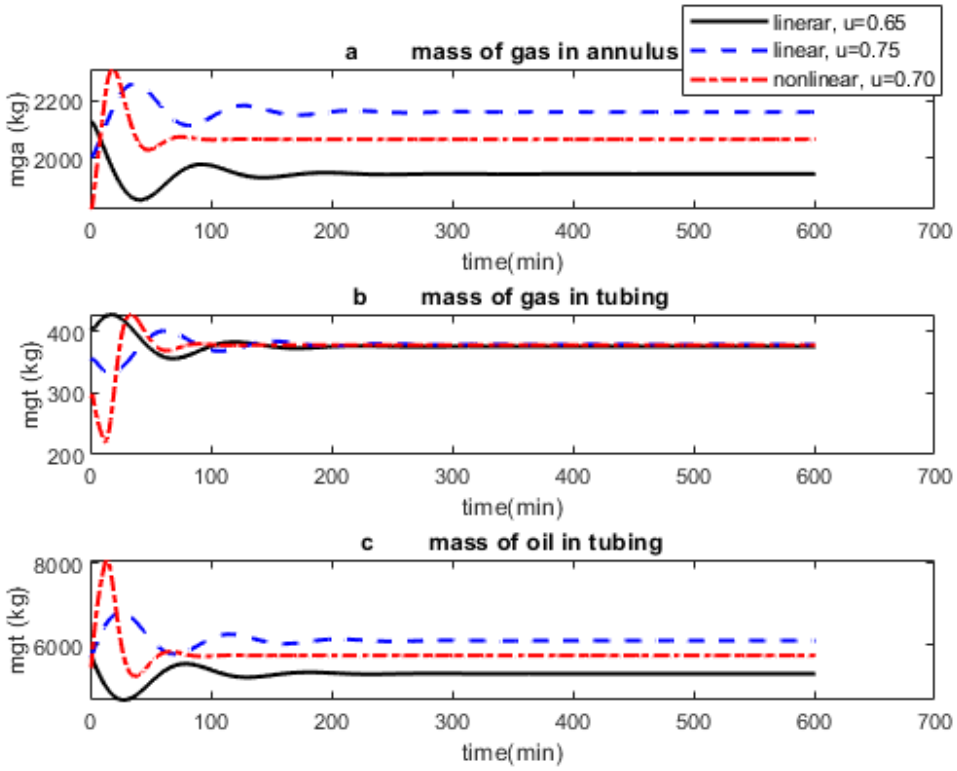

Figure 31: linear and nonlinear states of gas-lifted system for u=0.70. The linear states do not converge to the nonlinear state

It is seen that the three states converged to the steady states corresponding to the input which is $u = 0.6$ despite starting from different initial state values. The implication is that the gas-lifted system does not settle far away from the steady state corresponding to the input irrespective of the initial conditions for the nonlinear case.

The situation is different in Figure (31) that compares nonlinear response with two linear responses. The initial conditions for the linear states correspond to $u = 0.65$ and $u = 0.75$ respectively. A step input of $u = 0.05$ and $u = -0.05$ were applied to the linear models respectively while an input of $u = 0.70$ was applied to the nonlinear model. It is expected that the three states converge at steady state to the same value since all three states operate at $u = 0.70$. Only Figure (31b) however shows convergence in the states from different initial conditions. The state that starts from steady state corresponding to $u = 0.65$ converges to a value below the nonlinear state while the state that starts from $u = 0.75$ converges above the nonlinear states in both Figures (31a) and (31c). This only creates uncertainty further as all three states are supposed to converge as they are all operated at $u = 0.70$. This implies that operating the system using linear models will produce different trajectory at a neighbourhood of the equilibrium point that is a bit far. To get accurate state prediction hence optimisation result, nonlinear approach was to be

used.

4.4.3 Bifurcation

The dynamics of the gas-lifted system is highly dependent on parameters. One of these parameters is the gas/oil ratio (GOR) and the parameter within our control is the input which is the percentage valve opening when we consider one input or flow rate into the annulus as second input when it is two input. By parameterising the input, we can observe the behaviour of the gas-lifted system output as the input changes from u=0%(0.00) to u=100%(1.00). This reveals the critical point at which the system changes from stable to unstable oscillatory regime. This critical point is GOR dependent as shown in Figure 32 for GOR of 0.0001, 0.001, 0.01 and 0.1 respectively. The black dash lines are the minimum and maximum flow rates of produced oil while the red solid is the average flow rate.

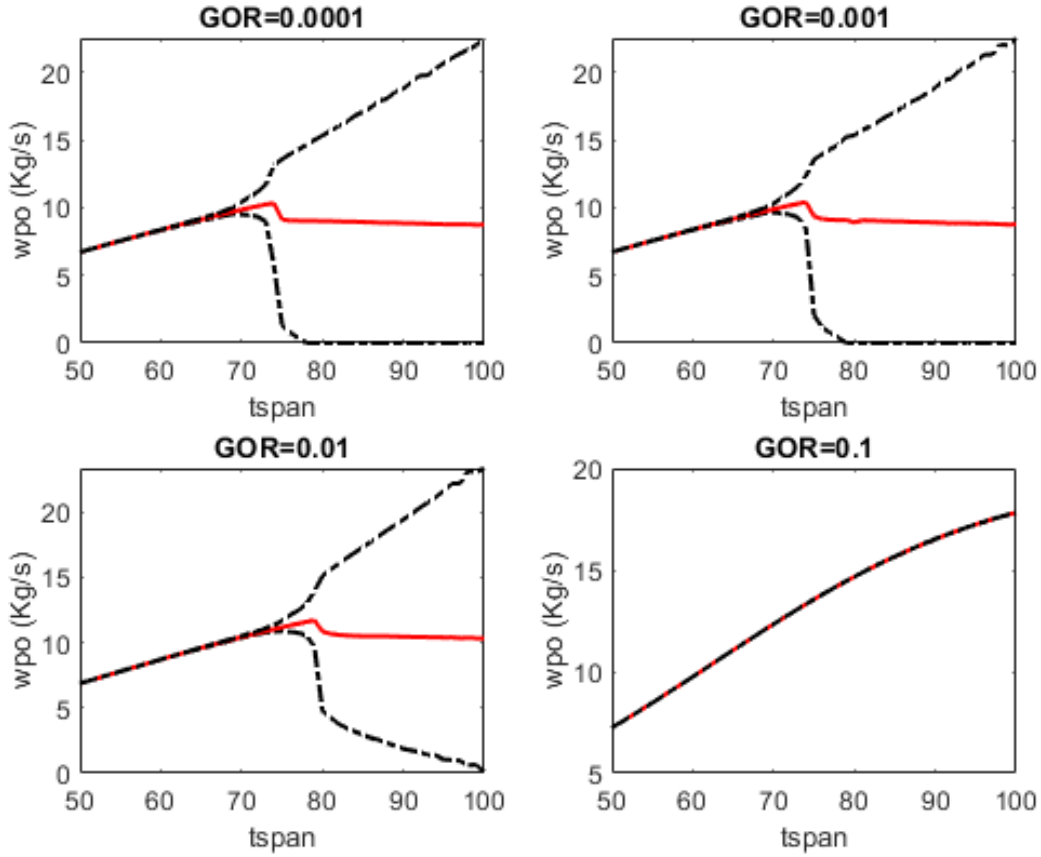

Figure 32: Bifurcation diagrams for GOR = 0.0001, 0.001, 0.01 and 0.1. Mean production (red solid) is reduced after the system goes into instability. A GOR of 0.1 shows no instability for any input value.

In all the four cases in Figure (32), during the stable region, both the minimum, mean

Table 9: Eigenvalues at equilibrium points for GOR = 0.01.

Equilibrium point	**Eigen value**	**casing-heading situation**
u=0.7	-0.0171, -0.0003±0.00014	none
u=0.8	-0.0201, -0.0001±0.00017	partial
u=0.9	-0.0261, 0.0001±0.0020	full

and maximum oil production are the same. This stable production starts from u=0 (0%) to about u=0.67 (67%) for both GOR of 0.0001 and 0.001 while it is u=0.75 (75%) for GOR of 0.01. Slight oscillation starts at u=0.67 (67%) and the bifurcation point is at u=0.73 (73%) for GOR of 0.0001 and GOR of 0.001. Slight oscillation starts at u=0.75 (75%) for GOR of 0.01 while its bifurcation point is at u=0.8 (80%). Thereafter, full oscillation sets in. In the case of GOR of 0.1, there is no oscillation for any input value. This is because high GOR implies more gas in the tubing and low chance of casing-heading instability. Also note that there exists slight difference in the critical points for the GOR of 0.0001 and 0.001 implying that a GOR of 0.001 is almost the same as a no gas in the reservoir. The critical point is the same when any of the variables of the system is selected in place of oil production rate (w_{po}).

The behaviour of the equilibrium points around the bifurcation point changes from stable to unstable regime. The eigenvalues for the equilibrium points corresponding to u=0.7, 0.8 and 0.9 for the system with GOR = 0.01 are given in table 9. These points correspond to points before bifurcation, at bifurcation point and when the system is fully into oscillation respectively. In the equilibrium points corresponding $u = 0.7$ and $u = 0.80$, the real parts of the eigenvalues do not cross the imaginary line. Beyond the bifurcation point, two conjugate eigenvalues crossed into the right hand plane hence the system becomes unstable. The eigenvalues and the result from Figure (32) which shows a change in the behaviour of oil production rate as the bifurcation point is crossed indicate that the gas-lifted system with the given parameter values exhibit local bifurcation. The fact that there is a change in the stability of the system based on eigenvalues crossing the imaginary line during bifurcation favours nonlinear control application. This is because the use of nonlinear prediction models takes into account all these behaviour in one prediction.

4.4.4 Phase Portrait

We then considered the visualization of the solution to the gas-lifted system at the critical points in section 4.4.1 above. We considered the state matrix corresponding to the equilibrium points at $u = 0$, $u = 0.65$ and $u = 0.95$ and used these points for the

plot of phase portrait and discussion on the stability at these points. As said earlier, the behavior of nonlinear system is more complex about these equilibrium point. One of the most important behaviors is stability of the equilibrium point. An equilibrium point is stable if nearby trajectories converge to it and it is unstable if they diverge from it.

The gas-lifted system presented here is a third order system which is difficult to visualize the trajectory using phase portrait. We first reduced the third order system to second order system using the method described in (RAMESH; GANESAN; MAHALAKSHMI, 2017). There, a third order system is reduced to second order by providing the desired transfer function of the second order system. The coefficients of the reduced (second) order system are solved for simultaneously after comparing coefficients of the third order system with that of the second order system. Thereafter we presented the phase portrait. Figure 33 compares the reduced model with the originally linearized counterpart for $u = 0.65$.

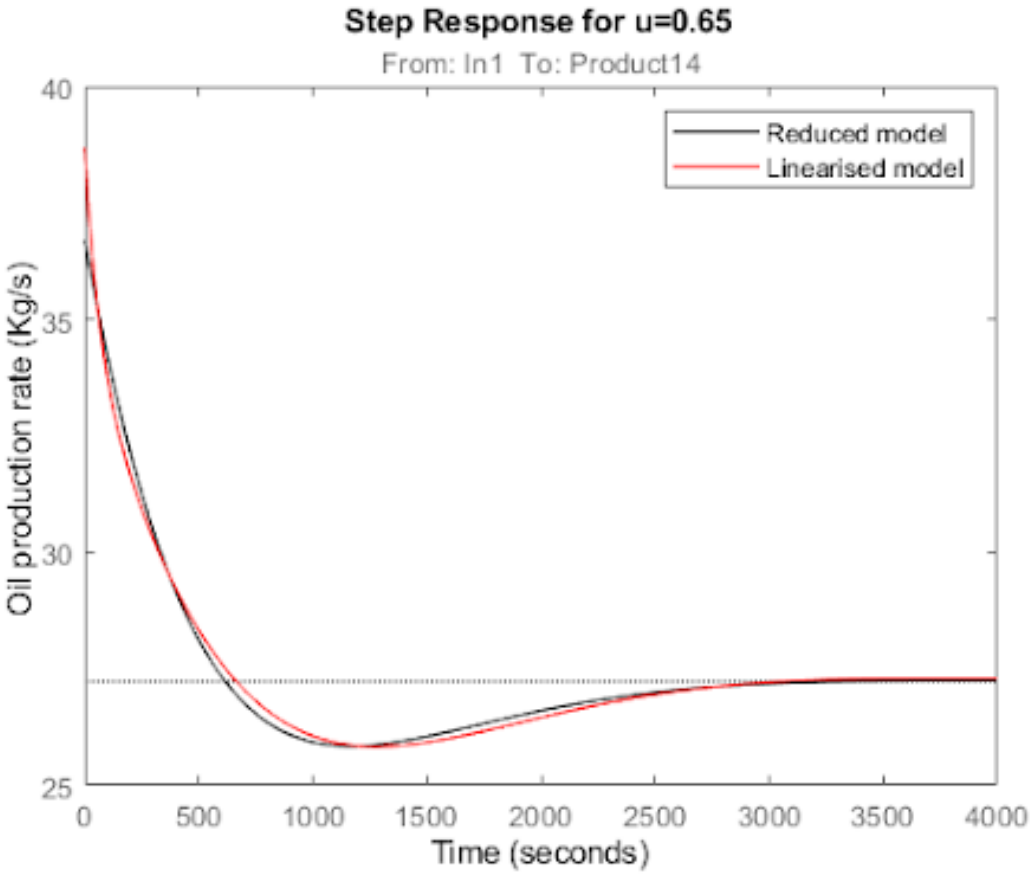

Figure 33: Reduced and linearised model for u=0.65

It is seen in Figure 33 that both responses match almost exactly hence the phase portrait for the reduced model represents that of the original linearized model but it is now easy to plot the two-state model. But for $u = 0$ (not shown), the two models

converged perfectly. On the other hand, the reduced and linearized models have very poor convergence for $u = 0.95$ but they are almost as close as possible hence we can still use the reduced model to represent the linearized model for the purpose of the phase portrait plot.

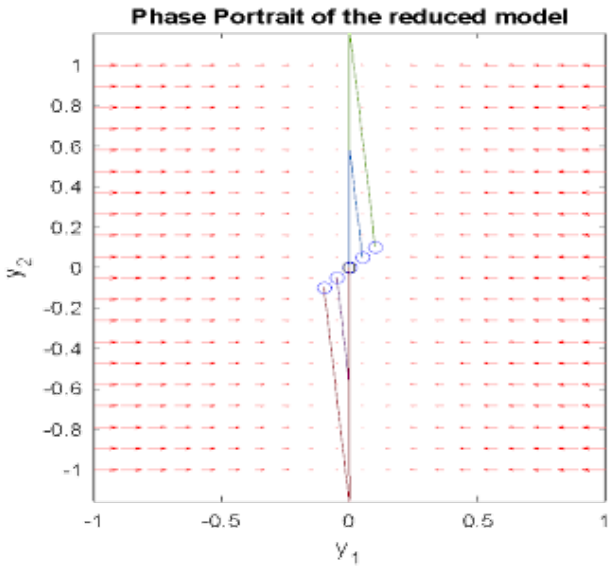

Figure 34: Phase portrait for the reduced model at u = 0

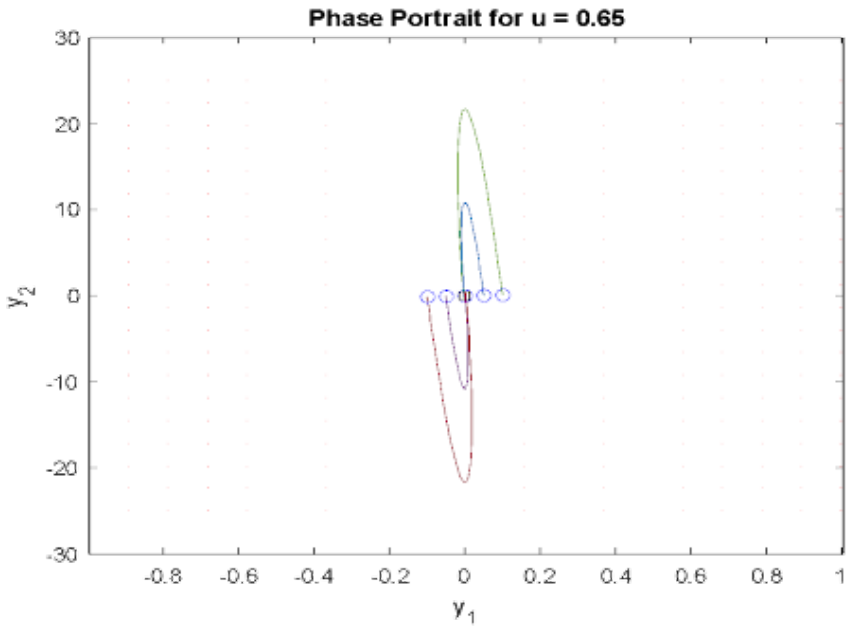

Figure 35: Phase portrait for the reduced model at u = 0.65

Figures 34, 35 and 36 are the phase portraits for $u = 0$, $u = 0.65$ and $u = 0.95$ respectively. The trajectories start from the point marked 'o' and terminate at '□'. It can be seen that for all three cases, the trajectories terminate at the origin showing that the origin is stable. In Figure 35, the velocity vector is not visible due to difficulty of

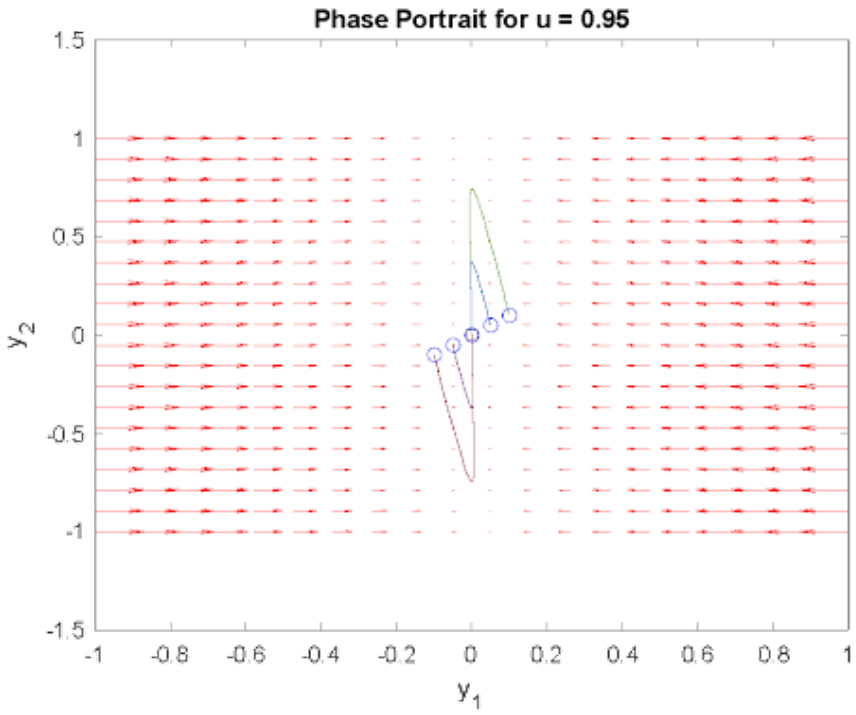

Figure 36: Phase portrait for the reduced model at u = 0.95

showing it simultaneously with the state trajectory for this particular fixed point. The velocity vector is the same as that shown in Figures 34 and 36.

Note that the reduction of the order of the system has left the states in the portrait plots above to be meaningless as it is not sure if the states are m_{ga} and m_{gt} or m_{ga} and m_{ot} or m_{gt} and m_{ot}. Also, the positions and number of the poles and zeros have changed due to order reduction. Nevertheless, it is used for the purpose of visualizing the portrait.

4.4.5 Limit Cycle

A limit cycle is a type of close orbit where there is no other close orbit in its neighborhood and any trajectory within the neighborhood converges to (stable limit cycle) or diverges from (unstable limit cycle) or converges to on one side and diverges on the other side (half- stable). Unlike the phase portrait we drew in section 4.4.4 above which can be a property of both linear and nonlinear system, limit cycle is a property of a nonlinear system only. The closest a linear system can get to is to have periodic orbits that are not limit cycles since they may not be isolated. A good example is a center which is an equilibrium point that is purely imaginary (has no real part). We identify the presence of limit cycle or eliminate the presence of limit cycle both analytically or geometrically but here geometrical approach is used.

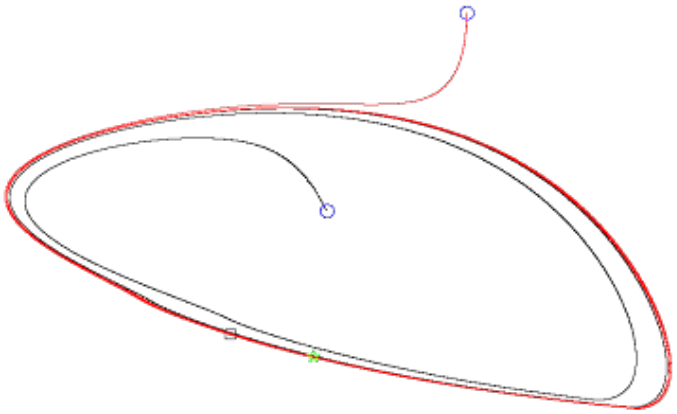

Figure 37: Limit circle corresponding to u = 0.95

Details of how we ascertained whether or not this is a limit cycle is not provided here. We just showed here that the state trajectory converged to a periodic orbit that was isolated here. The states are x_1 and x_2 since it is again difficult to show limit cycle for higher order systems. Figure 37 is the limit cycle drawn by using the data obtained from the simulation of the entire gas-lifted system and plotting the state trajectory for x_1 and x_2. This is done for $u = 0.95$ that is in the oscillating region.

It is seen from Figure 37 that trajectory starting from outside the limit cycle (begins from blue circle and ends in a black square) converges on the limit cycle. Also, the trajectory that starts from inside the limit cycle (begins from blue circle and ends in green pentagon) also converges on the limit cycle. Although it takes the inner trajectory longer curve before converging on the limit cycle, its curve does not form another periodic orbit, hence there is no isolated orbit here which is the limit cycle. The limit cycle in Figure 37 is a stable limit cycle since all trajectories converge on it.

4.4.6 Linearised Gas-Lifted System

We examined the behaviour of the gas-lifted system around the equilibrium point to guide the comparison of the controller presented in this thesis with the PI controller. We therefore revisited the concept of linearisation earlier discussed. This time, the gas-lifted system was linearised around the operating points corresponding to the input values from

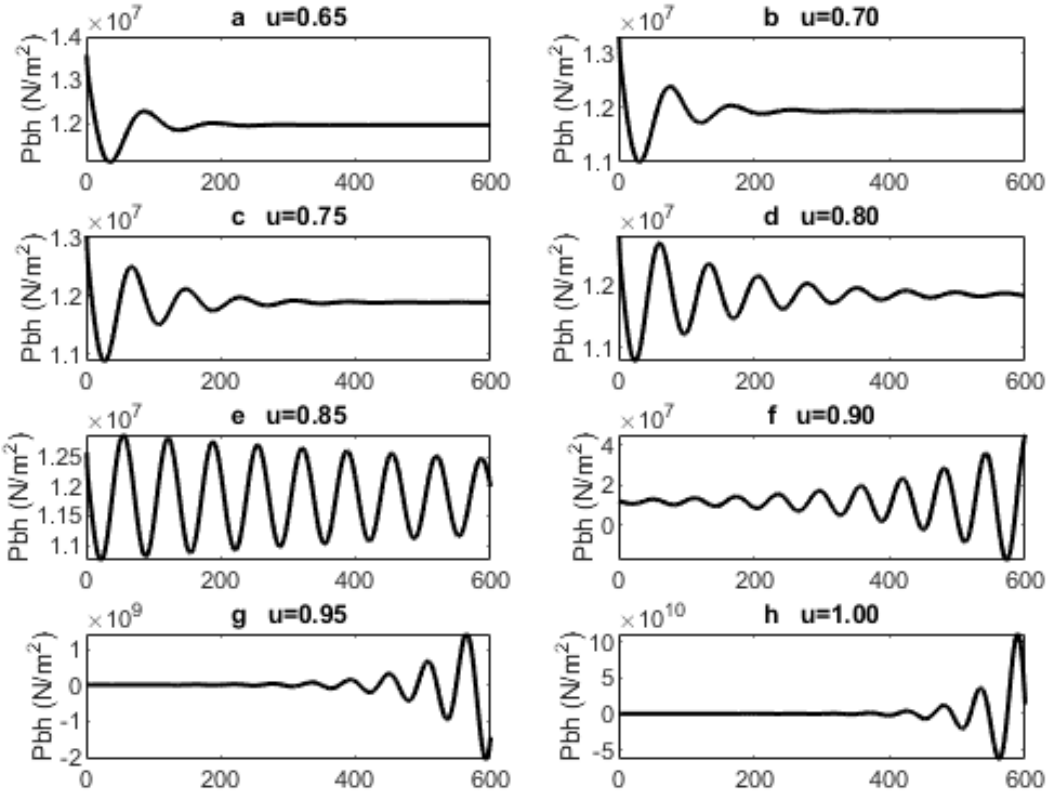

Figure 38: Step responses of the linearised gas-lifted system in stable and unstable mode. The output is the downhole pressure and the steady states correspond to input values from $u = 0.65$ to $u = 1.00$.

$u = 0.65$ to $u = 1.00$ incrementing by 0.05. The resulting state space model for steady state were used to obtain step responses around the bifurcation point. Figure (38) shows these step responses around the bifurcation point.

The step response for the linearised system in Figure (38) shows gradual change in the oscillatory behaviour of the system. At $u = 0.65$, the step response converge to a fixed value while at $u = 0.80$, where bifurcation occurs, the system experiences damped oscillation. Beyond this point however, the system goes into oscillatory behaviour as seen in Figure (38e) and becomes unstable at $u = 0.90$ and beyond. The situation was made more obvious in Figure (31) that compared nonlinear response with two linear responses as discussed earlier. This brings the issue of model uncertainty as input (which determines operating points) changes making linear control application insufficient hence necessitating the use of nonlinear control.

The gas-lifted system presented conflicting behaviour as observed here. The bifurcation diagram showed a change in the stability of the system as input changed, the

eigenvalues showed change in stability with input. However, the limit cycle shown in the unstable region showed that it is a stable limit cycle. Since the oscillatory behavior we intended to remove (in this thesis) is called casing-heading instability, this instability may be Lyapunov instability. This is due to fact that Lyapunov stability is assured for system in which the energy or output or trajectory decays to zero when little or no perturbation is given to it. But in the gas-lifted system, the system trajectory grew until it entered the limit cycle hence it is Lyapunov unstable. The instability may also be due to the effect it has on downstream equipment. The gas-lifted system is a DAE system and one property of a DAE system is that the stability cannot easily be detected from local stability analysis of the linearized system (NIKOUKHAH, 1998). This could explain why the system exhibits the casing-heading instability while the limit cycle is stable.

4.5 Concluding Remarks

We presented in this chapter the simplified model of a gas-lifted well. The ODE models describing the mass balances were presented and the algebraic variable controlling the flow rate, the pressure and density were derived too. Then the stability behavior of the system was examined by linearizing the system around equilibrium points provided by the states corresponding to inputs of $u = 0$, $u = 0.65$ and $u = 0.95$. The phase portraits show that every trajectory starting near the equilibrium points converged to the origin. Before the bifurcation point, the eigenvalues have negative real parts all indicating the linear stability of equilibrium points. After the bifurcation point, the real part of the complex eigenvalue crossed into the right-half plane (RHP). The nonlinear system also showed a stable limit cycle as all trajectories starting near the limit cycle converged to the limit cycle.

The gas-lifted system with the parameters presented therefore is stable except when operated at the input which is in the oscillatory region. But since the oscillatory behavior of the system is called a casing-heading instability, this instability may not be linear one but Lyapunov. This is owing to the fact that the system trajectory grows until it entered the stable limit cycle whereas for Lyapunov stability, the trajectory is meant to decay to zero.

5 GAS LIFT STABILITY USING FINITE HORIZON NMPC

5.1 Background

Gas-lifted system in matured oil well experiences casing-heading instability which reduces mean oil production and it is not healthy for the downstream equipment. This instability can be removed by implementing terminal equality constrained nonlinear model predictive control (NMPC) with input targets and control zones on the system. Input-dependent stability behaviour of the gas-lifted system was visualised through the bifurcation diagram, limit cycle and step responses of the linearised model at various operating points in chapter 4. The controller was earlier presented in chapter 3 and the close-loop feasibility and convergence discussed.

In this chapter, we used Euler method for the solution of the differential equation to first obtain the states. We then simulated the casing-heading instability and its removal by end-constrained finite horizon NMPC in problem P_3. The controller stabilised the undisturbed gas-lifted system improving production by 5.63% compared to the open-loop operation when the system was in casing-heading instability region. For the disturbed system, the additional degree of freedom from using two inputs attenuated the disturbance quickly compared to one input especially when the desired input was out of input bound. The steady state production, aided by the high input target, reached 12.25kg/s which is far more than 9.57 kg/s for the one input case. This controller showed a 3.76% improvement over PI controller for the same purpose. The stabilisation of the casing-heading improves flow assurance in gas-lifted system which is highly desired in oil production because it leads to optimal operation of the system.

5.2 Gas Lift Models Evaluation

In this chapter, the input to the gas-lifted system is the percentage opening of the production choke when we consider one input, but for two inputs case, the flow rate (in Kg/s) into the annulus is the second input. As said in chapter 4, this input is applied through the valve characteristic function (f(u)) shown in (4.5) and defined in (4.16)

The model in chapter 4 gives rise to a differential algebraic equation (DAE) of the form:

$$\dot{x} = f(x, z, u) \tag{5.1a}$$

$$0 = g(x, z, u) \tag{5.1b}$$

Where (5.1a) is the differential part and (5.1b) is the algebraic part. Differential equations are usually solved numerically using many methods available such as ODE45, explicit Euler, ODE15s, ODE23t, shooting techniques among others to produce the evolution of the states. The shooting approach and Euler approach were used on the CSTR where the model did not present a stiffness problem. But for the gas-lifted system, where the presence of oscillatory behavior causes variation in speed of solutions between adjacent parts, stiffness issue results, making it difficult to implement multiple shooting techniques.

We solved this problem here using ODE15s and in some cases the Euler method with sample time (h=1 minute). We used two sets of parameters here which correspond to field values in table 6 and the parameters corresponding to laboratory values in table 10 based on (EIKREM; AAMO; FOSS, 2008). We started the simulation close to the steady state values for a gas-lifted system based on field data and simulated over 2 hours. The initial states are $x_0 = [1285\ 745\ 5826]^T$. We took the flow rate of the injected gas into the annulus, w_{gl} to be equal to the initial flow rate of the injected gas from the annulus into the tubing, w_{iv} as 1 kg/s. Figure 39 shows the states of the system.

Figure 39, shows that the gas-lifted system is a positive system as all the states are nonzero as pointed out in chapter 4. The dependence of the states is indicated by for example x_1 and x_2. As the mass of gas in the annulus is declining, the mass of gas in the tubing is increasing and when the mass of gas in annulus starts increasing, that of gas in tubing starts declining. The dependence of the mass of oil in the tubing on the rate of oil production and the rate at which oil flows from reservoir into the tubing as indicated by equation (4.3) is evident in Figure 39. Figure 40 shows the rate of oil production and rate of oil flow from the reservoir into tubing.

From Figure 40, the net mass change of oil ($w_{ro} - w_{po}$) is initially positive since w_{ro}

Table 10: List of the constants, definitions, units and values for laboratory scale

Parameter	Definition	Unit	Value
H_a	Height of annulus	m	0.907
H_t	Height of tubing	m	14
H_{bh}	Height of bottomhole	m	4
A_a	Area of annulus	m^2	$0.314\text{x}10^{-3}$
A_t	Area of tubing	m^2	$0.314\text{x}10^{-3}$
C_r	Reservoir valve coefficient	m^2	$12\text{x}10^{-6}$
C_{iv}	Injection valve coefficient	m^2	$1.6\text{x}10^{-6}$
C_{pc}	Choke valve coefficient	m^2	$0.156\text{x}10^{-3}$
ρ_0	Reservoir oil density	Kg/m^3	1000
GOR	Gas/oil ratio	-	0.001
P_r	Reservoir pressure	N/m^2	$2.9\text{x}10^6$
P_s	Separator pressure	N/m^2	$1\text{x}10^5$
T_a	Annulus temperature	K	293
T_w	Tubing temperature	K	293
M_w	Molar mass of gas	Kg	0.028
R	Gas constant	J/KM	

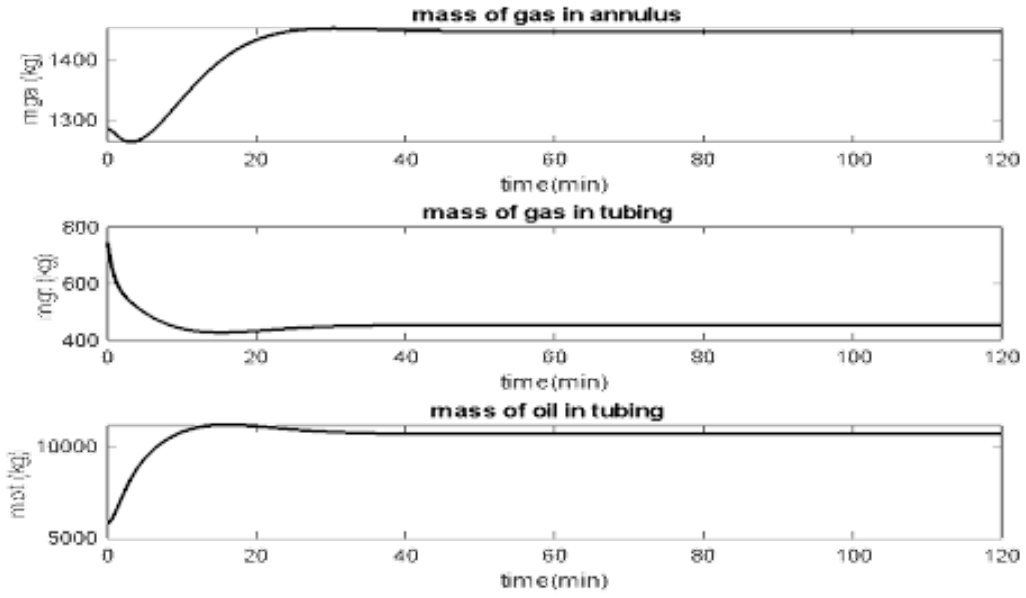

Figure 39: Gas lift states for field scale data.

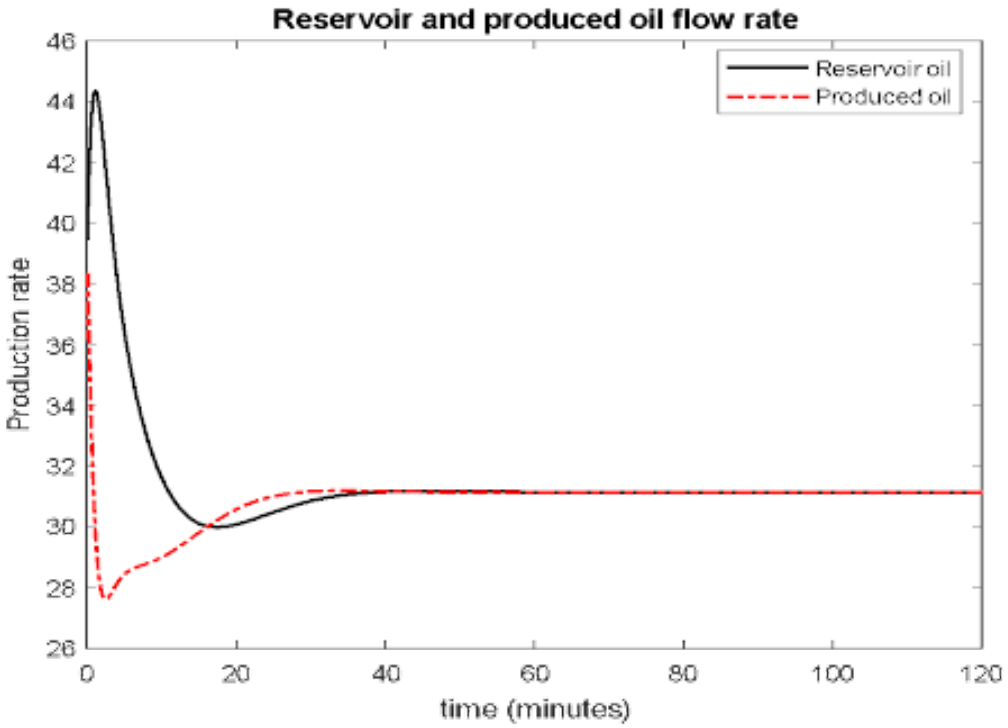

Figure 40: Gas lift oil flow for field scale data.

is greater than w_{po} which corresponds to the increase in m_{ot} in Figure 39. The next point in Figure 40 where the net mass flow is negative corresponds to when the m_{ot} in Figure 39 is decreasing (not very much visible). Thereafter, the mass of oil in the tubing, m_{ot} increases till steady state is reached in Figure 39. Notice that at steady state, the rate of production equals the rate of oil flow into the tubing from the reservoir which is in agreement with (4.3) when m_{ot} is constant. Also observe that despite the flow rate from the reservoir is declining while the flow rate of produced oil through the production choke is increasing, the net flow rate is still positive till a steady state is reached where this net value equals zero.

Similarly, Figure 41 shows the flow rates for the gases. In Figure 41, at steady state, the flow rate of the produced gas is the sum of the flow rate of gas through the injection valve (w_{iv}) and the flow from the reservoir (w_{rg}) which is in agreement with (4.2). Also, at steady state, the flow through the injection valve (w_{iv}) equals the rate of gas injection (w_{gl}) which we take as $1kg/s$ here. This is also in agreement with (4.1). The pressures for the system are shown in Figure 42. For flow from reservoir to the well to be possible, the reservoir pressure must exceed the bottom hole pressure which is confirmed in the figure.

The constant reservoir pressure used here is 150 bars which exceeds the bottom hole pressure in Figure 42 at any time hence there is flow. Also, for flow to occur between

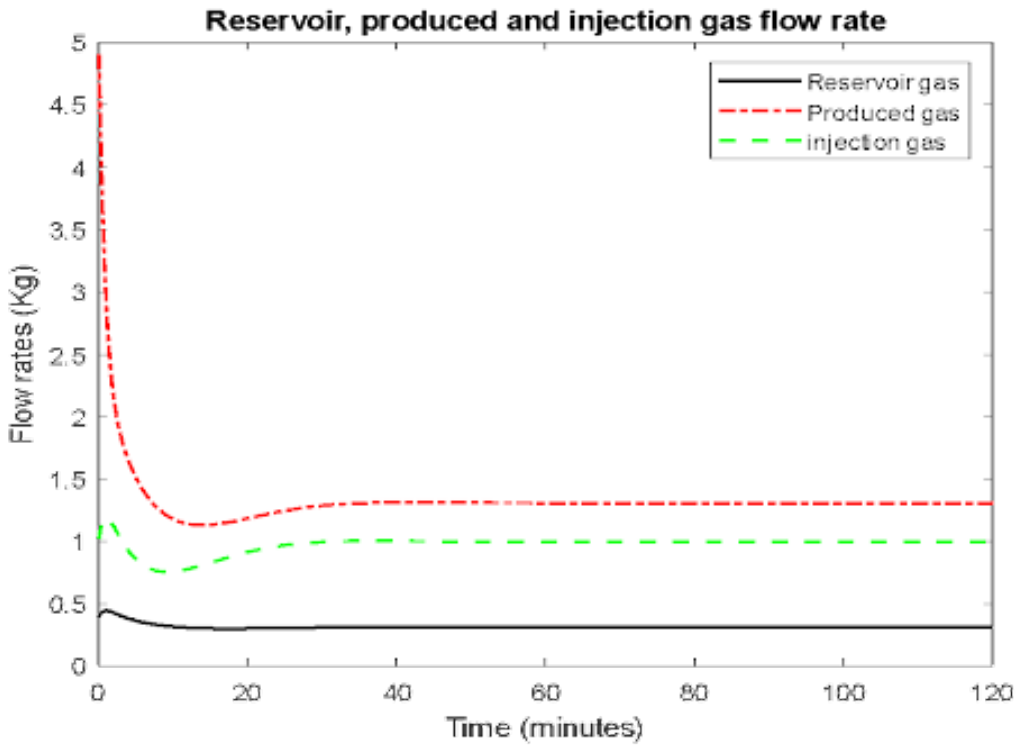

Figure 41: Gas flow rates.

annulus and tubing, the annulus pressure must exceed the tubing pressure at the injection point. If this is not maintained like this by any means, there will be alternate 'flow and no flow' situation of gas through the valve resulting in casing-heading instability discussed in the next section.

Similar result was obtained when the DAE system was solved using Euler approach. But for the Euler approach, we tested this on small scale data presented in (EIKREM; AAMO; FOSS, 2008). Figure 43 shows the states of the gas-lifted system using laboratory scale data solved with Euler method. Because the dimensions and the parameters values for the laboratory scale data are very small, the system attained steady state faster hence we simulated over 2 minutes unlike 2 hours for the field scale data. The initial conditions are $x_0 = [0.0320\ 0.0052\ 0.2000]^T$.

As expected, the solutions for the small-scale data was faster than the field scale and it showed the behaviour of gas-lifted system varies from field to field and from well to well and from time to time. Figure 44 shows the equivalent flow rate for the oil through the production choke and from the reservoir into the tubing. It can be seen that similar pattern to the flow behaviour presented in Figure 40 was obtained. Notice again that the flow rate from the reservoir into the tubing is declining as oil is produced but never goes below the production rate through the choke. At steady state, these two are again

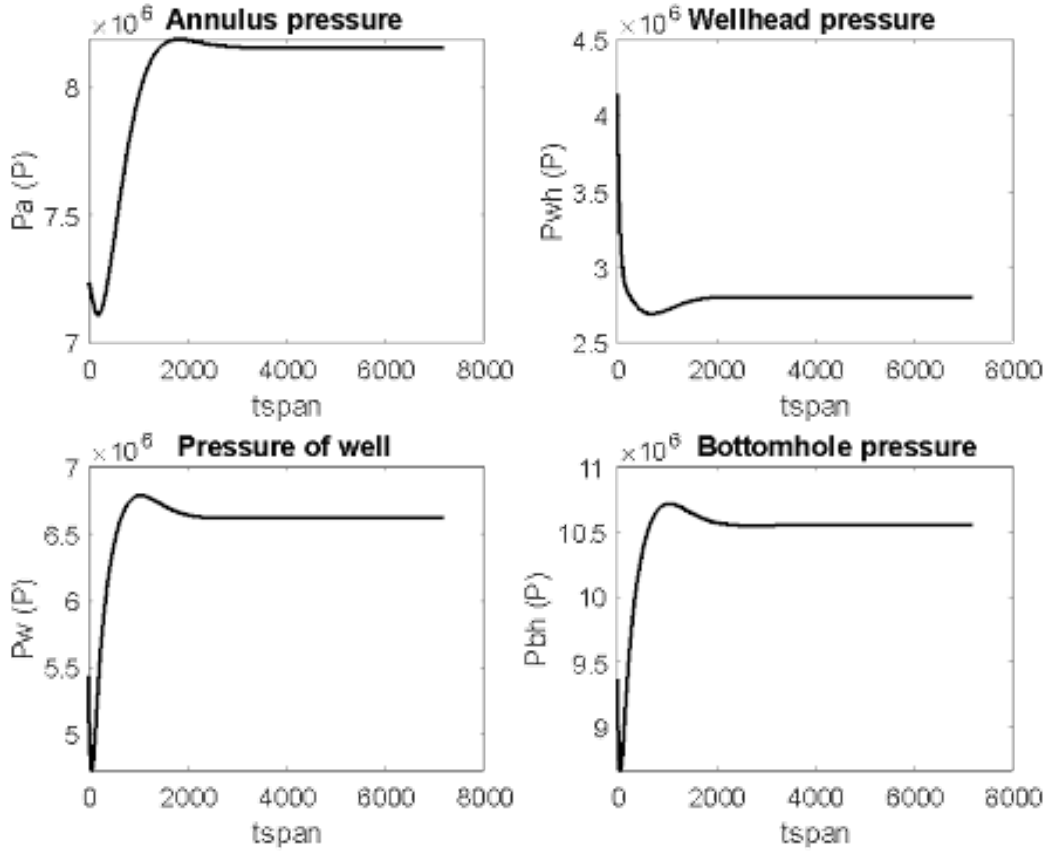

Figure 42: Gas lift pressures.

equal. It can be seen that the Euler method despite its shortcoming of inaccuracy and numerical instability can also be used to solve the DAE gas-lifted system. Hence over a short horizon and with very low sampling time, we used the Euler method in computing the predicted states for the designed controller and enjoyed the advantage of its simplicity.

5.3 Casing-Heading Instability

Casing-heading instability, a factor that affects flow assurance results from periodic variation of the pressures for the gas-lifted system. This affects the mean oil production over a time since at some conditions within a cycle there might be no flow or very low flow. In this section we first simulated the instability. Further on, casing-heading instability particularly conditions that minimise casing-heading instability hence improve mean oil production is now discussed in subsequent sections.

The input is u=0.65 (65% valve opening) while w_{gl} (flow rate into the annulus) was fixed at 0.4kg/s. Starting from initial condition of x_0=$\begin{bmatrix}2100 & 400 & 5700\end{bmatrix}^T$ kg, and with

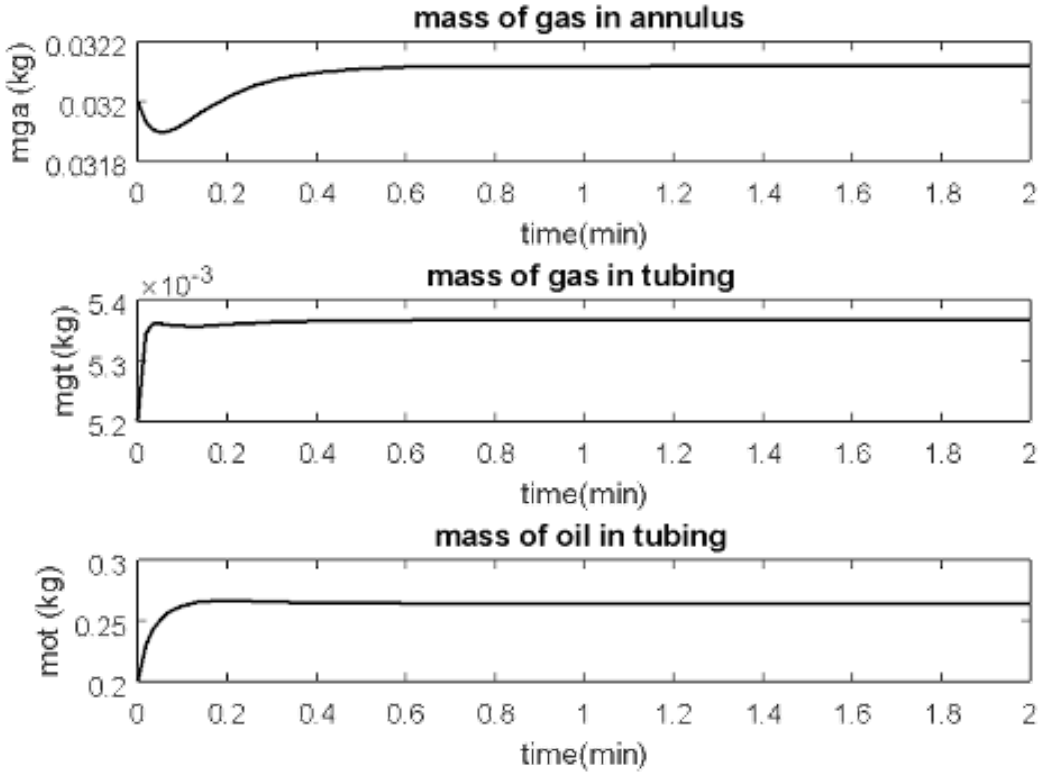

Figure 43: Gas lift states for laboratory scale data.

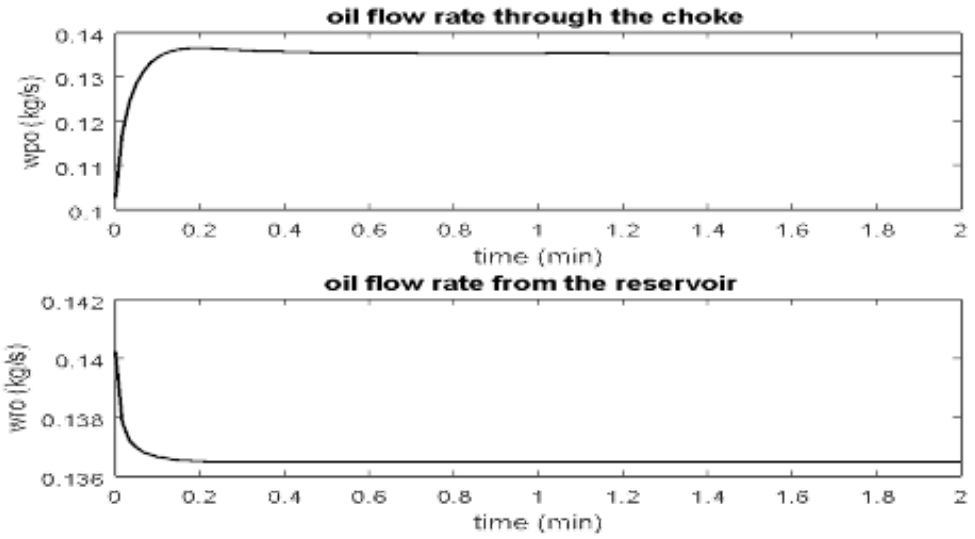

Figure 44: Gas lift oil flow for laboratory scale data.

GOR fixed at 0.01, the system was simulated over 5 hours. For a GOR of 0.01 (shown later), the system remained in stable mode till the inputs became u=0.75. Figure (45) shows the states of the gas-lifted system. In Figure (45) the system shows no oscillatory behaviour as the states converge to a steady state value of x_s=$\begin{bmatrix}2131 & 347 & 6429\end{bmatrix}^T$ kg,

showing the system is stable. Operating the gas-lifted system at $u = 0.65$ therefore prevents the casing-heading instability but the system operates at low production rate as flow rate depends on input.

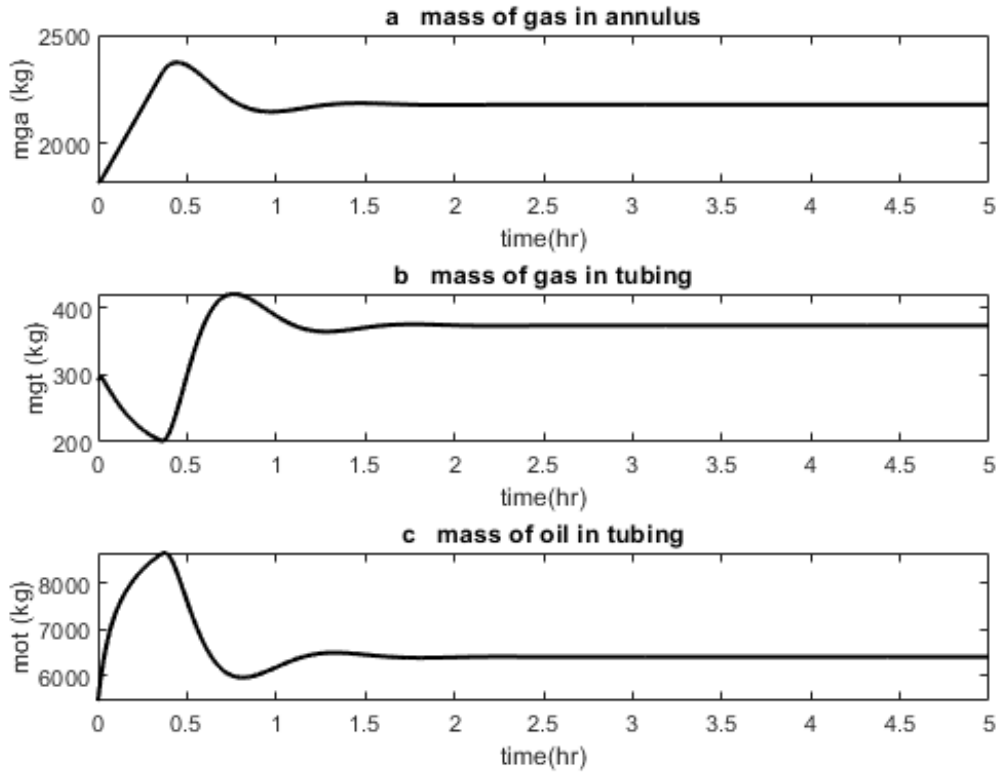

Figure 45: States of gas-lifted system for $u = 0.65$ in stable mode. These states are mass of gas in annulus x_1, mass of gas in tubing x_2 and mass of oil in tubing x_3. All three states are positive including other algebraic variables of the system. The states converged to fixed values as there is no oscillation

For the unstable regime, we used a choke opening of 95% (0.95) which falls into the unstable region. Figure (46) shows the oscillating states of the system. The system oscillates with a period of about 53 minutes (0.88 hrs). All algebraic variables of the gas-lifted system also showed the oscillatory behaviour. This period can be as low as 100s (1.7 minutes) in laboratory scale to few hours in some fields (SCIBILIA; HOVD; BITMEAD, 2008). Further simulations showed that any input such that $0.0 \leq u \leq 0.75$ produced a gas-lifted system that was completely stable. For $0.75 \leq u \leq 0.80$, there was a slight oscillation, however, bifurcation point is at u=0.80 after which the system goes into oscillation. Next, we discuss the stabilisation of the system using the NMPC.

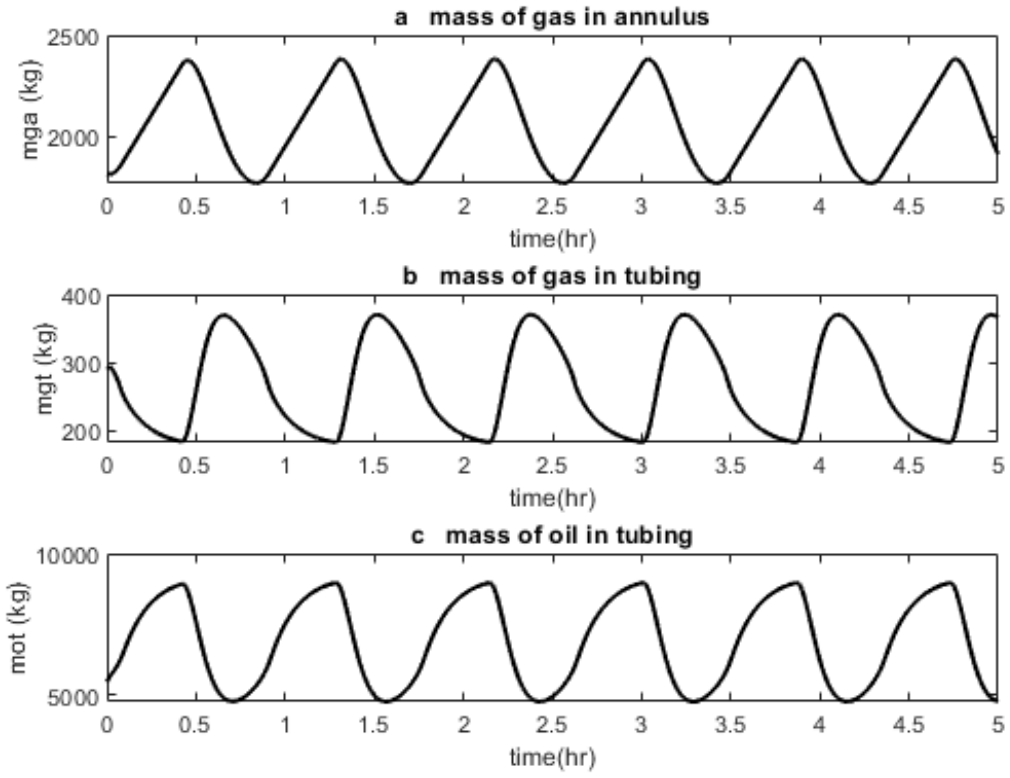

Figure 46: States of gas-lifted system for $u = 0.95$ in unstable mode. The states do not converge to fixed values but oscillate with a period of about 53 minutes. This oscillation is not healthy for the downstream equipment and it also reduces the mean oil production.

5.4 Stabilisation of Gas-Lifted System Using Terminal Equality Constrained NMPC with Input Target and Control Zones

The pressure of gas in the annulus depends on the mass of annulus gas. If the mass of gas in the annulus can be maintained above a certain value, pressure in the annulus can be kept above certain value that favours unidirectional and continuous flow of gas from annulus to tubing. The third order model of gas-lifted system has one of the states of the system being mass of annulus gas (x_1). Oscillatory behaviour can be minimised if the mass of annulus gas can be kept at a permissible minimum value. An NMPC with terminal equality constraint whose first objective is to ensure the states are in their zones before enforcing input target can set a zone for the annulus gas. This gives the controller the flexibility to maintain the mass of annulus gas (x_1) at value that favours flow from the annulus to the tubing while the controller solves the input that approaches the optimal input from the RTO (real time optimsation) as much as possible. Various scenarios for

the gas-lifted system stabilisation which followed the results in (ADUKWU; ODLOAK; KASSAB, 2023b) are presented below.

5.4.1 Undisturbed Gas-Lifted Well Stabilization Using NMPC with Desired Input within Input Bound: One Input Case

We considered a case where the system was undisturbed and the desired input was within the input bound. There was only one input which is the percentage valve opening. The controller presented in (3.15), (3.16) section 3.3.3 was used. The controller parameters are: $m = 4$, $p = 100$, $Q_x = diag([111]\text{x}10^{-1})$, Q_u=$diag([1]\text{x}10^{6})$ and $R_u = diag([1]\text{x}10^{5})$. We showed the closed loop behaviour for the system with desired input $u_{des} = 0.95$ which is in the unstable region.

The estimated states from the EKF and the optimal states were compared. The parameters of the EKF are: the state covariance, $P_0 = diag([100\ 10\ 1000])$, the state noise, $Q = diag([100\ 16\ 160])$ and the measurement noise, $R = diag([1000\ 1000\ 40])$. The measurements used for the EKF are the mixture density, annulus pressure and top-side pressure (SCIBILIA; HOVD; BITMEAD, 2008) while the detailed EKF procedure is described in (SIMON, 2006). The continuous time gas-lifted system model was discretised using zero-order hold. This was to accommodate the UKF that is descrete and the measurement also that is discrete. The sample time is the same for the simulation (1 minute).

Zone control and input target was implemented for the closed loop system. The zones were selected based on the limitation imposed by the gas-lifted system volumes and the desire to increase the annulus pressure while reducing the well pressure. This implies a large lower bound of the mass of gas in annulus x_1 and a small upper bound of the mass of gas in tubing x_2 and mass of oil in tubing x_3. From several simulations around steady state, the control zones were selected as $x_{min} = \begin{bmatrix}2000 & 100 & 1000\end{bmatrix}^T$kg, $x_{max} = \begin{bmatrix}2600 & 800 & 7000\end{bmatrix}^T$kg.

Figure 47 shows the estimated and optimal states. The estimated states were used in the controller for prediction and were obtained from measurements as detailed in (SIMON, 2006). The optimal states were obtained from using the first element of the optimal input sequence on the gas-lifted system model. The blue dashed lines are the upper and lower limits for the states (control zone) while the black solid line is the system optimal states and the red dash-dotted line is the estimated states.

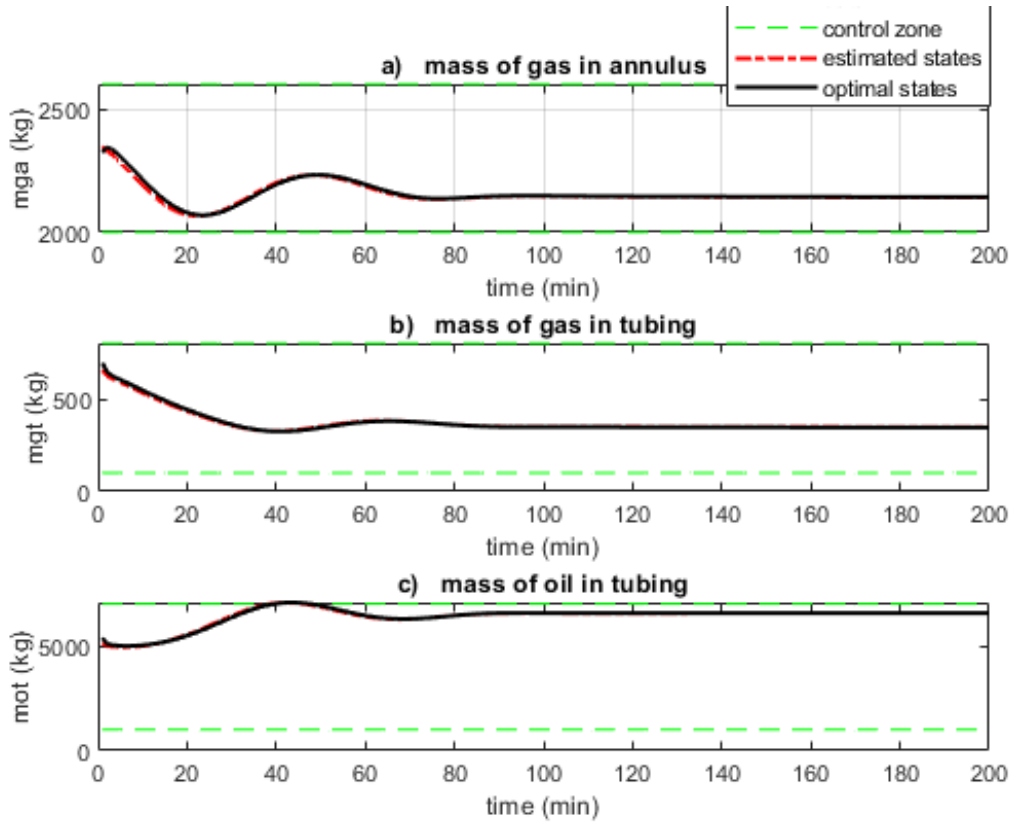

Figure 47: Optimal and estimated states of the gas-lifted system. The optimal states are the true states of the system while the estimated states are the EKF outputs. The states are within the state zones and the states are stabilised by NMPC despite the input target falls within the unstable region.

Figure 47 shows the control zones are respected. The controller can enforce zone control for narrower control zones but at the expense of low optimal input sequence which results in low oil produced rate. Hence for an adverse case where the controller is unable to stabilise the oscillatory behaviour, the lower bound of x_1 can be increased to a limit dictated by the annulus volume while the upper bounds of x_2 and x_3 can be decreased. This will however jeopardise feasibility as the control zones will be made narrower. The estimated states (red long-dotted line) is seen converged to the optimal states (dark continuous lines) obtained from the actual measurement. This shows the performance of The EKF.

Figure 48, is the oil production rate at 95% valve opening (u = 0.95). The optimal production from the controller (black solid line), unstable production (red dashed line), mean production (blue dash-dotted) were obtained at GOR = 0.01 while the stable production (green dotted line) was obtained at GOR = 0.4. The mean production is the average production when the gas-lifted system is in the unstable region at u = 0.95. The

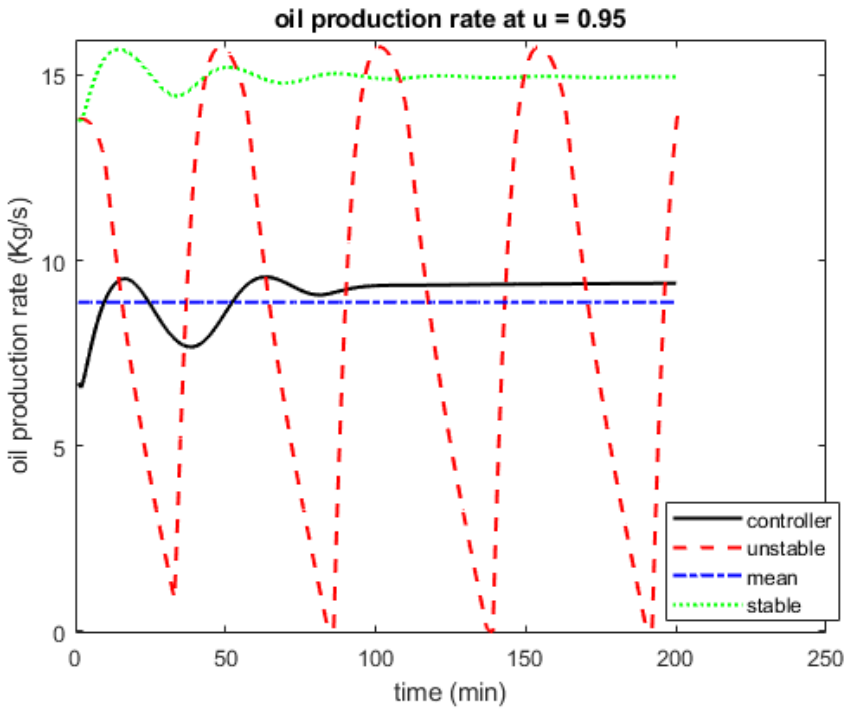

Figure 48: Oil production rate at 95% valve opening (u = 0.95). The optimal production from the controller (black solid line), unstable production (red dashed line), mean production (blue dash-dotted) were obtained at GOR = 0.01 while the stable production (green dotted line) was obtained at GOR = 0.4.

steady state optimal production rate from the controller is 9.38kg/s, while the mean production is 8.88kg/s and the stable oil production is 14.95 kg/s. If the reservoir parameter, GOR is high enough to keep the gas-lifted system in stable mode, oil production will be at its highest rate for an input u = 0.95. But if GOR is not sufficient enough to naturally remove the instability at the given input, the NMPC is better. The NMPC increased steady state oil production by 5.63% over mean oil production when the gas-lifted system was operated at u = 0.95.

5.4.2 Undisturbed Gas-Lifted Well Stabilisation Using Terminal Equality Constrained NMPC with Desired Input out of Input Bound : One Input Case

When it is desired to approach the input limit as close as possible, the input from RTO (real time optimsation) is no longer selected as the desired input. Since this controller respects the control limits, a desired input outside this limit was selected to force the optimal input close to the control limit without violating the control limit. We started with $u_{des} = 0.65$ and switched to $u_{des} = 1.25$ (which is out of control limit) after 90

minutes (1.5hours). Figure 49 shows the states of the system while Figure 50 and Figure 51 show the input target and cost function respectively.

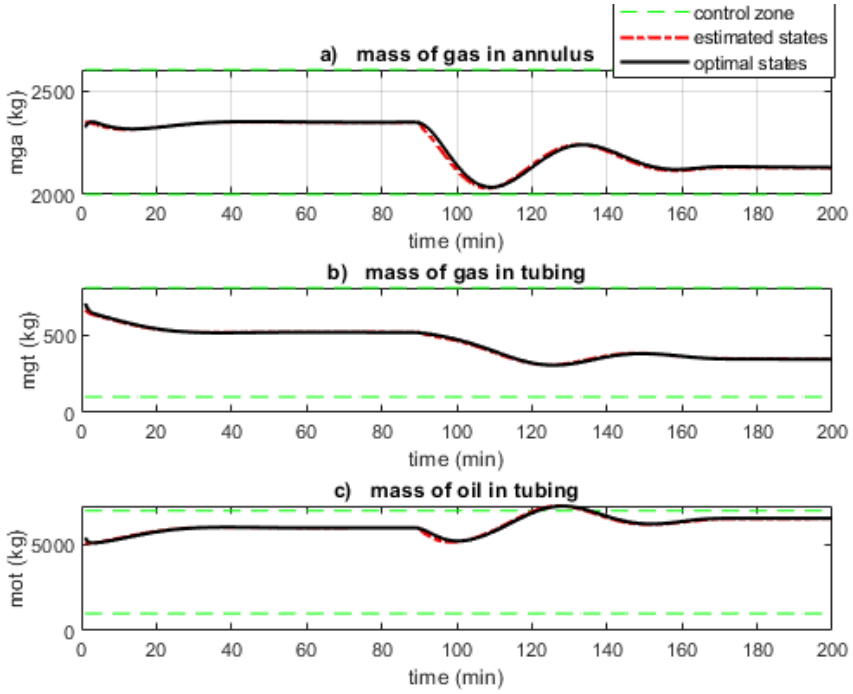

Figure 49: The states of the gas-lifted system when the desired input (u_{des}) switches from input bound to out of input bound. The states bounds are still respected.

The second part of Figure 49 where $u_{des} = 1.25$, is out of input bound. The control zones are respected except for mass of oil in tubing that temporarily violated the zones after the switch from stable input within bound to input out of bound. In Figure 50, the first part where u = 0.65 is both within bound and reachable. The optimal control input converged to the desired input and the cost function corresponding to the portion in Figure 51 decays to zero monotonically. This is not evident in the diagram but on zooming, it showed how the cost decreased to zero. The second part of Figure 50 however is out of input bound and unreachable. The optimal input is unable to reach desired input as well as the input bound. The corresponding cost function in Figure 51 decreases to a point where it leaves an offset due to the desired input being unreachable. The steady state oil production however increased to 9.57kg/s compared to 9.38kg/s when the desired input was kept at u = 0.95.

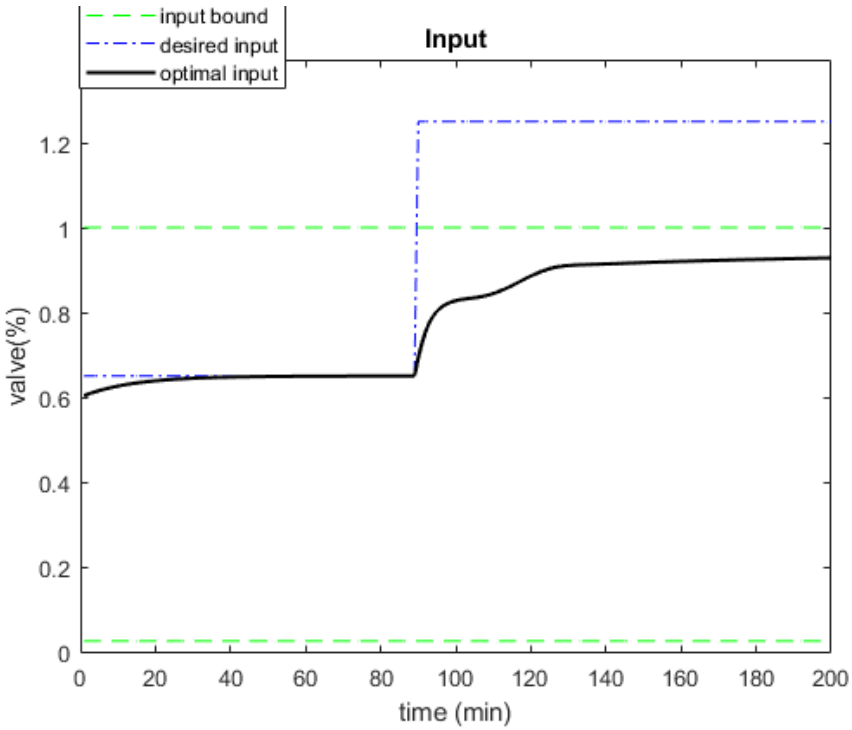

Figure 50: Desired input (blue dash-dotted), optimal input (black solid) and the input bounds (green dash) when the desired input switches from within bound to out of bound. The optimal input approaches the upper bound as far as possible but does not converge to it.

5.4.3 Disturbed Gas-Lifted Well Stabilisation Using NMPC with Input within Bound : One Input Case

A system where disturbance caused the state to go out of zone was considered here. The new state bounds are $x_{min} = \begin{bmatrix} 2000 & 100 & 1000 \end{bmatrix}^T$ kg, $x_{max} = \begin{bmatrix} 2600 & 500 & 7000 \end{bmatrix}^T$ kg which is a reduction of the upper limit of x_2. The initial condition is $x_0 = \begin{bmatrix} 2300 & 450 & 5800 \end{bmatrix}^T$ kg, which is a reduction of the initial condition of x_2. The disturbance is a 5% decrease in x_1, 20% increase in x_2 and 20% decrease in x_3 occurring between 60th and 65th minutes where the system is in steady state. The desired input is u = 0.95 which is in the unstable region. Figure 52 shows the states of the system.

The disturbance caused the states to violate the control zones in Figure 52 but the NMPC restored the states to their zones. State x_1 was restored in about 11 minutes while the disturbance effect was removed in about 67 minutes after the disturbance was introduced. It took 2 minutes to restore the x_2 to the zones after the disturbance ended while x_3 took 40 minutes. The disturbance effect was removed after 87 minutes and 77 minutes for x_2 and x_3 respectively.

The input target (u_{des}) of 0.95 was not met as the optimal input sequence reached

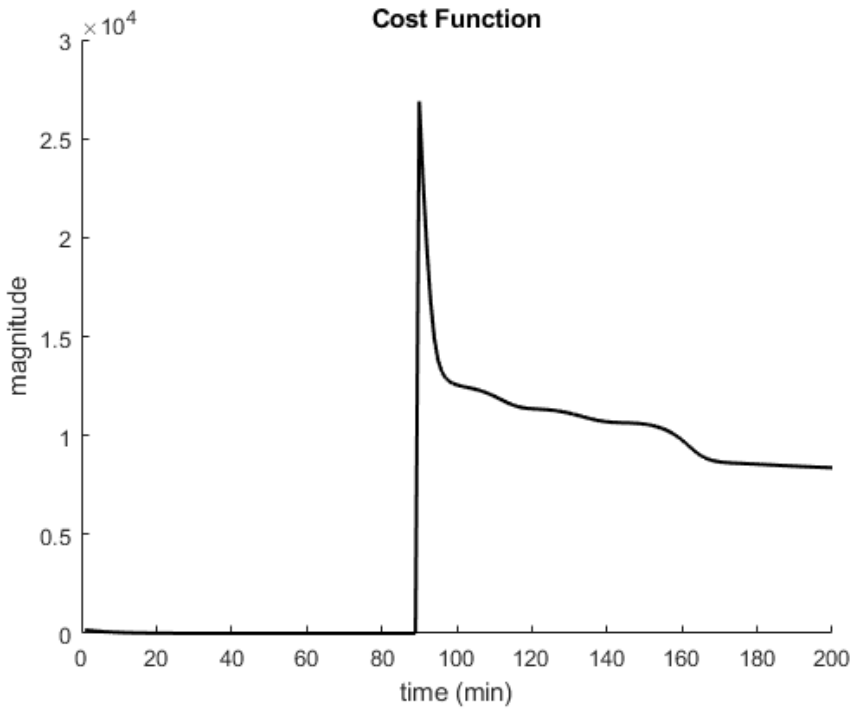

Figure 51: Control cost function for the gas-lifted system. The first part corresponds to $u_{des} = 0.65$ which is in the stable region. The second part corresponds to $u_{des} = 1.25$ which is out of input bound. The cost function decreases to zero for the first part that the input is reachable but leaves an offset for the unreachable part

a steady state value of 0.901. The optimal production attained a steady state value of 8.78kg/s which is lower than 9.38kg/s for the undisturbed system. On simulating using $u_{des} = 1.25$ which is out of input bound and unreachable, the optimal input from the controller attained steady value of 0.92 while the oil production steadied at 9.09 kg/s which again is less than the undisturbed system. This shows the controller has been able to restore the states to their zones but could not attain the optimal production for the undisturbed system.

5.4.4 Disturbed Gas-Lifted System Stabilisation Using Terminal Equality Constrained NMPC Having Input within Bound : Two Input Case

Most control solutions to operation of gas-lifted system use only one input (the production choke) to control the flow through the system. The flow into the annulus (w_{gl}) is usually fixed by regulatory controller (mostly PID) and the setpoint depends on available gas from the compressor station. In few cases, both valves are manipulated to control the flow in multivariable approach for optimal operation as shown in (RASHID; DEMIREL; COUËT, 2011), (DIEHL et al., 2018). We examined the effect of the additional degree

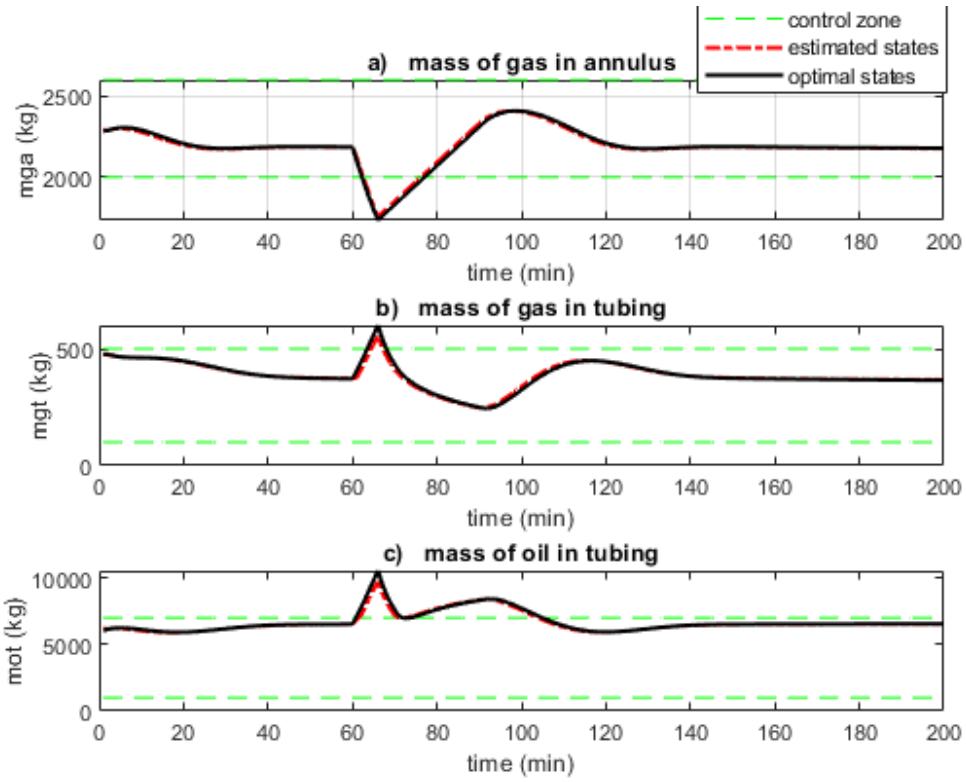

Figure 52: States of gas-lifted system with disturbance occurring between 60th and 65th minutes. The NMPC restored the states to their zones after the disturbance made the states to temporarily violate the control zones.

of freedom on disturbance attenuation and improvement of oil production rate. All the values in the one input case were retained but w_{gl} that was fixed in the one input case was here an input where the desired value is given as $u_{des} = 0.4$ kg/s. Also the simulation time is 400 minutes to give room for the inputs to converge to the desired values. Figure 53 shows the two inputs and Figure 54 shows the corresponding cost function.

The introduction of an extra degree of freedom made the optimal input for the valve opening in Figure 53 to be slightly closer to the input target than the one input case. For a longer simulation time, the input target will be met for both inputs. The cost function in Figure 54 declines to almost zero after the arrival of the disturbance. Increase in simulation time showed that this offset was removed after the disturbance. The production rate improved slightly to 8.87kg/s over the one input case which is 8.78kg/s. This was caused by the optimal input for the valve opening reaching a final value of 0.93kg/s compared to 0.901kg/s for the one input case. There was therefore just a very small advantage in using the two inputs case when the desired input for the second input (flow rate into the annulus) was chosen to be the same as the fixed value considered in one input system.

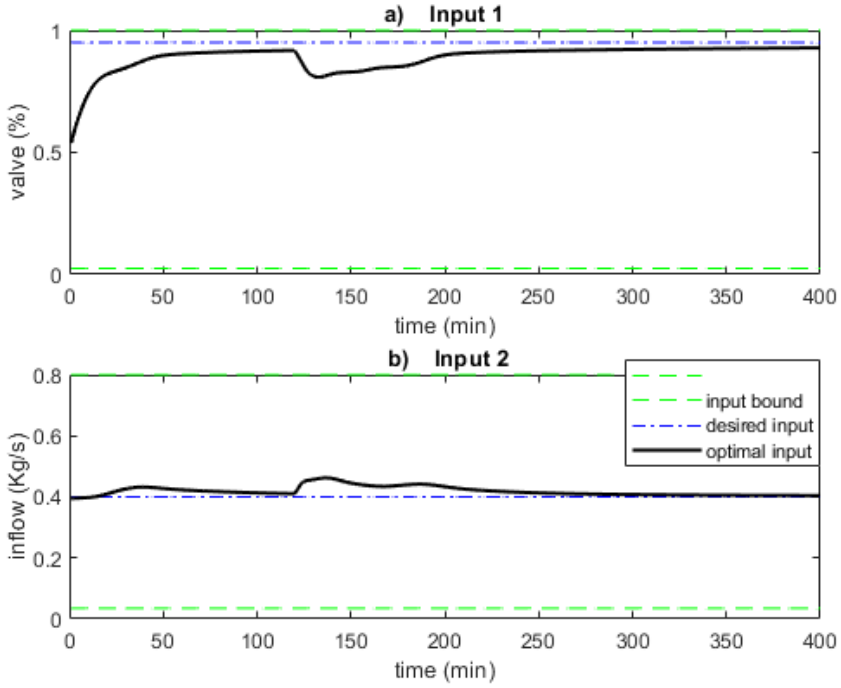

Figure 53: Two inputs of the gas-lifted system. The second optimal input follows the desired input u_{des}=0.4kg/s as close as possible.

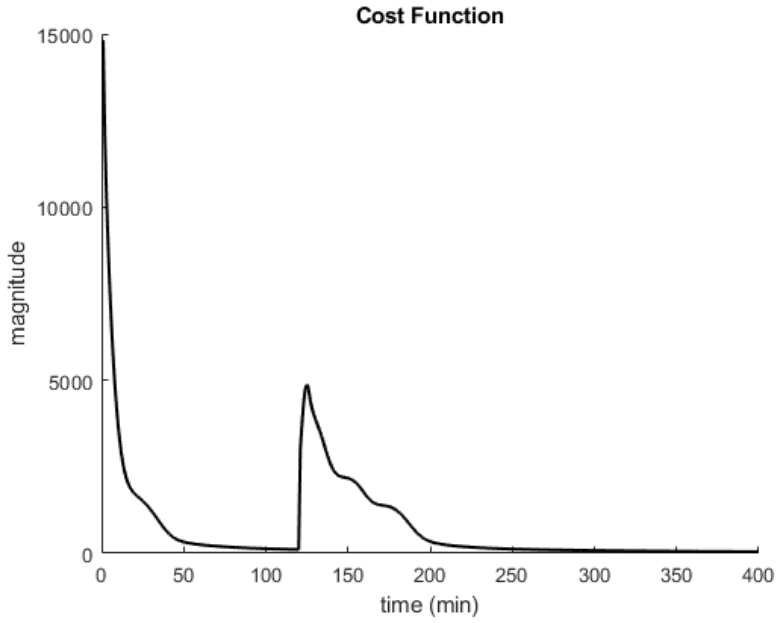

Figure 54: Control cost function for the gas-lifted system with disturbance. The first part corresponds to the time before the disturbance arrival and the second part corresponds to the part after the disturbance arrival. The cost function decreased to a value permitted by time for the first part but decreased to zero for the second part

The state plot was almost identical to Figure 52 hence not shown here. This is due to the controller being able to fix the second input at almost the constant value of $u =$

0.4kg/s in Figure 54 which is the value of the w_{gl} in the one input case. The first optimal input therefore approached the optimal input corresponding to Figure 52 hence the state trajectories were almost identical.

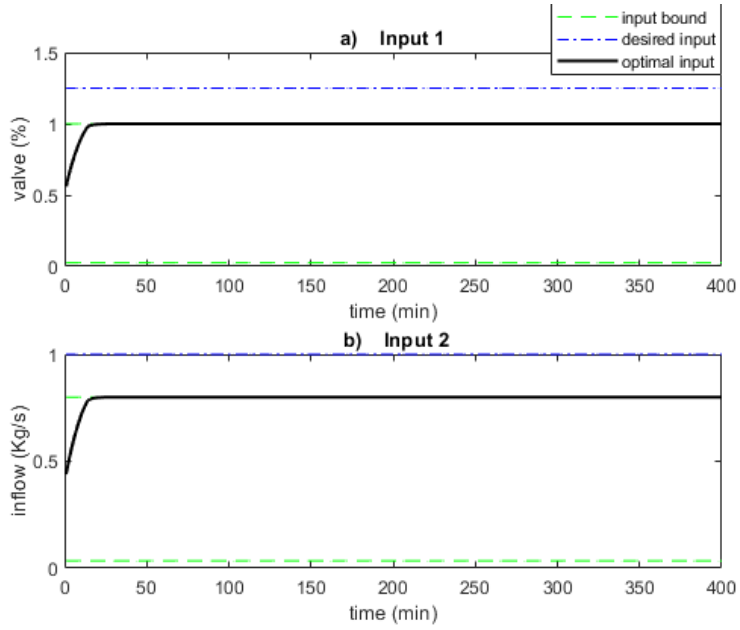

Figure 55: Optimal inputs when the desired inputs are out of input bounds. The two inputs saturated on the upper boundary of the control input even when disturbance arrived. This helped attenuated disturbance effect much quickly.

If however, the unreachable input is considered, the advantage of the two input case over the one input case in terms of disturbance attenuation and improved flow of oil becomes obvious. In under 20 minutes, the unreachable input targets forced the two inputs to converge to the upper control limits as shown in Figure 55. Following the arrival of disturbance, the optimal inputs remained at the upper boundary of the control limit hence maintaining states x_2 and x_3 in their zones despite the disturbance. State x_1 however violated the state zones briefly and was quickly restored to the zones by the saturated inputs as shown in Figure 56. The steady state production reached 12.25 kg/s which is far more than 9.57 kg/s for the one input case. This is expected as the rate of production and the stability of the gas-lifted system depends on the flow rate of the gas into the annulus which saturated at 1.0 kg/s.

5.4.5 Stabilisation with PI Controller

In section 4.4.6 it was observed that the gas-lifted system presented here is highly nonlinear necessitating the use of nonlinear control approach to its optimisation. We compared the performance of the end-constrained NMPC with the PI controller described

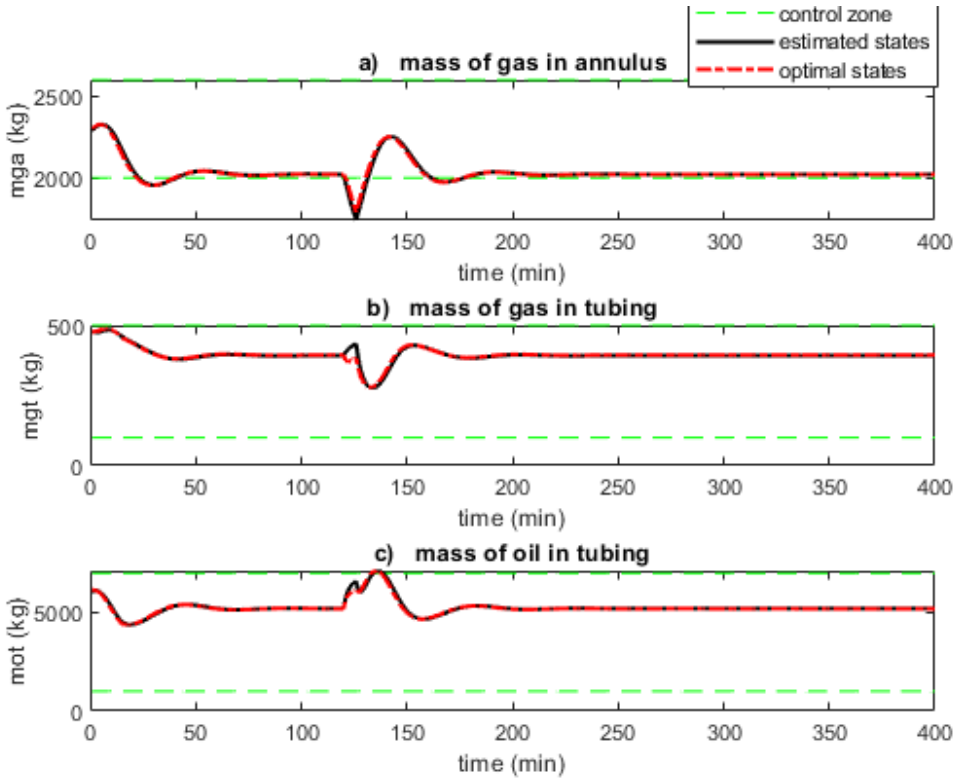

Figure 56: States of gas-lifted system with disturbance occurring between 120th and 125th minutes. The saturated optimal inputs ensure faster disturbance attenuation than when the input target is within limit.

in (SCIBILIA; HOVD; BITMEAD, 2008). Balanced rather than aggressive tuning of the PI controller discussed in Klan and Gorez (2005) was used here since the gas-lifted system is a very slow system. The system was linearised around an operating point corresponding to $u = 0.70$ which is in the stable region based on Figure 38. The output is the downhole pressure whose measurement is available hence no need for estimation. The setpoint for the downhole pressure was selected such that the steady state input is $u = 0.95$. Figure 57 shows the gas-lifted states following the application of the PI controller while Figure 58 shows the PI controller output (gas-lifted system input).

The controller stabilised the gas lift states in Figure 57 at steady state after damping the oscillation. This is achieved by the PI controller gradually opening the valve further from the equilibrium value of $u = 0.70$ to the steady state value of $u = 0.95$ as shown in Figure 58a. The oil production increased slightly to 9.04 Kg/s in Figure 58b which corresponds to a meagre 1.08% increase over the open loop mean production rate. Choosing lower setpoint for the downhole pressure can increase oil production rate but this might lead to computed controller output being different from input to the gas-lifted system since the valve cannot handle input above 1 (100%). Also since the objective of

casing-heading instability removal is to increase mean production and protect downstream equipment, using PI controller is still better than open loop operation despite the slight difference above. There was also a meagre 3.76% increase in production rate when NMPC was used compared to the PI controller. Despite this value is small to compensate for the rigor of using the NMPC, the fact that NMPC incorporates constraints in its formulation makes its use better than the PI controller.

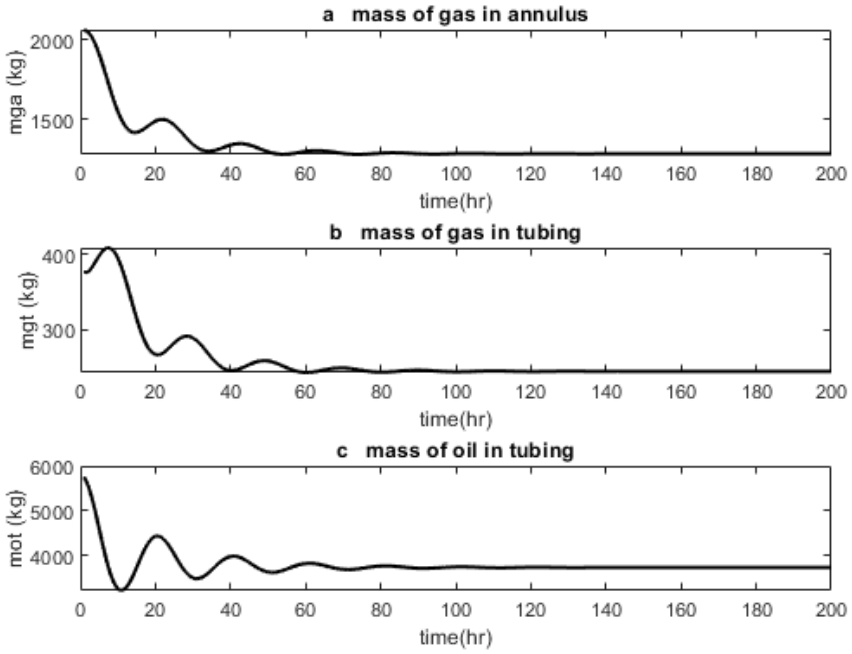

Figure 57: Stablised states of gas-lifted system with PI controller. The oscillation is damped out slowly compared to the use of NMPC.

5.5 Concluding Remarks

End equality-constrained NMPC was used to stabilise a gas-lifted system. The stability and convergence of the controller was discussed in section 3.3.3 and some behaviours of the system were first discussed in chapter 4. The controller stabilised the gas-lifted system for one input (production valve) and two inputs (production valve and lift gas injection valve). The two input case has more advantage over the one input case when the input targets are out of input bound as the controller forced the inputs to saturate at the upper bound of the inputs. The saturated inputs helped attenuate disturbance much quicker and also improved flow rate of produced oil. The NMPC performs slightly better than the PI controller both in terms of slight increase in production rate and speed of damping of the oscillation.

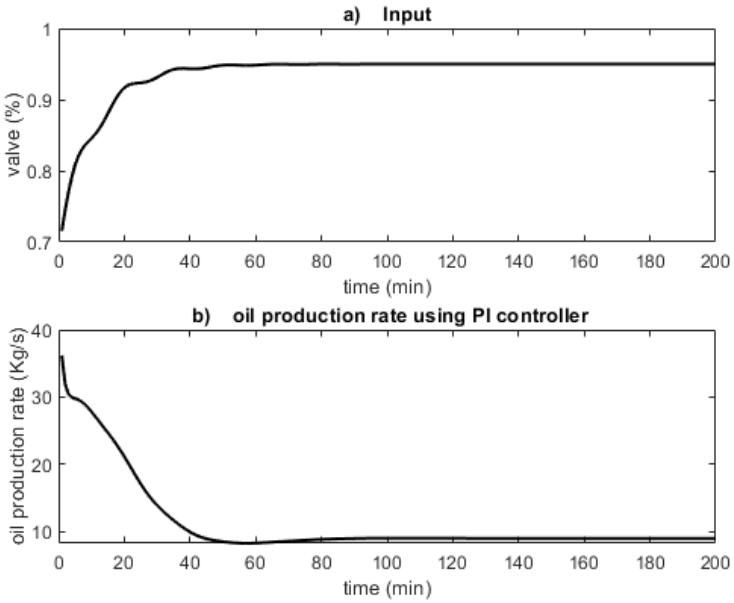

Figure 58: Input and output of the gas-lifted system using PI controller. The PI controller opens the valve gradually from the equilibrium point to $u = 0.95$ which is in the unstable region making the oil production to steady at 9.03 Kg/s) .

6 STATE ESTIMATION OF GAS-LIFTED SYSTEM

6.1 Background

Gas-lifted systems are usually situated in harsh environments or deep below the sea surface for sensors to produce reliable measurements. This is due to the difficulty encountered when deploying the sensors in the location required to provide good measurement, excess heat effect on the sensors, reaction between the sensors and the harsh environments among other reasons. In addition, sensors that could take more accurate measurements could create additional cost that is higher than the additional output due to their deployment. Gas-lifted system is naturally nonlinear but linear estimation method has been applied in the state estimation with no reported work on nonlinear state estimation.

The focus of this chapter therefore is the extension of nonlinear state estimation methods to gas-lifted system. Extended Kalman Filter (EKF), unscented Kalman Filter (UKF) and particle Filter (PF) were used to estimate the nonlinear states. Brief description of the filters were first presented starting from the linear Kalman filter. Hypothesis test on the expectation of the residuals were performed to show how close to optimal the estimation methods are and it showed the UKF estimates to be slightly better than EKF while PF performs least. The PF have poor accuracy using residual visualisation, hypothesis test and the root mean squared error (RMSE) values of the residuals. Gas-lifted system exhibits casing-heading instability where the states show oscillatory behaviour depending on the value of the input as discussed in section 5.4 but the results here did not change in a given pattern for each filter as the input was changed from the non oscillatory region to the oscillatory region. Therefore, for this noise distribution and model assumption, either of EKF or UKF can be used for nonlinear state estimation with UKF better preferred if computational cost is not considered when control solutions is used.

6.2 Gas-Lifted System State Estimation

Most control solutions in gas-lifted systems rely on sensor measurements that are not completely reliable due to the reasons above, hence the states or variables used in the controllers are unreliable. This is the case in Eikrem et al. (2002), Rashid, Demirel and Couët (2011) where a control solution was used to remove casing-heading instability assuming all measurements were available and reliable. However, in Eikrem, Imsland and Foss (2004), Eikrem, Aamo and Foss (2008), Aamo et al. (2005) top-side measurements were used by the observers and Kalman filters to estimate the states for the controller.

The performances of these filters on gas-lifted system vary due to the dependence of model on the underlying assumptions used at the modeling stage, in addition to the noise assumption. In the linear case, the Kalman filter is the optimal estimation methods used (SCIBILIA; HOVD; BITMEAD, 2008; KRISHNAMOORTHY; FOSS; SKOGESTAD, 2016). Gas-lifted system is inherently nonlinear and if it is used in this form, nonlinear filters such as Extended Kalman Filter (EKF) (SCHNEIDER; GEORGAKIS, 2013), Unscented Kalman Filter (UKF) (WAN; MERWE, 2000; BRADFORD; IMSLAND, 2018) or Particle Filter (PF) (ARULAMPALAM et al., 2002) among other nonlinear state estimation methods should be used. These nonlinear state estimation methods have been applied successfully in many fields such as navigation (KONATOWSKI; KANIEWSKI; MATUSZEWSKI, 2017), robot localization (WILBERS; MERFELS; STACHNISS, 2019), fault detection in chemical process, (MAHMUT; LIN; FU, 2017) but have not found much application in gas-lifted system. A close application to gas-lifted system are the use of EKF for leak detection in pipes (which may not necessarily be gas lift pipes) (TORRES et al., 2020) and UKF with linear model predictive control (MPC) for optimisation of gas-lifted system (SHARMA; GLEMMESTAD, 2012).

This limited application of nonlinear filters in gas-lifted system is due to the fact that linearizing the system about an operating point and applying the linear Kalman filter is usually sufficient in most control applications. However, as the demand for optimal operation of the system is increasing, using the nonlinear filters makes it possible to estimate the states at various points, hence making it easier to approach these demands as much as possible. The choice of filter type to use in state estimation depends on the accuracy requirements, the complexity of the filter, the computational demand, the speed of convergence and the degree of linearity of the system among others factors.

A hybrid approach to optimisation of gas-lifted system proposed in Krishnamoorthy, Foss and Skogestad (2018) reduces the steady state wait-time associated with static

real-time optimisation (RTO). This hybrid approach uses model adaptation that involves parameter update using dynamic models while optimisation takes place using static nonlinear models. To meet up with the model adaptation, speed of convergence is the most important consideration for filter selection. Faster filters such as that proposed in Zhang et al. (2019), which uses direct approach to parameter estimation are used to decrease convergence time of the parameter estimation. And when the sensor measurements are unreliable, this hybrid approach can be implemented at more optimal level using both state and parameter estimation approach.

State estimation in gas-lifted system is necessary for casing-heading instability minimisation or removal (AAMO et al., 2005) which was the subject of chapter 5. It is also necessary for fault diagnosis in gas-lifted system which is the subject of next chapter.

6.3 State Estimation

We present key features of various estimation techniques before comparing their performances. We first present the linear Kalman filter on which the nonlinear filters that we want to apply were built upon. In all the filter types presented, the estimation processes follow the same pattern of prediction and update. What differentiates the estimation processes is the method of prediction and update. Also, within the same filter type, these procedures can differ depending on the computational demand, accuracy or other considerations.

6.3.1 Kalman Filter (KF)

The Kalman filter (KF), introduced in 1960 estimates states of linear system whose model is not exactly known and the inaccuracy represented by the model noise as given in (6.1), with the noise itself given in (6.2) (KALMAN, 1960):

$$x_k = Ax_{k-1} + Bu_k + w_k \tag{6.1a}$$

$$y_k = Cx_k + v_k \tag{6.1b}$$

$$w \approx N(0, R), v \approx N(0, Q) \tag{6.2}$$

where w and v are the state and output noise respectively which are assumed to be white, uncorrelated and follow Gaussian distribution of zero mean and non-zero covariance. A, B and C are state transition matrix, input matrix and output matrix respectively.

The Kalman filter is an optimal estimator for linear system even if w and v are still not Gaussian. The Kalman filter combines information from system prediction and measurement to obtain the best estimates of the system by multiplying their probability density functions (PDFs). The gain is selected based on which provides more reliable information between the state estimates up to a given time instant and the measurement at the given time instant which are indicated by the covariance. This is done in stages which involves prediction stage and correction stage as described below:

Prediction:

$$\hat{x}_k^- = A\hat{x}_{k-1} + Bu_k \tag{6.3a}$$
$$P_k^- = AP_{k-1}A^T + Q \tag{6.3b}$$

Correction:

$$K_k = P_k^- C^T (CP_k^- C^T + R)^{-1} \tag{6.4a}$$
$$\hat{x}_k^+ = \hat{x}_k^- + K_k(y_k - C\hat{x}) \tag{6.4b}$$
$$P_k^+ = (I - K_k C)P_K^- \tag{6.4c}$$

where P, Q and R are the state error covariance, state noise covariance and measurement noise covariance respectively while K is the Kalman gain. The initial values for the estimated state and error covariance are (SIMON, 2006):

$$\begin{aligned} \hat{x}_0^+ &= E(x_0), \\ P_0^+ &= E\left[(x_0 - \hat{x}_0^+)(x_0 - \hat{x}_0^+)^T\right] \end{aligned} \tag{6.5}$$

where E implies expectation.

At prediction stage, the states are predicted based on the system model in (6.3a). Then the state error covariance matrix is obtained according to (6.3b), giving $\hat{x}_k^-$ (a priori

state) and P_k^- (appriori state error covariance) respectively. These are used to compute the Kalman gain (K) at the correction stage according to (6.4a). The estimated state is obtained based on available measurement and the state prediction according to (6.4b). The error covariance of the state estimates is then calculated from the estimated states according to (6.4c) giving $\hat{x}_k^+$ and P_k^+ which are the posterior states and error covariances respectively.

6.3.2 Extended Kalman Filter

Extended Kalman filter (EKF) is a variant of Kalman filter used for nonlinear optimal state estimation. The EKF is an improvement over the indirect approach for nonlinear state estimation called linearised Kalman filter. The indirect approach linearises the nonlinear system around a nominal point, form a new model based on linearisation error from the nominal point and apply the Kalman filter algorithm presented above. In EKF however, the state transition function can still be nonlinear while the covariances are computed based on linearisation of the state function and the output function. The nominal point in the linearised Kalman filter is replaced with the immediate past state estimate in a bootstrap process minimising the divergence of the estimated state.
Consider the nonlinear discrete system presented in (6.6):

$$x_k = f_{k-1}(x_{k-1}, u_{k-1}, w_k) \tag{6.6a}$$

$$y_k = g_k(x_k, v_k) \tag{6.6b}$$

The state estimates are obtained in a manner similar to the linear Kalman filter above except that prediction is preceded by finding the partial derivative of the state transition function at the previous state estimate to obtain the Jacobian matrices A and W in (6.7a). The update is preceded by finding the partial derivative of the measurement function at the predicted state to obtain the jacobian matrices C and V in (6.7b). These matrices are used in the prediction and correction stages for the EKF. This is because the EKF tries to use the most recent state. The most recent state during prediction is the recently estimated state at the immediate past sample time ($\hat{x}_{k-1}^+$). The most recent state during update is the just predicted state at the current sample time ($\hat{x}_k^-$). The state prediction however uses the nonlinear state transition function (6.6a) (SIMON, 2006).

Pre-Prediction:

$$A_{k-1} = \left.\frac{\partial f_{k-1}}{\partial x}\right|_{\hat{x}^+_{k-1}}, W_{k-1} = \left.\frac{\partial f_{k-1}}{\partial w}\right|_{\hat{x}^+_{k-1}} \tag{6.7a}$$

Pre-correction:

$$C_{k-1} = \left.\frac{\partial g_k}{\partial x}\right|_{\hat{x}^-_k}, V_{k-1} = \left.\frac{\partial g_k}{\partial v}\right|_{\hat{x}^-_k} \tag{6.7b}$$

The prediction and update procedure for the EKF is then given in (6.8) and (6.9) respectively.

Prediction:

$$\hat{x}^-_k = f_{k-1}(\hat{x}^+_{k-1}, u_{k-1}, 0) \tag{6.8a}$$
$$P^-_k = A_{k-1}P_{k-1}A^T_{k-1} + W_{k-1}Q_{k-1}W^T_{k-1} \tag{6.8b}$$

Correction:

$$K_k = P^-_k C^T_k (C_k P^-_k C^T_k + V_k R_k V^T_k)^{-1} \tag{6.9a}$$
$$\hat{x}^+_k = \hat{x}^-_k + K_k(y_k - g_k(\hat{x}^-_k, 0) \tag{6.9b}$$
$$P^+_k = (I - K_k C)P^-_K \tag{6.9c}$$

The partial derivative matrices (Jacobians) are used in the prediction and correction steps that use the nonlinear state transition function and output. Matrices W and V are identity matrices if the noises are additive which then makes (6.9a) to be equivalent to (6.4a). The use of the nonlinear function in the prediction in addition to the operating points being the immediate past state estimates makes this approach more accurate than the indirect (linearisation) approach for nonlinear filtering. Either approach is better than the linear Kalman filter in nonlinear estimation

Other variants of the EKF exist that minimise the linearisation error inherent in the EKF. These variants are called higher order EKF as they consider higher order terms in the Taylor series linearization (EINICKE, 2019).

6.3.3 Unscented Kalman Filter

The Extended Kalman filter (EKF) is adequate for a system that is not very nonlinear. As the EKF represents the entire system space with Gaussian random variable (GRV) that captures only two terms of Taylor series linearisation around the mean only, it is inadequate for highly nonlinear system. Unscented Kalman filter (UKF) works better in this case where it represents the system space by few carefully selected sigma points. The UKF uses the unscented transform (UT) to obtain the statistics of the estimated states.

The prediction stage is a three-step process that involves:

1. Forming the matrix of sigma points:

   Let (6.6) be the system model, n the number of sigma points, X the matrix of the sigma points, X_i the vector of the sigma points and $\bar{x}$ the mean of the state to be transformed. X contains $2n+1$ vectors distributed around and including $\bar{x}$ as given in (6.10):

   $$X_0 = \bar{x} \tag{6.10a}$$
   $$X_i = \bar{x} + (\sqrt{(n+\lambda)P_x})_i \quad i = 1.....2n \tag{6.10b}$$
   $$\lambda = \alpha^2(n+\kappa) - n \tag{6.10c}$$

   These sigma points are weighted and the weights, W are calculated as:

   $$W_0^{(\bar{x})} = \frac{\lambda}{L+\lambda} \tag{6.11a}$$
   $$W_0^{(P)} = \frac{\lambda}{L+\lambda} + (1 - \alpha^2 + \beta) \tag{6.11b}$$
   $$W_i^{(\bar{x})} = W_i^{(P)} = \frac{1}{2(L+\lambda)} \quad i = 1...2n \tag{6.11c}$$

   λ is a tuneable parameter. α determines the spread of the sigma points around $\bar{x}$. κ is a scaling parameter usually set to zero. β depends on knowledge of the distribution. It is 2 if the distribution is Gaussian.

2. Propagation through the nonlinear model:

   Each of the sigma points is then propagated through the nonlinear model (6.6a) to obtain $x_{predicted}$ which is the apriori state at the given sample time.

3. Obtain the estimates for the mean and covariances:

   The mean ($\bar{x}$) and covariance (P_x) are obtained as the weighted sum of the transformed sigma points as given in (6.12) (WAN; MERWE, 2000).

$$\bar{x} = \sum_{i=0}^{2n} W_i^{(\bar{x})} x_i \tag{6.12a}$$

$$P_x = \sum_{i=0}^{2n} W_i^{(P)} (x_i - \bar{x})(x_i - \bar{x})^T \tag{6.12b}$$

The correction involves:

1. Transform the sigma points into measurement space using (6.6b) to obtain y_t and compute transformed mean and co-variance similar to (6.12):

$$\bar{y} = \sum_{i=0}^{2n} W_i^{(\bar{y})} y_i \tag{6.13a}$$

$$P_y = \sum_{i=0}^{2n} W_i^{(P)} (y_i - \bar{y})(y_i - \bar{y})^T \tag{6.13b}$$

2. Obtain Kalman gain K as:

$$K = \sum_{i=0}^{2n} W_i^{(P)} (x_i - \bar{x})(y_i - \bar{y})^T P_y^{-1} \tag{6.14}$$

3. Compute the estimated state at k using:

$$\hat{x} = \bar{x} + K(y - \bar{y}) \tag{6.15}$$

By propagating the states through the nonlinear function approximated by three term approximation of Taylor's series, the statistics of the states hence the states are more accurate. This comes with higher computational cost in terms of memory space and processor cycles leading to increased calculation time.

6.3.4 Particle Filter

When the system is nonlinear and the state distribution is non-Gaussian, the UKF becomes insufficient for the state estimation hence particle filter is used. The PF represents the system states with particles similar to sigma points in UKF although the particles are randomly selected not using algorithm as in UKF. The estimate is determined by the probability that the state takes a certain value hence the state transition function, the state estimates and other variables are expressed as PDF. The final estimate is then obtained from the PDF using any method that is desired such as mean, expectation, states with maximum weight etc. The PF has prediction, correction and re-sampling stages.

At prediction stage, state hypothesis or particles are generated from the initial states of the system and propagated through the state transition function expressed in PDF as $p(x_k|x_{k-1})$. The state estimates at immediate past sample time, $p(x_{k-1}|Z_{k-1})$ combines with the state transition function to form the state prediction $p(x_k|Z_{k-1})$ as given in (6.16) (ELFRING; TORTA; MOLENGRAFT, 2021).

$$p(x_k|Z_{k-1}) = \int p(x_k|x_{k-1})p(x_{k-1}|Z_{k-1})d_{k-1} \tag{6.16}$$

At correction, conditional PDF of the measurement, $p(z_k|x_k)$ is computed based on the measurement function in (6.6b) and the knowledge of the PDF of the noise (v_k) while the PDF of measurement based on available measurements up to time $k-1$ is computed as in (6.17) (ELFRING; TORTA; MOLENGRAFT, 2021).

$$p(z_k|Z_{k-1}) = \int p(z_k|x_k)p(z_{k-1}|Z_{k-1})d_k \tag{6.17}$$

The PDF of the estimated state is therefore obtained as (ELFRING; TORTA; MOLENGRAFT, 2021):

$$p(x_k|Z_k) = \frac{p(z_k|x_k)p(x_k|Z_{k-1})}{p(z_k|Z_{k-1})} \tag{6.18}$$

The measurement Z_{k-1}, refers to measurement from time t = 0 to t = $k-1$ which is $Z_{0:k-1}$, but (Z_{k-1}) is used because it is assumed that the information in all the previous measurements is already contained in it. Similar reason is given for (x_{k-1}). Also, to differentiate between sensor output and measurement obtained using the measurement function (6.6b), we use upper case Z for sensor output and lower case for the function

output. Equation (6.18) can be converted to summation by transforming the integral PDF into discreet form using the Dirac function which is 1 at the given point and zero everywhere else thereby approximating it in (6.19)

$$p(x_k|Z_k) = \sum_{i=1}^{N} W_k^i \delta(x_k - x_k^i) \tag{6.19}$$

Where W is the weight of the particles and N is the total number of particles. From (6.19) the desired statistics such as mean, maximum particle value or machine learning approach are used to obtain the state estimates. At the resampling state, new particles are selected again based on the weights. The weights are used to compute a value that shows if the current particles still represent the state distribution accurately enough. This value called effective number of particles denoted as N_{eff} is given in (6.20) as:

$$N_{eff} = \frac{1}{\sum_{i=1}^{N} (W_k^i)^2} \tag{6.20}$$

Since the weight w is normalised to sum to 1, the more particles that still contribute to the distribution (particles with reasonable weights), the more the value of N_{eff}. Hence a threshold is set which when N_{eff} falls below, resampling takes place. Resampling can also take place at fixed time interval or using a threshold defined based on the inverse of the particle weights. But Elfring, Torta and Molengraft (2021) showed that using the N_{eff} reduces the number of resampling steps compared to the other methods described above.

Table (11) presents a summary of the major estimation types discussed briefly. It is seen there that the complexity of the estimation type varies from the very simple linear Kalman filter to the very complicated particle filter which also shows the variation of the performance.

6.4 Gas-Lifted Input and Measurements

The input in this chapter is the percentage valve opening represented as u that controls the flow rate of produced fluid through the production choke as discussed in chapters (4) and (5). The measurements are annulus pressure (P_a), wellhead pressure (P_{wh}) and mixture density (ρ_t) which are readily available from the sensors and are reliable (SCI-

Table 11: Summary of the main estimation methods

Estimator type	System Type	Key Method Used	Complexity
Kalman Filter	Linear with gaussian noise	Multiplication of the covariances	Very simple
Extended Kalman Filter	Nonlinear with Gaussian noise	Linearisation/Kalman filter or partial derivative with nonlinear state transition function	Simple
Unscented Kalman Filter	Highly nonlinear with Gaussian noise	Selection of sigma points and utilisation of UT	Complex
Particle Filter	Highly nonlinear with non Gaussian noise	Propagation of randomly selected particles from the initial states/use Bayesian approach for state estimates	Very complex

BILIA; HOVD; BITMEAD, 2008). The estimated variables are usually the downhole pressure which are controlled to a given setpoint to allow the continuous flow of gas from annulus into the tubing. In our case here, the estimated variables are the gas lift states.

6.5 Filters Performances on Gas-Lifted System

In this section, we compare the performances of the three nonlinear filters on the gas-lifted system. The assumed distribution is Gaussian for all three filters. The initial condition, x_0=[2300 750 5800] kg is the same for all three filters and the input is fixed at $u = 0.6$ throughout for all three filters. The state covariance, $P_0 = diag([100\ 10\ 1000])$, the state noise, $Q = diag([100\ 16\ 160])$ and the measurement noise, $R = diag([1000\ 1000\ 40])$ are the same for all three filters. All these were selected by trial and error but putting into consideration, the ratio of the values of the states and measurements. The sampling time is $60s$ (1 minute) for all three filters and the system was simulated over 150 samples (2.5hrs). For the UKF, $\alpha = 10^{-3}$ was chosen by trial and error, $\beta = 2$ due to the assumed Gaussian distribution and $\kappa = 0$. The PF used maximum weight to obtain the state estimates from the posterior distribution, since the weight reflects the probability that the true state is the given particle (the states with higher weight has higher chance of being the true state of the system). The threshold for triggering resampling was set to 0.8 to quickly remove particles that were not contributing significantly to the distribution while the sampling method was residual. All the simulations were done in MATLAB version R2021a (THE MATHWORKS, INC., 2021). Euler and ODE15S were used to solve state trajectories of the differential algebraic equation (DAE).

6.5.1 States and Residuals Visualisation

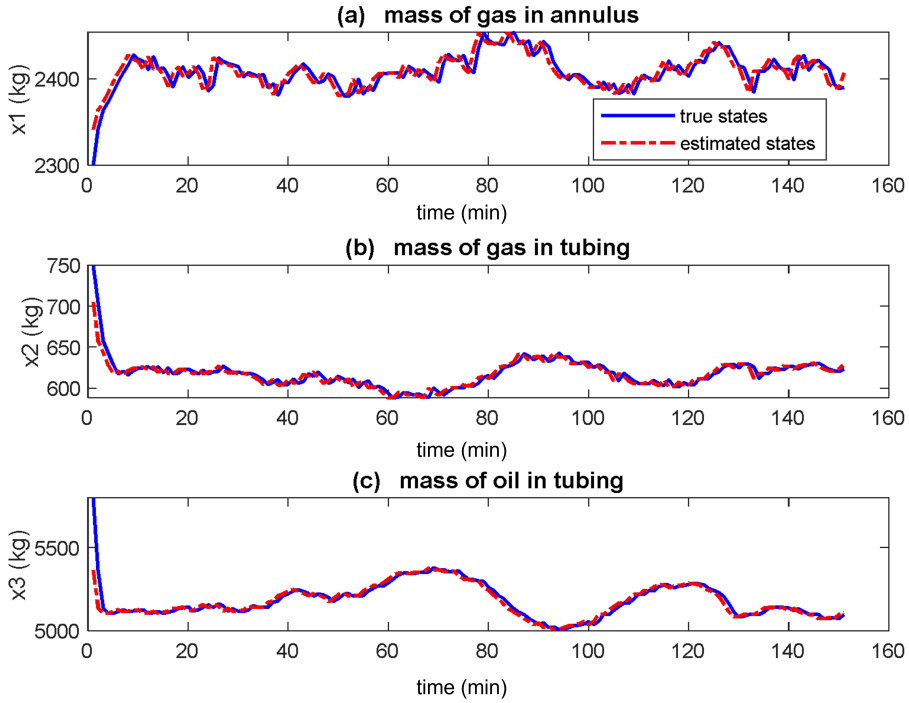

Figure 59: True and estimated states of gas-lifted system using extended Kalman filter (EKF). All three states estimates (red dash-dotted lines) converge to the true states (blue solid line) about the same time. These states are the mass of gas in annulus, the mass of gas in tubing and the mass of oil in tubing respectively.

Figure 59, Figure 60 and Figure 61 show the true and estimated states for the EKF, UKF and PF respectively. In Figure 59 the estimated states (red dash-dotted) converge to the actual states (blue solid) in under 10 minutes for all three states. The estimated states converge to the true states in Figure 60 too but at different times with x_2 fastest whereas x_3 being the slowest. Figure 61 shows that the estimated states track the actual states poorly.

The effect of random sampling of the states into particles and obtaining the state estimates from the posterior distribution is seen in the poor tracking performance of the PF. While the UKF also samples the states before using the unscented transformation to obtain the anterior state statistics, the sampling here was carefully and deterministically done hence UKF tracked better than PF. Unlike in the case of EKF and UKF where each state is propagated through the state transition function and are estimated individually, the PF propagates states hypotheses. The consequence of this is that the actual state is not being properly tracked like that of the EKF and UKF. The result was not better when the state estimate was obtained from the posterior distribution by using the mean

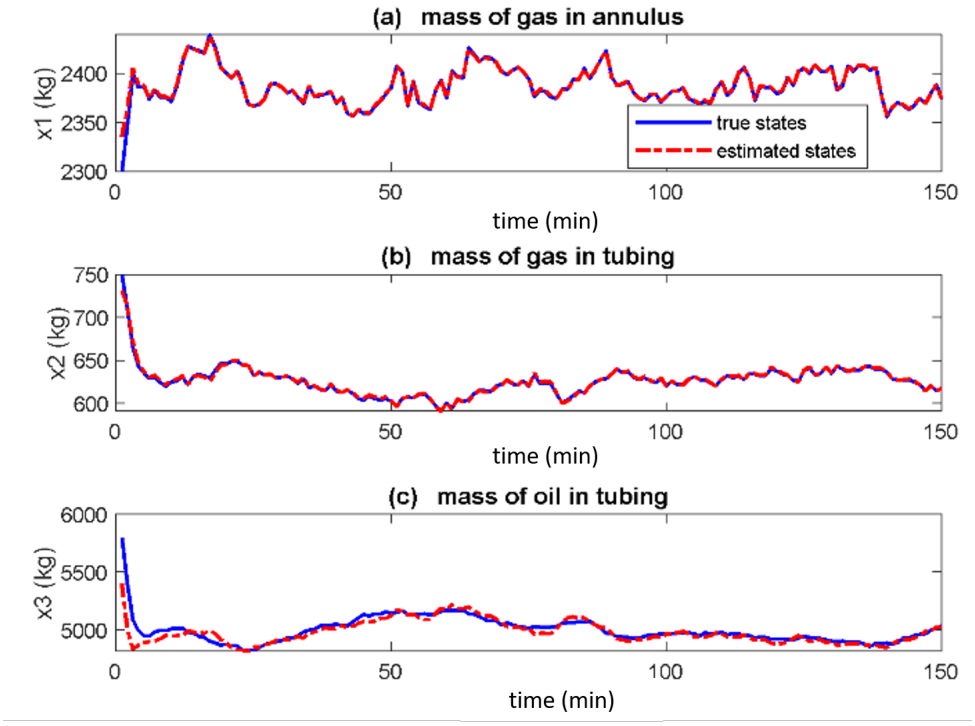

Figure 60: True and estimated states of gas-lifted system using Unscented Kalman Filter (UKF). The estimated states converge at different times with x_2 fastest and x_3 slowest.

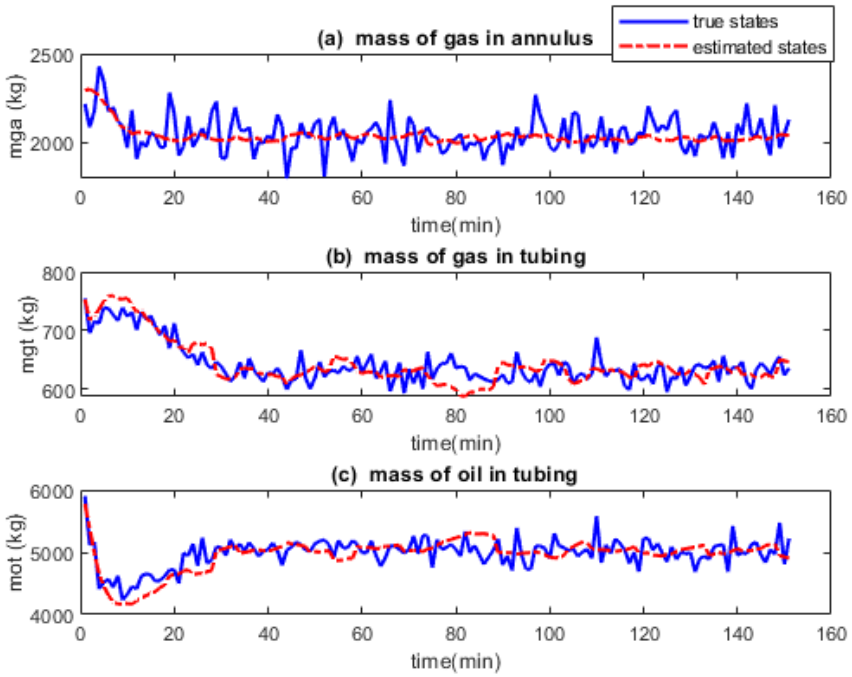

Figure 61: True and estimated states of gas-lifted system using particle Filter (PF). The estimated states do not converge to the true states exactly due to the particle sampling techniques used by PF.

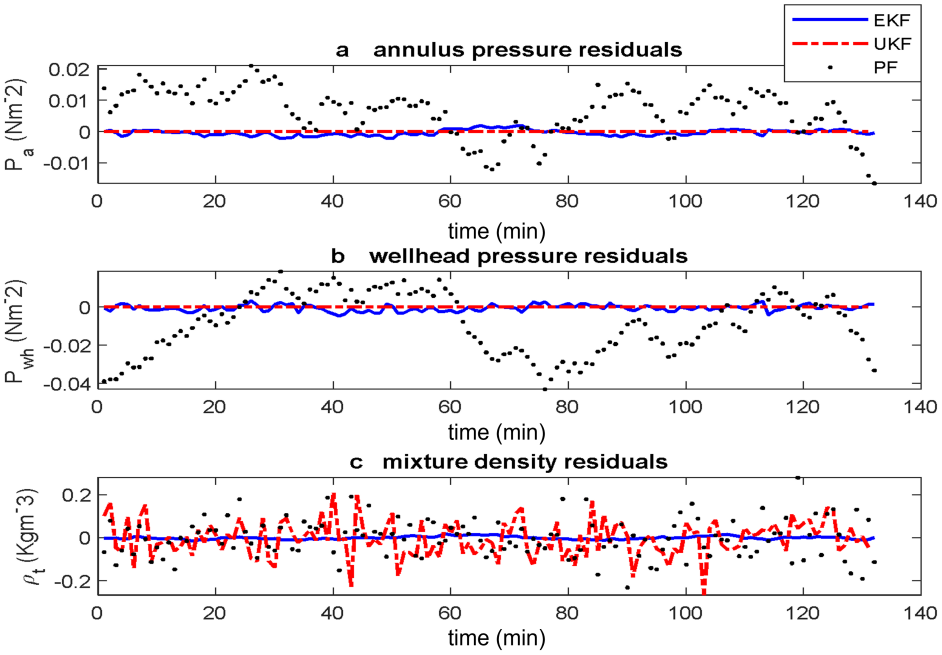

Figure 62: Estimated states full residuals of gas-lifted system using EKF, UKF and PF. The residuals from estimating using PF is the poorest for the three measurements.

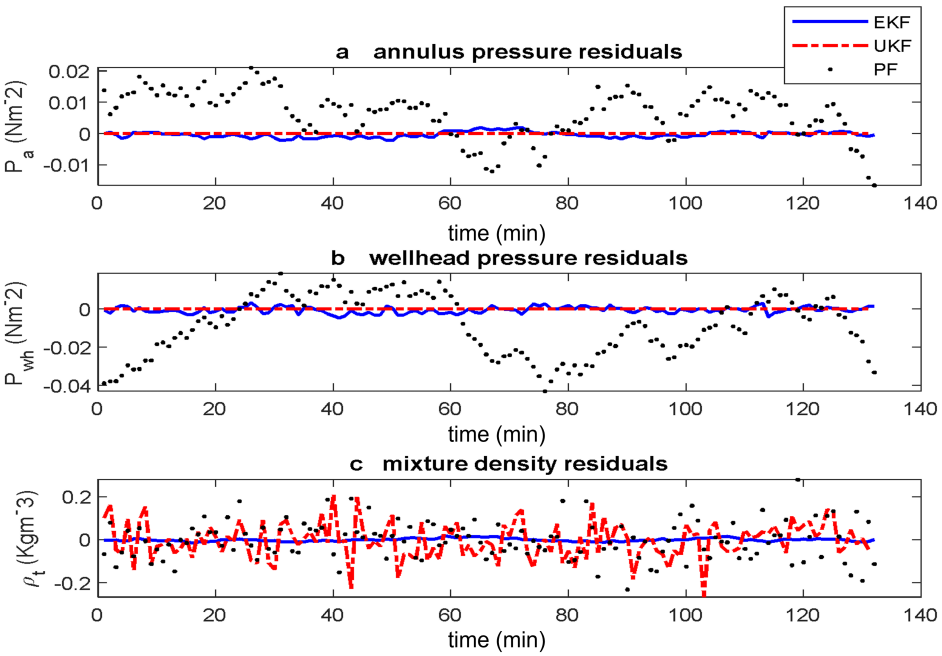

Figure 63: Estimated states normalised residuals of gas-lifted system using EKF, UKF and PF. The normalised residuals is obtained from the residuals by dividing each residual by the corresponding steady state value.

of the particles despite that the true state was believed to be around the mean of the 3,000 particles.

From Figure 59 and Figure 60, the UKF tracks better than EKF due to the use of

three term approximation of Taylor series of the nonlinear system by the UKF while EKF uses two terms. Hence based on visualisation of the true and estimated states, the UKF performs the best whereas the PF performs worst. This result is different from the one performed on mechanical system by Konatowski, Kaniewski and Matuszewski (2017) where EKF performed poorly while the performances of UKF and PF were similar. This justifies the extension of this methods to gas-lifted system as the performance of the filters depends also on the system whose states are estimated in addition to the noise distribution.

The initial slow convergence of the states means that the residuals have higher magnitude for the first few state estimates. We removed this transient part and show in Figure 62, the residuals. In all three measurements, the residuals from the PF is larger than the EKF and the UKF reaching a value of 2.1x10^5, -1.8x10^5 and 1.8x10^1 for P_a, P_{wh} and ρ_t respectively. The UKF has smaller residual than the EKF for P_a and P_{wh} but bigger for ρ_t indicating that the UKF still has the best estimation performance by residual visualisation.

We examined the residuals further by first considering the normalised residuals. The normalised residuals were obtained by dividing the residuals by the steady state values of the actual measurements given as $y_{True} = [P_a\ P_{wh}\ \rho_t] = [9930500Nm^{-2}\ 4678800Nm^{-2}\ 71.9316Kgm^{-3}]$. Figure 63 shows the normalised residual plots. For each output, the residuals resulting from EKF (blue solid line), UKF (red dash-dotted line) and PF (blue dotted line) were compared.

We observe from Figure 63 that normalised residual has very low value especially for the EKF and the UKF. On zooming Figure 63 at steady state, these values were of the order of $1X10^{-3}$ for UKF and $3X10^{-3}$ for EKF but about 0.2 and -0.2 for PF when the residual was the mixture density. This shows that the estimates are better in EKF and UKF than in PF with UKF still the best. Also for the three measurements, the distribution of the residuals around the zero line is poor for the PF except the case of ρ_t in Figure 63c. Furthermore, the distribution of the residual for EKF and UKF are however even around the zero line including in Figure 63c where the residual for the UKF is large. The more even the distribution of the residuals around the zero line, the better the estimated states.

The above estimation was performed at fixed value of $u = 0.6$ which was in the stable region. The performance of the filters depends on the degree of linearity of the system and the noise distribution. The gas-lifted system is known to exhibit different behaviour as

input increases from 0 to 1. We therefore performed statistical test on the residuals. The first check was to see if the residuals of the filters outputs follow Gaussian distribution of zero mean and non-zero variance. This we obtained from the expectation test on the residual. Next, we examined the RMSE for the residuals of gas-lifted system at three different inputs: $u = 0.60$, $u = 0.75$ and $u = 0.90$. These inputs correspond to the system in stable region, the system sliding into unstable region and the system fully into casing-heading instability region respectively.

6.5.2 Statistical Tests

Two tests were performed on the residual here: the expected value test to examine the shape of the residual distribution and the root-mean-square-error to show how close the estimates are to the true states.

6.5.2.1 Expected Value Test

Since it is impossible to perform infinite number of experiments to determine if the mean of the residual is close to zero, we used the expected value test to infer the centre of the residual distributions and with hypothesis test, we checked the mean of the entire residual distribution. The residual (innovation since it is stochastic) was obtained as the difference between the actual measurements from sensors and the outputs computed using output function in (6.6b) with the states being the estimated states. The residual that is more evenly distributed around zero produces a distribution that is close to normal and increases the accuracy of estimation. Non-normality of residual does not exactly translate into poor estimation especially in the case of nonlinear states with many samples, however, it helps to compare the performance of the estimation methods. 151 samples were used for each filter simulations and the mean value for the residuals was computed using (6.21).

$$\bar{r}(k) = \frac{1}{N}\sum_{i=1}^{N} r_i(k) \tag{6.21}$$

where r is the residual k is the measurement index corresponding to P_a, P_{wh} and ρ_t, N is the number of samples which is 151 here and $\bar{r}$ is the mean of the residuals.

The hypothesis test was conducted on the computed mean of the residuals for the three measurements and table 12 shows the results for the 9 residuals. Checkmark '✓' represents true hypothesis which is that the residual comes from a normal distribution while an 'X' represents an alternative hypothesis which is that the residual does not come

Table 12: Hypothesis test for the residuals for estimates with EKF, UKF and PF. ✓indicates true hypothesis (which indicates the mean of the residual is zero) while X indicates the alternative hypothesis (which is that the mean of the residual is not zero). The P-Values are also indicated.

Residual	EKF	UKF	PF
P_a	X	X	X
	$1.9\text{x}10^{-4}$	4.3x^{-3}	$3.8\text{x}10^{-36}$
P_{wh}	X	X	X
	$1.5\text{x}10^{-3}$	$3.2\text{x}10^{-12}$	$2.2\text{x}10^{-58}$
ρ_t	✓	✓	X
	$7.1\text{x}10^{-1}$	$6.6\text{x}10^{-1}$	$3.9\text{x}10^{-3}$

from a distribution that is normal. The corresponding p-values are also provided in the table.

Optimal estimation is associated with linear Kalman filter where the state and the measurement functions are linear and the noise is Gaussian. The effect of this is that when the state with Gaussian distribution is estimated, the residual (innovation) is Gaussian. This is not the case with other filters whose models are nonlinear. We therefore used the hypothesis test on the residual to see how close the nonlinear filter residuals are to being Gaussian. As seen in table 12, the entries for most of the hypothesis tests indicate that the residuals did not come from a distribution that is Gaussian except for the residual ρ_t for both EKF and UKF. The acceptance of true hypothesis in these two isolated cases is not enough to draw the conclusion that the residual of the mixture density is normal when estimated with EKF and UKF as this might have happened by chance.

The p-values that indicate the chance that the true hypothesis holds were also provided and they indicate that EKF and UKF have higher chance of having residuals that are normal since they have higher p-values than the PF. The p-values of UKF is better (bigger) than that of EKF except for P_{wh}. The PF has the least performance as the p-values are smaller than those of EKF and UKF. Both residual visualisation and the expected value test indicated that UKF is slightly more accurate than EKF with PF having the lowest estimation accuracy of the three filters for this system.

6.5.2.2 Root-Mean-Square-Error (RMSE)

The RMSE for the residual is the most common error metric for testing the accuracy of the filters (ATKINSON; RICHTER; THROCKMORTON, 2018; KONATOWSKI; KANIEWSKI; MATUSZEWSKI, 2017; SCHNEIDER; GEORGAKIS, 2013). We examined the RMSE for the filters under 3 different input conditions to see if the accuracy of

Table 13: RMSE for estimates with EKF, UKF and PF with casing-heading instability. Hypothesis test on the residual is provided where ✓indicates true hypothesis while X indicates the alternative hypothesis.

u	Residual	EKF	UKF	PF
0.60	P_a	X	X	X
		$9.1\text{x}10^3$	23	$6.4\text{x}10^4$
	P_{wh}	X	X	X
		$7.8\text{x}10^3$	$1.1\text{x}10^2$	$5.0\text{x}10^4$
	ρ_t	✓	✓	X
		0.52	6.4	6.2
0.75	P_a	X	X	X
		$1.4\text{x}10^4$	23	$7.1\text{x}10^4$
	P_{wh}	X	X	X
		$7.9\text{x}10^3$	$1.4\text{x}10^2$	$3.7\text{x}10^4$
	ρ_t	✓	✓	X
		0.97	6.6	6.3
0.90	P_a	X	✓	X
		$2.6\text{x}10^4$	25	$3.0\text{x}10^5$
	P_{wh}	X	X	X
		$7.6\text{x}10^3$	$1.2\text{x}10^2$	$1.4\text{x}10^5$
	ρ_t	✓	✓	X
		2.1	6.4	6.0

the filter depends noticeably on effect of the casing-heading instability. Casing-heading instability results from the oscillatory behaviour of system depending on the input value. These inputs are u=0.6, u=0.75 and u=0.9 which correspond to the stable region, the region going into casing-heading instability and the region inside casing-heading instability respectively. Table 13 shows the hypothesis test and the RMSE for the three filters for u=0.6, u=7.5 and u=0.9 respectively.

It can be observed from table 13 that for all the three input values, the hypotheses tests is the same except for the P_a that changes to true hypothesis when $u = 0.9$ while it is the alternative hypothesis for $u = 0.60$ and $u = 0.75$. Again this might have happened by chance. While the RMSE of P_a residuals resulting from estimating with EKF increases from $9.1\text{x}10^3$ to $14\text{x}10^3$ and $26\text{x}10^3$, for the same EKF, the P_{wh} residual increases from $7.8\text{x}10^3$ to $7.9\text{x}10^3$ and then decreases to $7.6\text{x}10^3$ for u=0.6, u=0.75 and u=0.9 respectively. The RMSE of the ρ_t residual for estimation using EKF increases from 0.52 to 0.97 to 2.1. The RMSE for estimates using UKF does not show much variation in values as u is changed into the unstable region. The estimation using PF behaves similar to UKF as the RMSE for P_a increases from $6.4\text{x}10^4$ to $7.1\text{x}10^4$ to $30\text{x}10^4$.

This shows that there is no defined behaviour of the estimation accuracy of the non-

linear filters as input changes from the non-oscillatory region to the oscillatory region. But using UKF still shows better prospect as it appears to have the least of the change in RMSE when gas-lifted system is operated within these input range. Also note that the best indicator of the accuracy of the measurement is the value of the RMSE of the residuals and residual visualisation. The statistical test does not affect significantly the acceptance of the estimation accuracy considering that the states are nonlinear. This will be different if the states are linear and the noise distribution is Gaussian where having a normally distributed residual gives us confidence of the degree of accuracy of our estimation. Also care should be taken to interpret $'X'$ in tables 12 and 13 as failure of the null hypothesis test and not as products (multiplication).

The estimation accuracy depends on the proper selection of the matrices P, Q and R as described in (SCHNEIDER; GEORGAKIS, 2013). We examined how the change in R affected the filter performance using EKF on x_1 (mass of gas in annulus). Figure 64 shows the true and estimated states for R = [10 10 4], [100 100 40] and [1000 1000 400] respectively. Figure 64 shows that there is no significant difference in the estimates for these different values of R. A minor difference exists during the transient state and during a major change in the direction of the graph. Similar results were obtained when the different filters were used with other states. This result indicates that for the gas-lifted system where we selected P, Q and R arbitrarily, the previous results were not affected significantly by these choices.

6.6 Concluding Remarks

It was shown here that the gas-lifted system nonlinear states can be estimated directly using one of EKF, UKF or PF without the need to linearise the system and apply linear Kalman filter. Based on the noise assumption here, UKF performed slightly better than EKF by examining the RMSE for the residuals, visualising the states and examining the residual using the hypothesis test. This is because the UKF uses three term approximation of Taylor series while EKF uses two terms. The additional term improve the accuracy of the UKF over the EKF for the system. The performance of PF was least. But with the computational advantage of the EKF, the states of gas-lifted system can be estimated using the EKF since there is just a small difference in performance between using it and UKF. Hence for nonlinear control applications such as casing-heading instability, fault detection and diagnosis and general optimal operation of gas-lifted systems, with Gaussian noise, EKF can be used for state estimation.

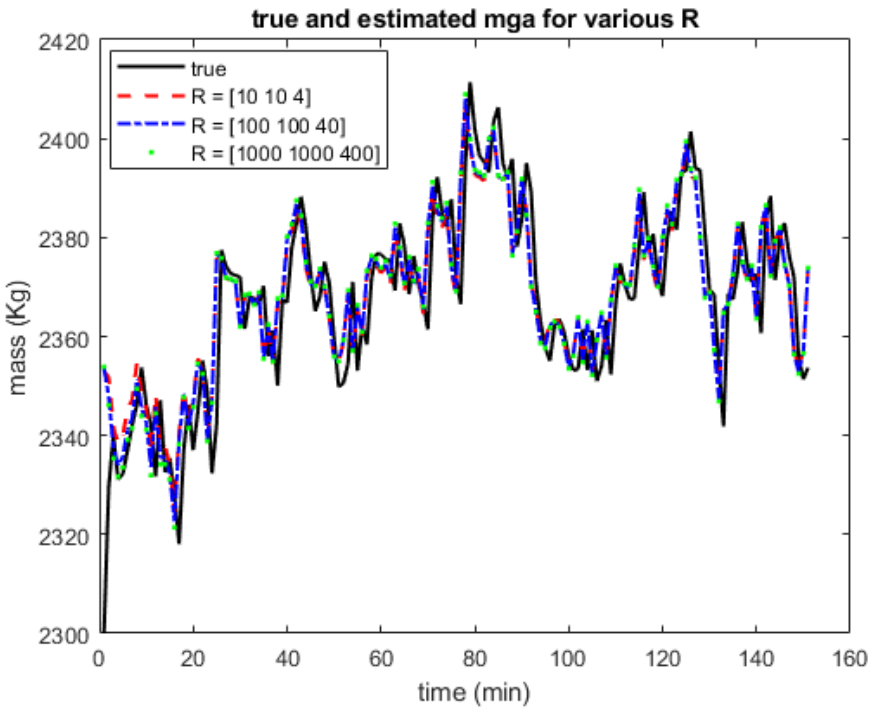

Figure 64: Estimated states and actual states for various values of R. The estimates did not change significantly with the values of R.

The comparison here was based on the estimation error and did not consider explicitly the speed of convergence of the estimates to the true states because sampling times are larger in gas-lifted system than in electrical and mechanical systems. Further works should consider both estimation error and the speed of convergence considering the importance of speed of convergence in parameter estimation for the hybrid optimisation in gas lift network.

7 FAULT-TOLERANT CONTROL OF GAS-LIFTED OIL WELL

7.1 Background

The gas-lifted system has inherent ability to hide the effect of fault hence the system can inject gas into the annulus and oil will still be produced even in the presence of fault of significant value. This however affects the optimal operation of the system and could move the system towards the undesirable casing-heading instability. Faults of step decrease in the valves coefficients in addition to limitation on the valve affect the optimal flow of the liquids through the system.

In this chapter, we detected and isolated valve faults using (GLRT) and (DOS). The states were estimated using (EKF). Model predictive control based (FTC) was then implemented on the system by using the robustness property of the zone control MPC and limiting the input bound in the optimiser. Both passive and active FTC were used to improve oil production or stabilise the system. Passive FTC provided more robustness but low output change. Reducing the upper control bound ensured stability but production could decline. Increasing the controller cost term that prioritises the input target increased production but it was prone to casing-heading instability.

7.2 Gas-Lifted System Fault-Tolerant Control

Gas-lifted system control is designed with the assumption of nominal operation of the system. The constraints for the optimisation or the controller are based on the fully functioning valves and sensors. But due to the nature of materials transported through the valve such as hydrates, wax, asphatenes, oil, gas (JAHANSHAHI, 2013) and its location, faults occur in the valves that tend to degrade the performance of the system or even make the operation of the system dangerous. This is in addition to the fact that all automated systems are prone to fault (BLANKE et al., 2000). Optimal and safe operation of the

gas-lifted system must therefore include fault-tolerant control (FTC).

Fault-tolerant control is an approach to use a controller in ensuring that a given safety-critical system functions to satisfactory level in the presence of fault of a given magnitude (BLANKE et al., 2000). FTC is implemented using either passive approach or active approach. Passive FTC, employs the robustness of controller without the need for model update or controller reconfiguration. Active FTC however apply accommodation or control reconfiguration based on knowledge of fault presence and the magnitude of the fault (OCAMPO-MARTÍNEZ et al., 2005). In general, any means where fault effect on the plant or controller parameters is considered during controller design and plant operation is taken as FTC (CAMACHO; ALAMO; PEÑA, 2010).

MPC exhibits inherent fault-tolerance capabilities hence its use in FTC which dates back to the 90's and now has wide applications in various industries (MACIEJOWSKI, 1997a),(MACIEJOWSKI, 1997b). In Ocampo-Martínez et al. (2005), the fault-tolerant capacity of MPC was used to monitor flow through actuators valves in Barcelona sewage system. Both passive FTC and active FTC performances on the sewage system were compared with the active case as expected, performing better in the network. In Rosich, Puig and Quevedo (2006), explicit MPC was used for low level control of fuel cell in power system. Faults that affect the compressor range of operation were accommodated by computing offline the control law that takes note of the fault effects on the compressor. The use of MPC for fault-tolerant control of a satellite system is presented in (SANTOS, 2011). However, the use of MPC in the fault-tolerant operation of gas-lifted system is yet to be reported in literature.

MPC fault-tolerant control is implemented by combining an online fault detection and identification (FDI) unit with a supervisory unit. The supervisory unit informs the MPC on either to modify the objectives to take into account the fault effect or change the constraints to reflect the current limitations of the inputs (ROSICH; PUIG; QUEVEDO, 2006). This is however possible under the assumptions that: (a) the FDI unit is working reliably (b) the MPC prediction model can be updated automatically and (c) the MPC control objective can be left unchanged after fault occurrence (MACIEJOWSKI, 2000). In cases where the system states can be measured accurately, the FDI unit takes the plant input and output to analyse the fault and provide the supervisory unit with the fault magnitude and presence as in the case of sewer models state (OCAMPO-MARTÍNEZ et al., 2005). Where the state measurements are not reliable, the FDI unit is combined with estimation or filter unit to provide the fault information to the supervisory unit and also provide the MPC with updated state estimates as used in the satellite models in

(SANTOS, 2011).

Optimal operation of gas-lifted system using nonlinear model predictive control (NMPC) with zone control for casing-heading stabilisation was presented in (ADUKWU; ODLOAK; JUNIOR, 2020),(ADUKWU; ODLOAK; KASSAB, 2023b) and discussed in chapter (5). This zone control NMPC has inherent FTC capabilities which were not considered in the article but the controller can accommodate fault of low magnitude while still keeping the system states in their zones as shown in (ADUKWU; ODLOAK; KASSAB, 2023a). In the passive FTC, the gas-lifted system zones can be carefully selected to aid continuous flow of gas from the annulus to the tubing and the controller parameters selected such as to keep the system far from the zone boundaries in the event of minimal fault. In the active case, the zone control MPC can combine this robustness property with model adaption, constraint change and objective prioritisation to obtain better FTC performance.

The flow rate through the gas lift valves depends on the valve coefficients which is a lump parameter that determines the flow per unit pressure drop across the valve at constant temperature and density of the liquid. Faults in valve affect this parameter which are to remain constant when pressure drop is constant. The occurrence of cavitation and flash in addition to other sources of wears and tears in the gas-lifted system valves alter this gas coefficients hence change the controller internal model (ULANICKI; PICINALI; JANUS, 2015). This change in valve coefficient can be modeled as step fault in the valve coefficient hence fault-tolerant control using MPC implemented for optimal operation of the system.

In this chapter, we applied FTC in the optimal operation of gas-lifted system similar to Ocampo-Martínez et al. (2005) in sewage networks and Rosich, Puig and Quevedo (2006) in fuel cell. The key difference between the work here and these articles are: (a) the use of an NMPC to increase prediction range of our model. (b) the FDI unit combined with state estimation to form the FDI/filter unit. While the estimator component of the FDI/filter unit provided the state estimates to the controller, the FDI component used the state estimates to provide the supervisory unit with the health status of the system. (c) Passive FTC was applied to fault resulting from decrease in C_{pc} while active FTC was applied to faults resulting from increase in C_{pc} and decrease in valve operating range. (d) Gas-lifted system is a differential algebraic equation (DAE) system that is not straightforward to solve like the ordinary differential equation (ODE) system presented in those articles.

Figure 65 shows the schematic of the FTC implemented in this chapter. The state

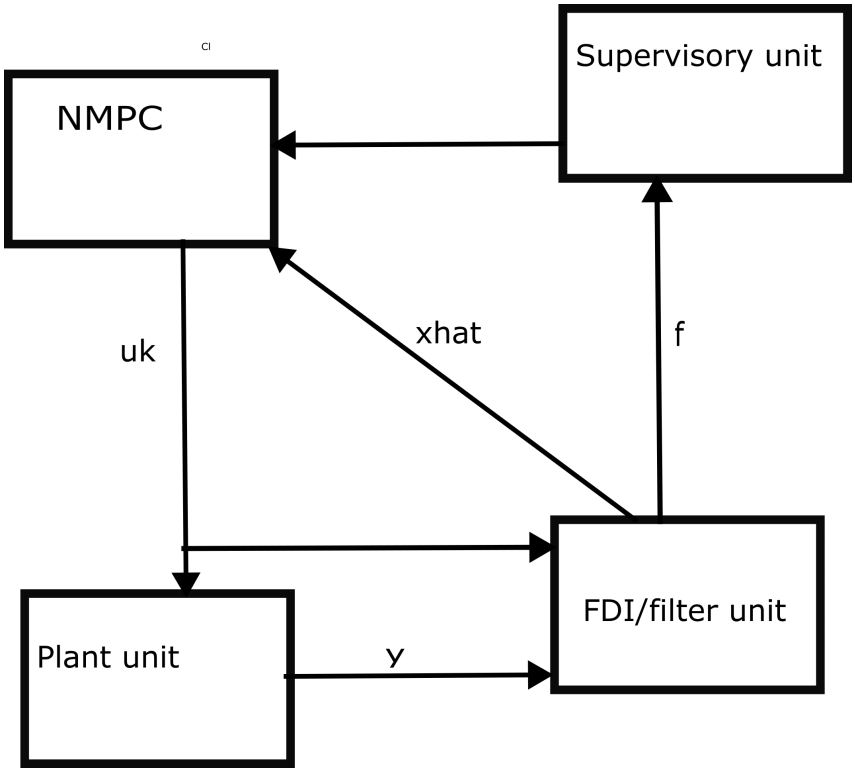

Figure 65: Schematic of fault-tolerant control (FTC). The fault diagnosis and identification (FDI) unit combines with the estimation unit to provide the supervisor unit with fault information and the NMPC with the estimated states.

estimation/FDI unit operated separately from the optimisation/control unit. The state estimation used Extended Kalman filter (EKF) to provide the FDI sub-unit with the state estimates and also provided the MPC with updated state estimates (ADUKWU et al., 2022; BLANKE et al., 2006). The EKF used here is presented in Apendix D while further details are found in (SIMON, 2006). The FDI used generalised likelihood ratio test (GLRT) to detect fault and estimate its magnitude (BLANKE et al., 2006). When fault was detected, the supervisory unit of the system operation determined the next operation. This action was either to change the upper bound of the valve constraints or alter the objective function priority in the controller. This takes advantage of MPC ease of representation of faults. While model modification is used for representing process fault like change in valve coefficients, input constraints modifications are used for valve faults (MACIEJOWSKI, 2002; CAMACHO; ALBA, 2013).

7.3 Preliminaries

This chapter deals with fault-tolerant control (FTC) for gas-lifted system with valve faults using model predictive control. The controller used is the NMPC presented in

chapter (3). It is a zone control MPC with input target. Further details of zone control MPC can be found in (GONZÁLEZ; ODLOAK, 2009; CAPRON; ODLOAK, 2018). A brief discussion of fault-tolerant control in gas-lifted system valves using nonlinear MPC is therefore presented in this section. Gas-lifted system description is detailed in (XU; GOLAN, 1989)

7.3.1 Valve Faults

Fault is an uncommitted deviation in the characteristics of all or a part of the system making the system unable to perform its function satisfactorily. Fault diagnosis involves three activities: (a) fault detection: detecting the occurrence of a fault, (b) fault isolation: identifying faulty components and (c) fault identification: determining the magnitude and type of fault.

Valve faults could either be a stuck fault where the valve remains in one position irrespective of the control command, an outage fault when the valve delivers no input to the gas-lifted system or partial degradation where the performance of the valve decays with time. Partial degradation is considered as either a sudden change in the valve coefficient leading to an abrupt fault, a gradual change in the valve coefficient leading to a incipient fault/ramp fault or impulse in the coefficient.

Faults in valve include: valve clogging, positioner supply pressure drop, fully or partially opened bypass valve, flow rate sensor fault, internal leakage, stem displacement fault (VENKATA; RAO, 2019). Some of these faults such as valve clogging, positioner supply pressure drop etc can have a jump effect on the flow rate. Also, the occurrence of cavitation and flashing degrade the performance of control valves (ULANICKI; PICINALI; JANUS, 2015). In deriving flow rate equation in gas-lifted system, all the constants that affect the flow rate through the valve are lumped together as the valve coefficients. For the flow through the injection valve, the C_{iv} is seen as the flow rate per unit pressure change (P) and percentage valve opening at a given temperature for a fluid of fixed density. Consequently, the flow rate through the valve is controlled by the coefficient and the percentage valve opening if the pressure, density and temperature are fixed. Similarly, fault affect the control of flow rate using the parameter, C_{pc}. These consequently affect the system dynamics that is purely determined by the flow rates. We therefore perform the fault diagnosis assuming these faults lead to a step change in the valve coefficient.

7.3.2 Generalised likelihood Ratio Test (GLRT)

The gas-lifted system considered here is noisy resulting from both measurement and process noise. A Gaussian noise assumption was made in this chapter. For our fault detection and diagnosis, we used the generalised likelihood ratio test (GLRT). The GLRT is a hypothesis testing algorithm for a sequence of random variables whose parameter dependent PDF is suspected to have changed due to the change in parameter from a value θ_0 to another value θ_1, where $\theta_0 \neq \theta_1$. θ_0 is usually known and if θ_1 is unknown, the GLRT is employed to obtain a decision function. But if θ_1 is known, the cummulative sum (CUSUM) approach is employed in obtaining the decision function to detect the change in the random sequence (WILLERSRUD et al., 2015).

Fault has the tendency to change this parameter from θ_0 to θ_1 as shown in Figure 66. In Figure 66, the residuals for the faulty and faultless cases have the same variance but the mean of the two cases differ. The presence of fault caused the mean of the residual of the system to change from zero in the no-fault case (dark solid) to 2 in the faulty case (red dashed). The GLRT for such change detection is based on the decision function given in (7.1).

$$g(k) = (\frac{1}{2\sigma^2})_{\max_{k-N+1<j<k}} \frac{1}{k+j-1} \left[\sum_{i=j}^{k} (y(i) - \mu_0)\right]^2 \tag{7.1}$$

Where k is the sample time, σ is the standard deviation of the faultless system, N is the window size and μ_0 is the vector of mean for the parameters when fault is not applied (WILLERSRUD et al., 2013b). N must be selected such that the time between detection and occurrence of fault is less than N. Meaning if K_0 = time of fault occurrence, K_a is the alarm time (time in which the fault is detected) and N_f is the detection delay (the time interval between fault occurrence and alarm time), then:

$$K_0 = K_a - N_f, \tag{7.2a}$$

$$N_f \leq N \tag{7.2b}$$

This ensures that the window is large enough for occurrence and detection to take place. But N must be kept small to reduce the computational demand. The magnitude of change in the parameter resulting from the fault is estimated by:

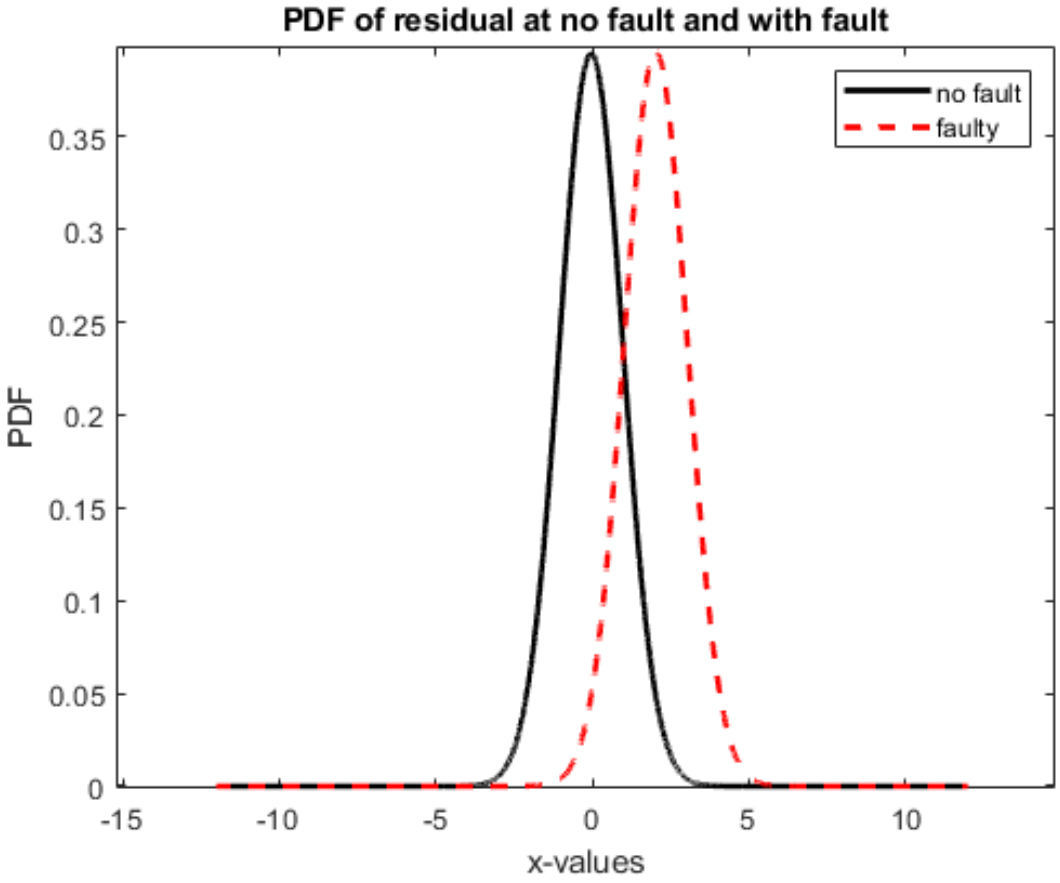

Figure 66: PDFs of residuals of faultless and faulty system. The presence of fault caused the mean of the PDF to change from zero to two.

$$\hat{\theta}(k) = \frac{1}{k+j-1}\left[\sum_{i=j}^{k}(y(i))\right] \tag{7.3}$$

The parameters in this case are the mean and standard deviation of the residual. But we assume the standard deviation is constant and the fault leads to a change in mean of the error distribution hence $\theta = \mu =$ mean of residual while y(k) is the residual. Once the decision function is obtained, then the threshold is selected such as to maximise the mean time between false alarm and minimise the mean detection delay. These performance requirements are given as:

$$\hat{\bar{T}}_D = \bar{L}(\mu_s), \tag{7.4a}$$

$$\hat{\bar{T}}_{fa} = \bar{L}(-\mu_s) \tag{7.4b}$$

L is defined according to Basseville and Nikiforov (1993) as:

$$L(\mu_s) = \frac{\sigma_s^2}{2\mu_s^2}(\exp\left[-2(\frac{\mu_s h}{\sigma_s^2} + 1.166\frac{\mu_s}{\sigma_s})\right] + 2(\frac{\mu_s h}{\sigma_s^2} + 1.166\frac{\mu_s}{\sigma_s}) - 1) \tag{7.5}$$

Where $\hat{\bar{T}}_D$ is the estimated mean time for detection and $\hat{\bar{T}}_{fa}$ is the estimated mean time between false alarm. σ_s is $\frac{(\mu_1-\mu_0)^2}{\sigma^2}$, μ_s is $\frac{(\mu_1-\mu_0)^2}{2\sigma^2}$, μ_0 is the mean of the residual distribution before change and μ_1 is the mean after change (BLANKE et al., 2006; BASSEVILLE; NIKIFOROV, 1993).

7.3.3 Dedicated Observer Scheme (DOS) System

The dedicated observer scheme shown in Figure 67 for three output system applies one output to each observer while the observer estimates the entire output variables if possible. For a no fault situation, the estimates of an output variable from all the observers is the same and equal to the true output from the system. If however, the input to an observer is faulty, the entire output from the observer is erroneous. The observer still estimates the erroneous output (now input to the observer). The residual for the output variable that is the input to the given observer is zero while the residuals for the other variables are nonzero. While this scheme is capable of detecting multiple faults, it is only applicable to systems in which the full states are observable or large part of the full states are observable. In the gas-lifted system presented, all the states are observable.

The logic unit in Figure 67 determines if a variable is faulty or not by evaluating the residual using the true system outputs and the estimated outputs from the observers. The output of the logic unit indicates a fault in the given variable based on the algorithm employed. In this thesis, we took the valve coefficients as the output variables. Observer 1 was fed with C_{gl}, observer 2 was fed with C_{iv} while observer 3 was fed with C_{pc}. A fault in C_{gl} implies the estimates from observer 1 is erroneous while the estimates from observers 2 and 3 are accurate. The logic unit in Figure 68 extracted from 67 for only observer 1 shows the observer input as C_{gl} and provides the estimates for all the outputs. All these estimates are erroneous if C_{gl} is faulty including the estimate of C_{gl}. But because C_{gl} input into the observer is itself erroneous (faulty), its residual is zero while the residuals of the other variables are nonzero. Applying the logic discussed in section (3.3), the fault in C_{gl} can be isolated.

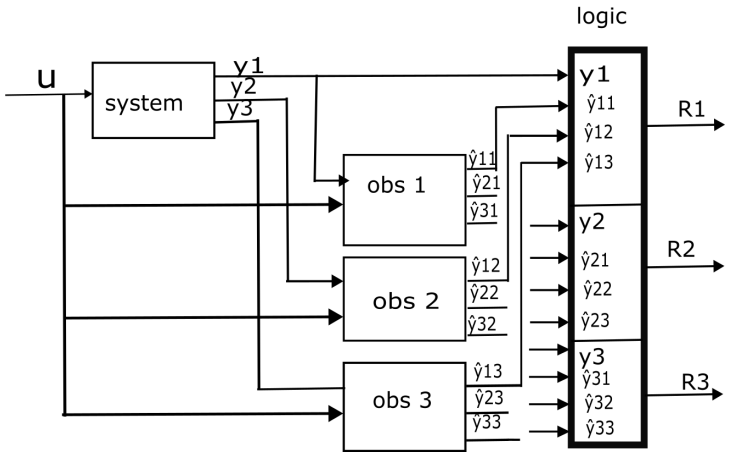

Figure 67: Dedicated Observer Scheme for a three-output system. In this fault isolation scheme, each observer is fed with one output of the system while the observer outputs the estimates of the three variables.

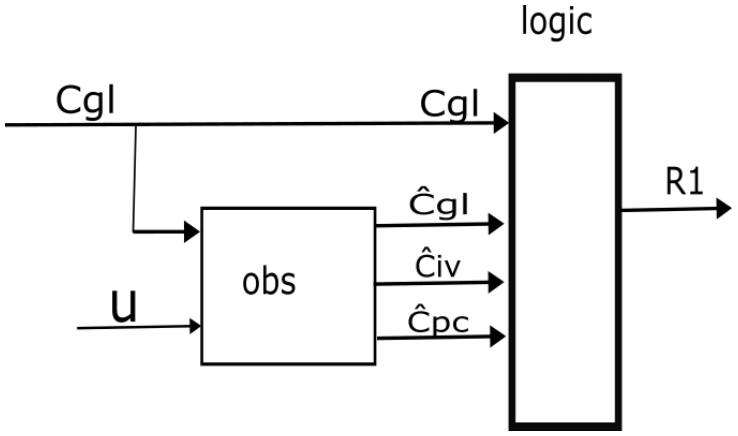

Figure 68: Logic unit having observer output as its input. If u_{cl} is faulty, all the inputs to the logic unit will be erroneous. If C_{gl} is fault-less, all the inputs to the logic unit will be correctly estimated.

7.3.4 Nonlinear Model Predictive Control

Model predictive control (MPC) is a control algorithm that uses an explicit model of the system to be controlled to predict the state trajectory over a given horizon (ROSSITER, 2017; QIN; BADGWELL, 2003). MPC solves an online optimal control problem to obtain the optimal input sequence in (7.6). The close-loop control law is defined by only the first element of this optimal input sequence in (7.7). This control law could be different for faulty system and fault-free system. At the next sample time, the horizon recedes, new measurements are taken and the process is repeated thereby minimising the effect of not only the mismatch between predicted model and actual plant but also disturbances in the plant.

$$U_k = \left[u(k|k)^T, u(k+1|k)^T, ... \right] \tag{7.6}$$

$$u_k = u(k|k) \tag{7.7}$$

MPC major features are the use of model, the multi-variable approach, the ability to incorporate constraints in its formulation, the receding horizon and the solution of the optimal control problem. The models are usually linear due to the fact that the resulting optimisation problem is convex hence global optimum are easy to be obtained. But research in nonlinear control that permits the use of nonlinear models now abound in the literature. The use of nonlinear model ensures that a wide range of prediction horizon is realised at the expense of high computational cost and risk of not getting the global optimum (ALLGOWER; FINDEISEN; NAGY, 2004).

MPC solves multiple objective function usually relating to state deviation from reference states, input moves, absolute inputs among others. The overall objective is the weighted sum of the individual objectives. Nonlinear MPC application to gas-lifted system is still very scanty. Nonlinear MPC was used by Diehl et al. (2018) for improving oil production using two inputs (choke valve and gas lift flow rate). Areas of MPC use in fault-tolerant control in gas-lifted system does not exist yet.

7.3.5 Fault-Tolerant Control

Depending on the type and degree of fault, the system performance can change from satisfactory performance through degraded performance, unsatisfactory performance to danger regions as shown in 69 (BLANKE et al., 2006). The objective of real time control of dynamical system is to operate the system in the region of satisfactory performance but the presence of fault makes the system performance move into any of the regions of performance including danger region where it becomes catastrophic to operate the system.

While the presence of fault moves the system behaviour from satisfactory performance towards danger or unsafe performance in Figure 69, the function of FTC is the reverse. The acceptance of what constitutes each performance above depends on the system and the management decision. In the case of gas-lifted system, satisfactory performance could be stated in terms of the mean oil production relative to supplied gas. Degraded performance occurs when the mean production relative to gas supplied declined noticeably.

The system enters unsatisfactory performance region when casing-heading instability sets in with its effects on the downstream equipment. The system enters unsafe zone if for example the faults causes excess production beyond the capacity of the storage tanks due to adverse casing-heading instability.

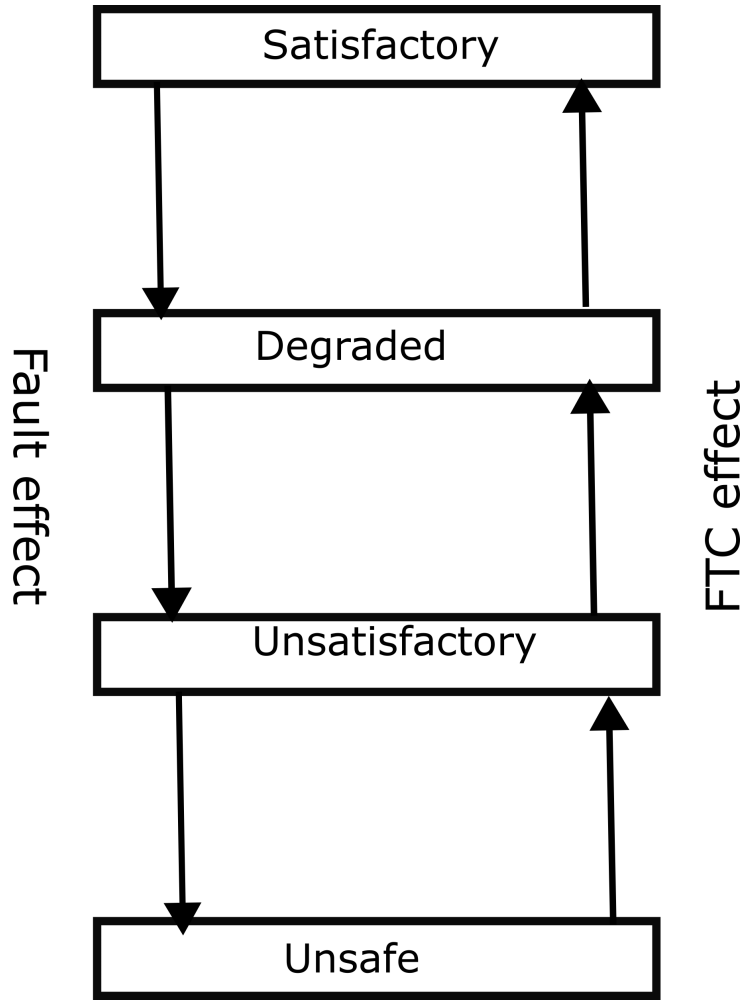

Figure 69: Fault and fault-tolerant control (FTC) of gas-lifted system. While the fault moves the operation of the system from satisfactory to unsafe performance, FTC moves the system performance in the reverse direction

7.4 Valve Fault Diagnosis in Gas-Lifted System

We augmented the states of the system by including the valve coefficients as additional states variables hence our augmented states are defined as:

$$x = [m_{ga}\ m_{gt}\ m_{ot}\ C_{iv}\ C_{pc}\ C_{gl}]^T \tag{7.8}$$

The additional states are the valve coefficients given in Appendix C. They are de-

scribed further in section 7.4.1. These augmented states vary for m_{ga}, m_{gt}, m_{ot} but remain constant for C_{gl}, C_{iv} and C_{pc} until the arrival of faults.

7.4.1 Parameter Description

The process of fault detection starts from generating a residual signal, r. At steady state, this signal remains constant for every sample even in the presence of input and disturbance but changes due to fault presence only. In the stochastic case considered here we assume the noise to be Gaussian distributed hence the residual (innovation in this case) has zero mean with non zero variance in the absence of fault but a non zero mean at some or all points in the presence of fault. In selecting the parameters for the gas-lifted system to be used in generating this residual for the fault signatures, there is no clear one in this case other than C_{gl}, C_{iv} and C_{pc} . But other variables change in known way to faults in the valves.

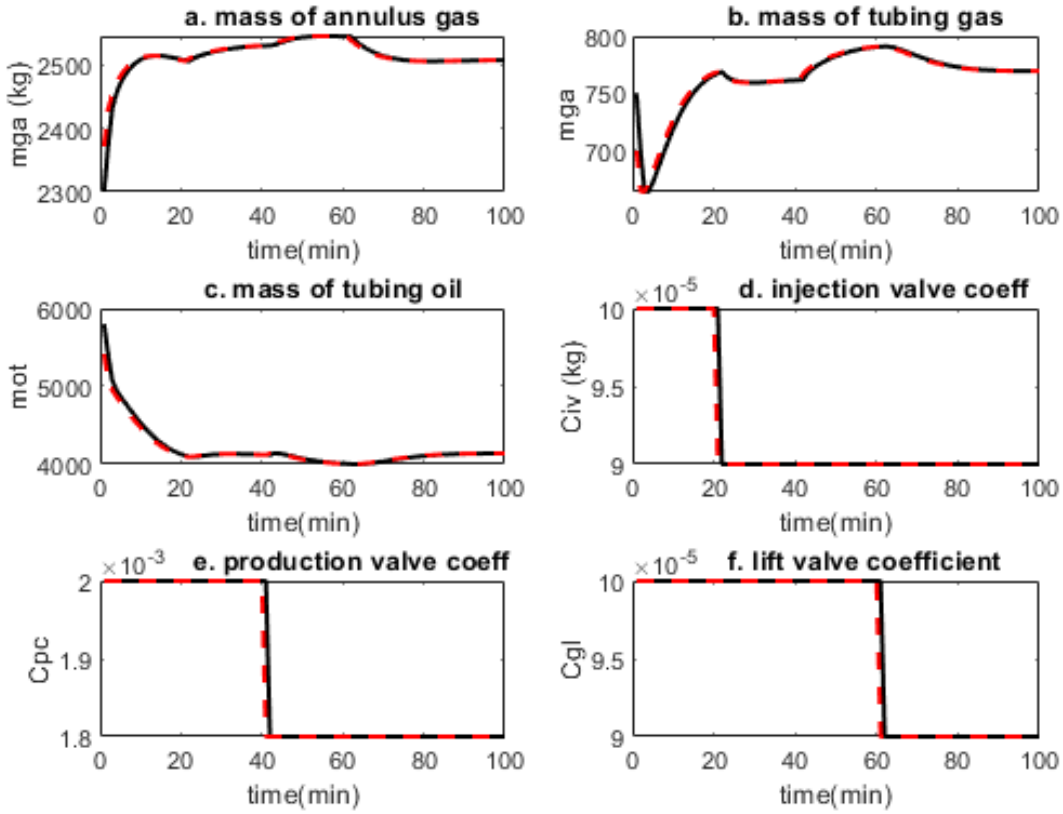

Figure 70: True and estimated states of the gas-lifted system. The true states are the dark continuous lines while the estimated states which are the red dash lines are the EKF outputs.

Figure 70 shows an abrupt fault of step decrease of 10% in C_{iv} introduced at the 20th

minute, C_{pc} introduced at the 40th minute and C_{gl} introduced at 60th. In Figure 70, a step fault in C_{gl} does not affect the performance of C_{iv} and C_{pc}. The same is true for any of the valve coefficients. Therefore, if a residual is generated for a fault in the C_{gl}, it will not affect the residual for the fault in the C_{iv}. Consequently, a strong detectability is ensured here.

Observe from Figure 70 the increase in m_{ga}, a decrease in m_{gt} and an increase in m_{ot} at t=20minutes corresponding to the time C_{iv} decreased. This is because a decrease in C_{iv} decreases flow from annulus into tubing hence increasing mass of annulus gas, decreasing tubing gas and increasing tubing oil due to reduced production. A decrease in C_{pc} implies low production through the choke. The mass of annulus gas increases since low production reduces flow from annulus to tubing, the mass of tubing gas increases and the mass of tubing oil increases. A decrease in C_{gl} decreases annulus gas mass, decreases tubing gas mass and increases mass of oil in tubing due to reduced production. The states therefore can also be used to to generate residual for fault diagnosis purpose like the valve coefficients. Unlike the valve coefficients that remain constant under input change, the states can change due to input change as well as fault hence should only be used with the valve coefficients for residual generation.

7.4.2 Hypothesis Testing for Fault Detection Using GLRT

The statistics of the residuals of the gas-lifted system change following the arrival of fault. It is the variation of the PDF with change in the residuals of selected parameters and variables that the GLRT discussed above rely through the formation of the log-likelihood ratio function of the residuals. The log-likelihood ratio is the ratio of the PDF (evaluated at time k) of the residual after a change has occurred to the PDF before the change. If the value exceeds a given threshold, an alarm occurs indicating the presence of fault. Figure 71 shows the GLRT function for the faultless gas-lifted system valve coefficients. It is seen that at no fault, these values are low.

The introduction of fault of reasonable value causes the values of the function to increase as seen in Figure 72 for the case of a 20% decrease in valve coefficients occurring at 400th minute for (C_{gl}), 500th minute for (C_{iv}) and 600th minute for (C_{pc}) respectively. In Figure 72a, the fault in (C_{gl}) is difficult to be detected as the threshold may not be exceeded while it is much easier to be detected in Figure 72b but the GLRT function can fall below the threshold later. In Figure 72c however, the fault can be detected easily as the residual can be exceeded and never returned to.

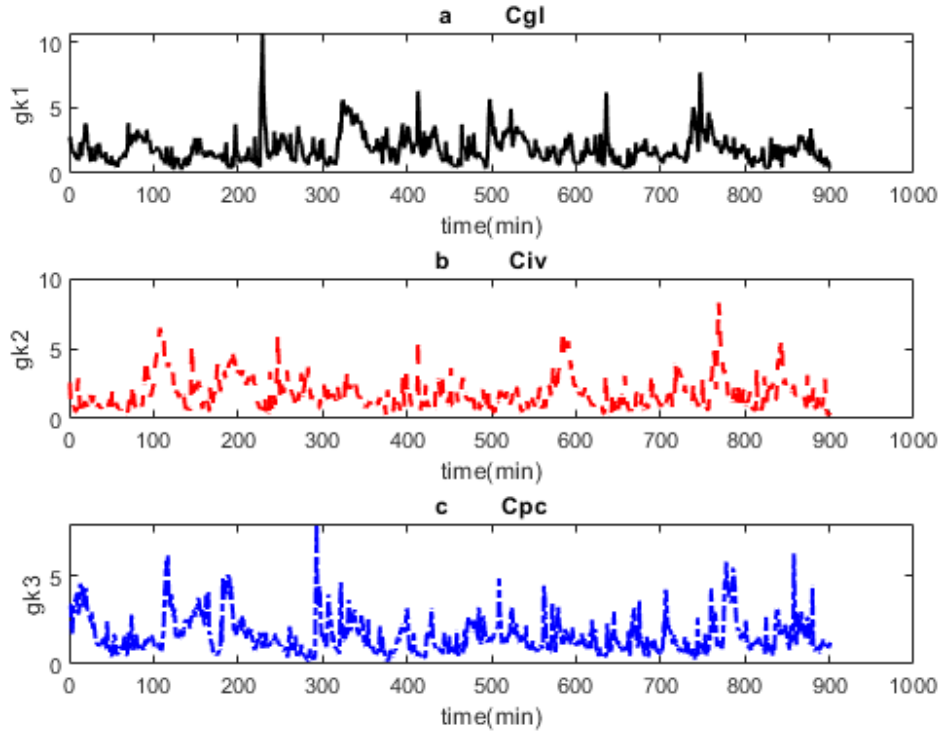

Figure 71: Generalised likelihood ratio test (GLRT) for the valve coefficients in the faultless case. The threshold can be approximated by selection of the maximum values for each residuals

Having discussed the GLRT, we present the hypotheses according to Basseville and Nikiforov (1993) as follows:

$$H_0 : \theta(k) = \theta_0 \qquad 1 \leq k \leq ct, \tag{7.9a}$$

$$H_1 : \theta(k) = \theta_0 \qquad 1 \leq k \leq k_f, \tag{7.9b}$$

$$\theta(k) = \theta_1 \qquad k_f \leq k \leq ct \tag{7.9c}$$

Where k is the time instant, ct is the simulation time and k_f is the fault occurrence time. We select H_0 if there is no change in decision function above the threshold for the entire simulation time, otherwise, H_1.

If we approximate $\sigma_s = 2\mu_s$, then L for (7.4a) reduces (7.5) to (7.10a). Similarly, L for (7.4b) can be obtained in like manner, reducing (7.5) to (7.10b).

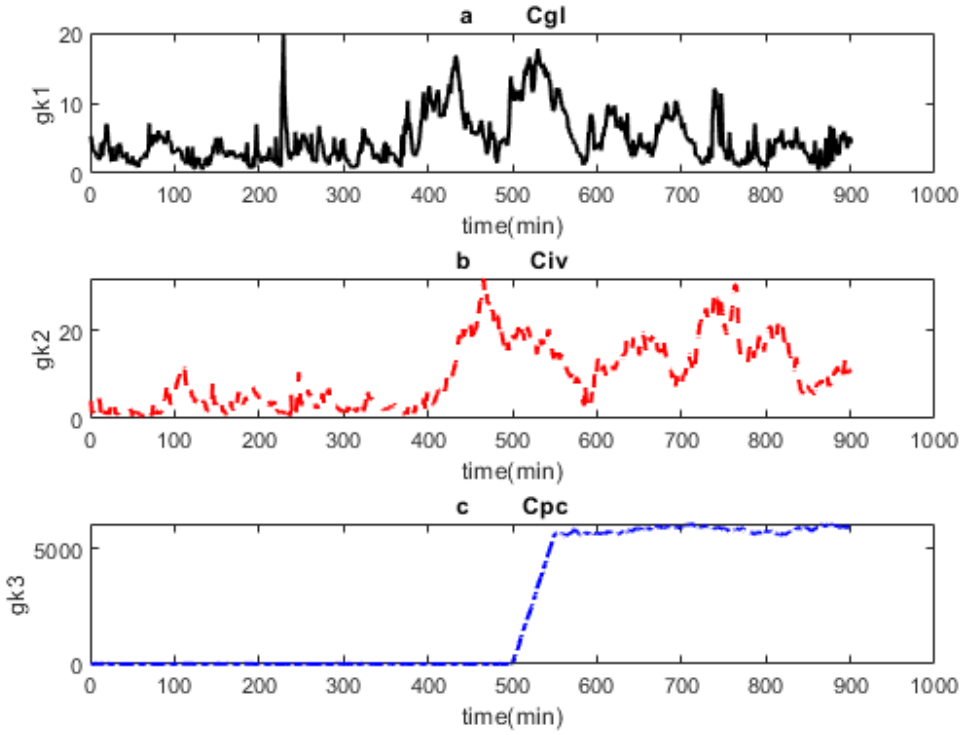

Figure 72: Generalised likelihood ratio test (GLRT) for the valve coefficients in the faulty case. Using maximum value as threshold makes the detection impossible for fault in C_{gl} while it is possible but difficult for C_{iv}. It is straightforward for C_{pc}.

$$\hat{\bar{T}}_D = L(\mu_s) = 2\exp(-0.5h - 0.583) + h - 0.834, \tag{7.10a}$$

$$\hat{\bar{T}}_{fa} = L(-\mu_s) = 2\exp(0.5h + 0.583) - h + 3.166 \tag{7.10b}$$

Solving for h in (7.5) is very demanding computationally. A common approach used is the secant method. But (BLANKE et al., 2006) plotted the graphs of $\hat{\bar{T}}_D$ and $\hat{\bar{T}}_{fa}$ for various values of h and obtained the value of h that meets the desired performance considerations from the graph. Here for each residual, we observed from the decision function plot in Figure 71, selected h that was greater than the maximum values for each of the residuals, then computed the performance from (7.10a) and (7.10b).

Results of equations (7.10a]) and (7.10b) increase with h but we desire that $\hat{\bar{T}}_D$ be small as possible while $\hat{\bar{T}}_{fa}$ be as large as possible. Consequently, if we choose h based on Figure 71, then the vector of threshold is given as $h = [C_{gl}\ C_{iv}\ C_{pc}] = [11\ 9\ 8]$. The corresponding vector of mean detection delay and mean time between false alarm are $\hat{\bar{T}}_D = [10\ 8\ 7]$ and $\hat{\bar{T}}_{fa} = [869\ 316\ 191]$ respectively. Recalling that the time is in

minute here implies that the detection delay for the production choke valve coefficient (C_{pc}) residual for example is 7 minutes which is adequate. However, the time between false alarm for (C_{pc}) residual is 191 minutes (3 hours) meaning regular occurrence of false alarms which is not desirable. With higher noise variance, $\hat{\bar{T}}_D$ was as high as 23 minutes which corresponds to a $\hat{\bar{T}}_{fa}$ of over a year which is desirable. Other factors can be used to choose the threshold in addition to the mean time between alarms and detection delay.

7.4.3 Fault Isolation with Dedicated Observer Scheme

We considered faults in the coefficients of the gas lift valves (C_{gl}), the injection valve (C_{iv}) and the production choke (C_{pc}). In the simulations, we selected the outputs from the augmented states where the outputs are these valve coefficients. The observers are labeled A, B and C respectively. Based on the DOS described earlier, we applied only the first output (C_{gl}) to the first observer (observer A) while (C_{iv}) and (C_{pc}) are applied to observers B and C respectively. Figure 73 shows the residuals for the gas-lifted system subjected to a step fault of 20% decrease in C_{gl}, C_{iv} and C_{pc}. A_{gl}, B_{iv} and C_{pc} correspond to residual of C_{gl} from observer A, C_{iv} from observer B and C_{pc} from observer C respectively.

The input to observer A is C_{gl} which was faulty starting at time t=200 minutes. Observer A therefore produced wrong estimates of all the outputs. But since C_{gl} was also wrong, the residual (A_{gl}) becomes zero. Since C_{iv} and C_{pc} were not faulty, the corresponding estimates were nonzero implying A_{iv} and A_{pc} were nonzero. Similarly, for Observer B, B_{iv} was zero while B_{gl} and B_{pc} were nonzero. For Observer C, C_{pc} was zero while C_{gl} and C_{iv} were nonzero.

If we assign 1 to observer A, 2 to B and 3 to C, based on Figure 73, the logic of the fault isolation can be given as: Variable i is faulty if (7.11) is true.

$$r_{ii} = 0, \tag{7.11a}$$

$$\prod_{i,j}^{m,n} r_{ij} \neq 0, i \neq j \tag{7.11b}$$

Where a logical 1 (high) implies a fault in the residual and a logical 0 (low) implies no fault while m and n are number of outputs and observers respectively. Note that the product can only be high implying a fault in the variable or low implying no fault in the variable. Also the product in (7.11) for any variable excludes r_{ii} as indicated in (7.11a). A high is returned only when none of the residuals in the product is zero, it returns a low

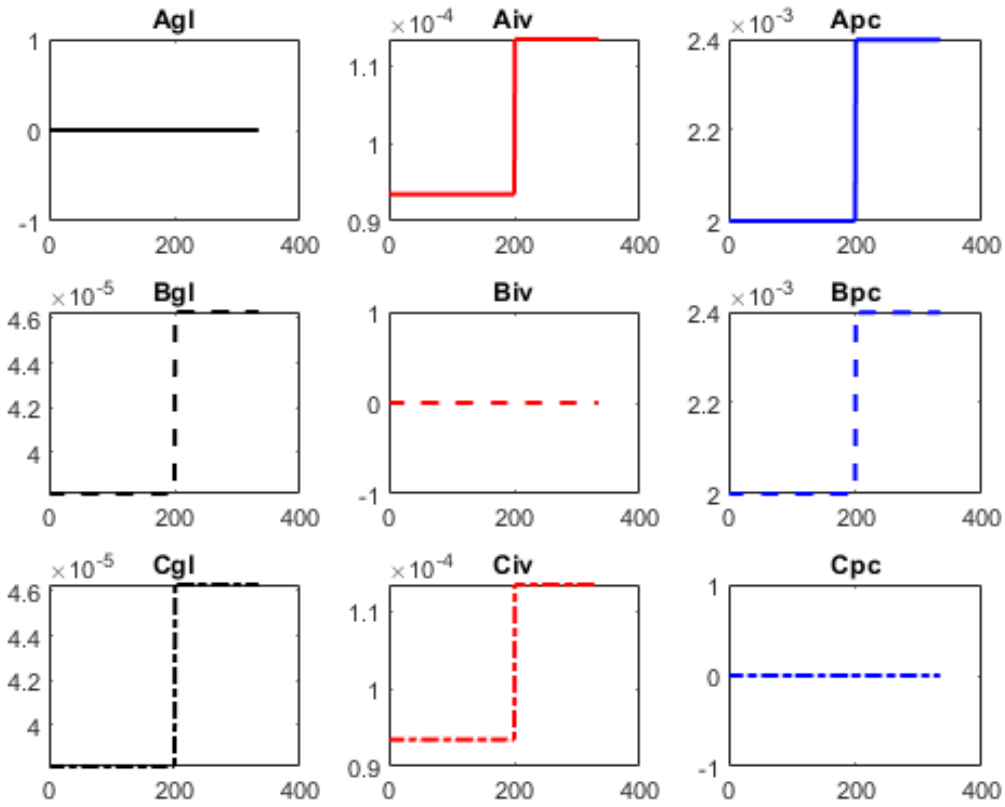

Figure 73: Residuals for gas-lifted system subjected to a fault of 20% step decrease in the valve coefficients using DOS. A_{gl}, B_{iv} and C_{pc} have zero values since the filter estimates for these variables agree with the true measurements.

otherwise. Applying the logic in (7.11), a fault detected in section (7.4.3) is isolated as fault in gas lift valve coefficient (C_{gl}).

7.5 Fault-Tolerant Control

After fault is detected and the effect is estimated, the next action is how to handle the effect of the fault so that the computed control law reflects the prevailing constraints due to fault presence while maintaining a level of production and preventing casing-heading instability. But if the magnitude of the fault is above a threshold, a more proactive measure other than control solutions are used if a fault is detected. We considered three FTC cases here: (i) passive FTC for decreased C_{pc}, (ii) active FTC for increased C_{pc} and (iii) active FTC for decreased valve range.

7.5.1 Passive Fault-Tolerant Control (PFTC) for Reduced C_{pc} Fault

In the passive case, there was no need for information from the FDI/filter unit during operation. The control zones were chosen offline such that the following objectives were met as far as possible:

(a) maintain the states in their zones at steady state.

(b) drive input towards the desired input target which will improve average oil production over open loop production.

(c) avoid casing-heading instability even if the system is operating at the input corresponding to unstable region.

(d) return the system to or close to the above after fault is detected.

The control zones were chosen based on the gas lift needs/limitations and the maximum/minimum values of the density obtained from simulations. In addition to this is the initial states that ensure the differential algebraic equation (DAE) has consistent solution. We note that the states which are masses depend on the density of the gas or mixture and the volume occupied. Based on the model and parameters values in the appendix, the volume of the annulus was calculated as $24.83m^2$ while that of the tubing was $17.25m^3$. The density of compressed annulus gas from simulation ranges between $57.84kg/m^3$ to $105.07kg/m^3$. These correspond to masses of 1436kg and 2608kg. It was desired to keep the minimum masses of gas in the annulus high hence keeping the annulus pressure high favouring constant flow of gas from annulus to tubing and reducing the chance of casing-heading instability. Therefore, we choose the minimum value of x_1 as 2000kg while the maximum is 2600kg.

From simulation, the density of mixture in tubing ranges between $50.82kg/m^3$ (at steady state with high gas content) and $800kg/m^3$ (when almost filled with oil only). These values correspond to masses of 876kg and 13799kg respectively. Based on this and the initial solution to the DAE system, x_2 zone was taken as 350Kg and 800kg while x_3 was taken as 5000kg and 7000kg. The upper bound for x_1 is strict for safety purpose and the lower bound is strict to enforce casing-heading instability removal. The lower bounds for x_2 and x_3 must be low enough to ensure bound for x_1 is achieved without infeasibility. The upper bounds are dictated by safety concern and the need to reduce the downhole pressure.

The controller parameters were chosen in similar way to meet the above objectives.

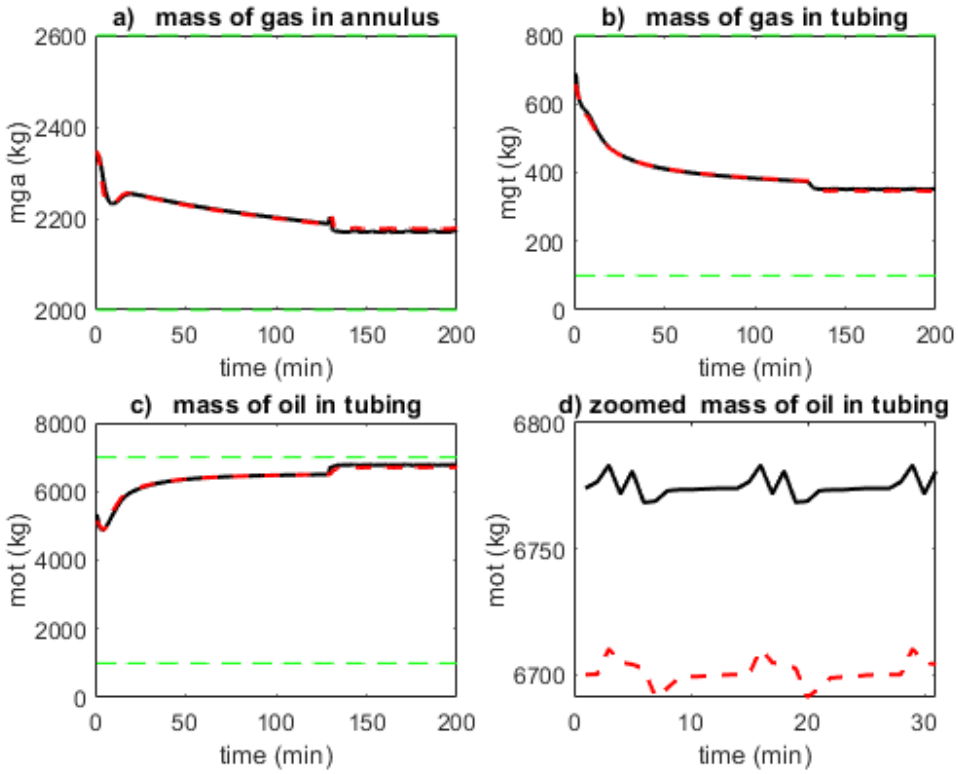

Figure 74: States of gas-lifted system subjected to a fault of 50% decrease in C_{pc}.

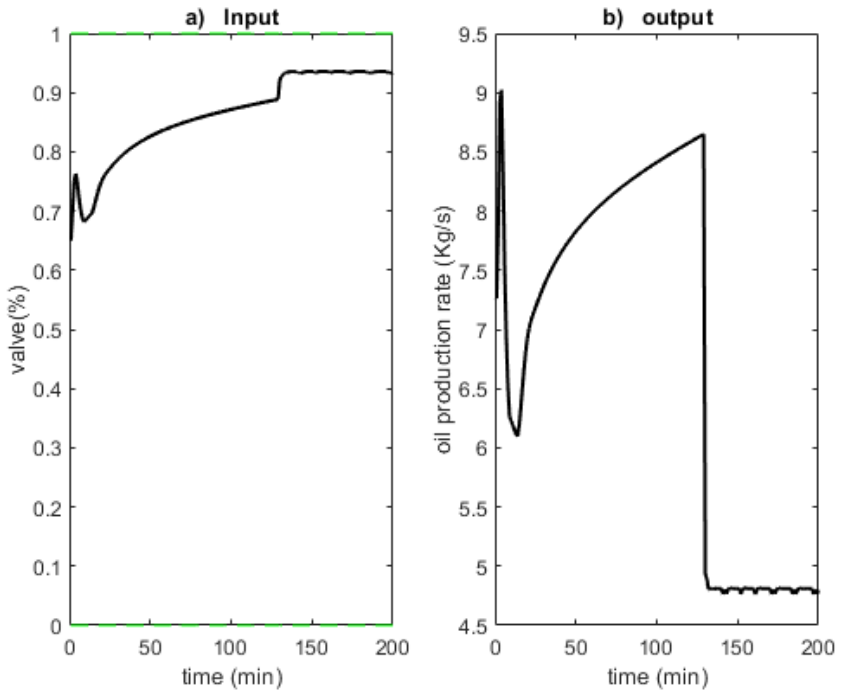

Figure 75: Input and output of gas-lifted system subjected to a fault of 50% decrease in C_{pc}. The reduced C_{pc}, forces the controller to compute higher inputs but the production rate still falls below the nominal value.

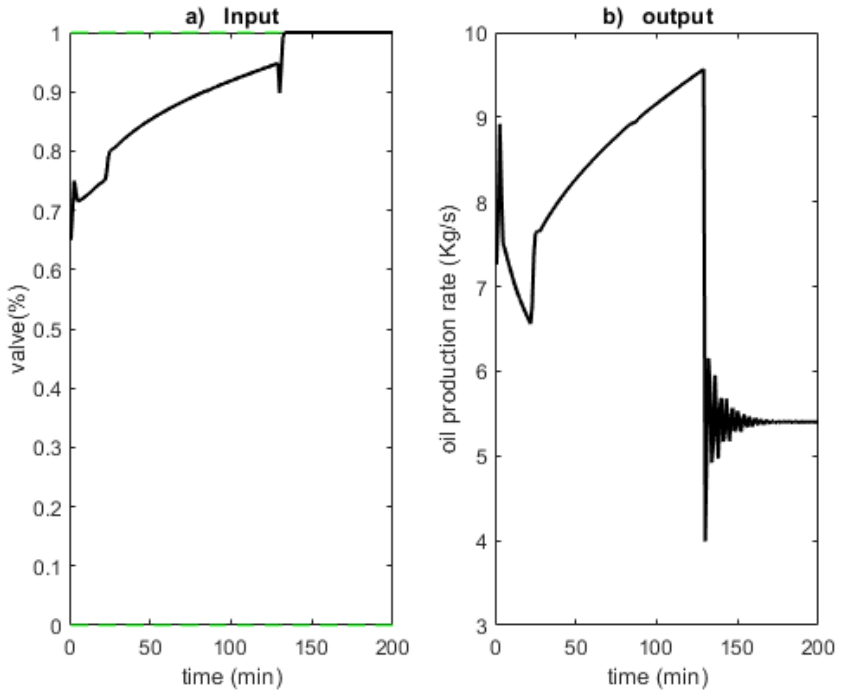

Figure 76: Input and output of gas-lifted system subjected to a fault of 50% decrease in C_{pc}. The increased control cost improves production but brought oscillatory behaviour.

In addition to this is that the controller parameters were chosen such that a large margin was provided for state zones in case of fault occurrence. Recall that if the lower bound of x_1 is not violated, casing-heading instability is minimised. Also if the upper bound of x_2 and x_3 are maintained, the downhole pressure will be lower favouring more flow of crude into the well.

From several simulation results, the controller parameters used for the PFTC were selected as: $m = 4$, $P = 200$, $Q_x = diag([1\ 1\ 1]\text{x}10^3)$, Q_u=$diag([1]\text{x}10^7)$ and $R_u = diag([1]\text{x}10^5)$, T=60s or 1 minute. When at time t=130mins, there was a 50% decrease in C_{pc}, the chosen controller parameters ensured that the state zones were not violated. Figure 74 shows the three states of the gas-lifted system. The dark solid lines are the optimal states while the red dash lines are the estimated states from the filter. The green dash lines are the states zones. Figure 74d is the zoomed portion of the mass of oil in tubing (x_3). Figure 75 shows the input and output corresponding to Figure 74.

In Figure 74, the state zones are respected despite the fault. The optimal states and the estimated states converged until the fault occurrence where they differ slightly showing the performance of the filter. Notice in Figure 74d that the zoomed portion of x_3 in the fault region shows slight disturbance and no real oscillatory behaviour. A decrease in Cpc implies a reduction of flow rate per unit percentage valve opening. This reduces

rate of flow through the valve hence the controller computed higher values of the input as shown in Figure 75a where the input increases from 0.88 to 0.93 following the arrival of fault. The optimal production however declined from 8.7kg/s to 4.8kg/s as shown in Figure 75b. When the same controller parameters were simulated for a fault of 50% increase in the C_{pc} and 10% decrease in the flow range, the corresponding flow rate due to these faults were 10.364kg/s and 8.7104kg/s respectively.

When higher priority was given to the deviation from the desired input, the rate of production increased but at the expense of oscillatory behaviour of the system. This scenario is shown in Figure 76 for $R_u = diag([1]\text{x}10^8)$. It is observed that the output increased to 5.4 kg/s compared to 4.8kg/s in Figure 75. However, oscillatory behaviour was experienced especially at the beginning of the fault occurrence time. This oscillatory behaviour is not desirable in gas-lifted system (EIKREM; IMSLAND; FOSS, 2004; SCIBILIA; HOVD; BITMEAD, 2008; GARCIA, 2013). This makes it difficult to attain higher production rate after fault occurrence using PFTC. Passive FTC does not depend on the reliability of the FDI/filter information hence the risk of poor performance due to wrong information is minimum, it is however conservative.

7.5.2 Active Fault-Tolerant Control (AFTC) for Increased C_{pc} Fault

For a high magnitude of fault, active fault-tolerant control is preferred to passive FTC to increase production or minimise the occurrence of instability. If the fault magnitude is large but the optimisation in the controller does not result in infeasibility and the states are in their zones, fault accommodation is implemented by changing the upper bound of the constraints on the input to reflect the faults presence. If the upper bound for the nominal constraint is Ub_n, that of the faulty system is Ub_f and the magnitude of the fault is f, then the fault accommodation is implemented by defining the new constraint as in 7.12.

$$Ub_f = \begin{cases} Ub_n, & \text{if } f \leq 0 \\ Ub_n - f, & \text{if } 0 \leq f \leq a \\ a, & \text{if } f \geq a \end{cases} \tag{7.12}$$

Where $0 \leq a \leq Ub_n$ which is the minimum constraint that will trigger operator intervention due to infeasibility of the optimiser.

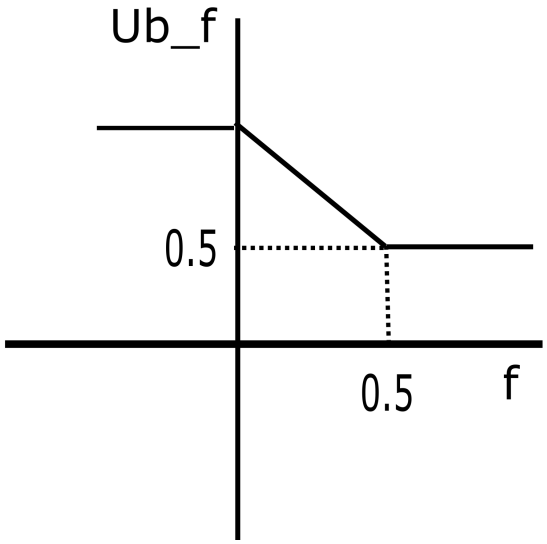

Figure 77: Modified constraint due to fault presence. The new constraint remains unchanged if there is no fault but decreases linearly with fault until 0.5 and remains constant afterwards.

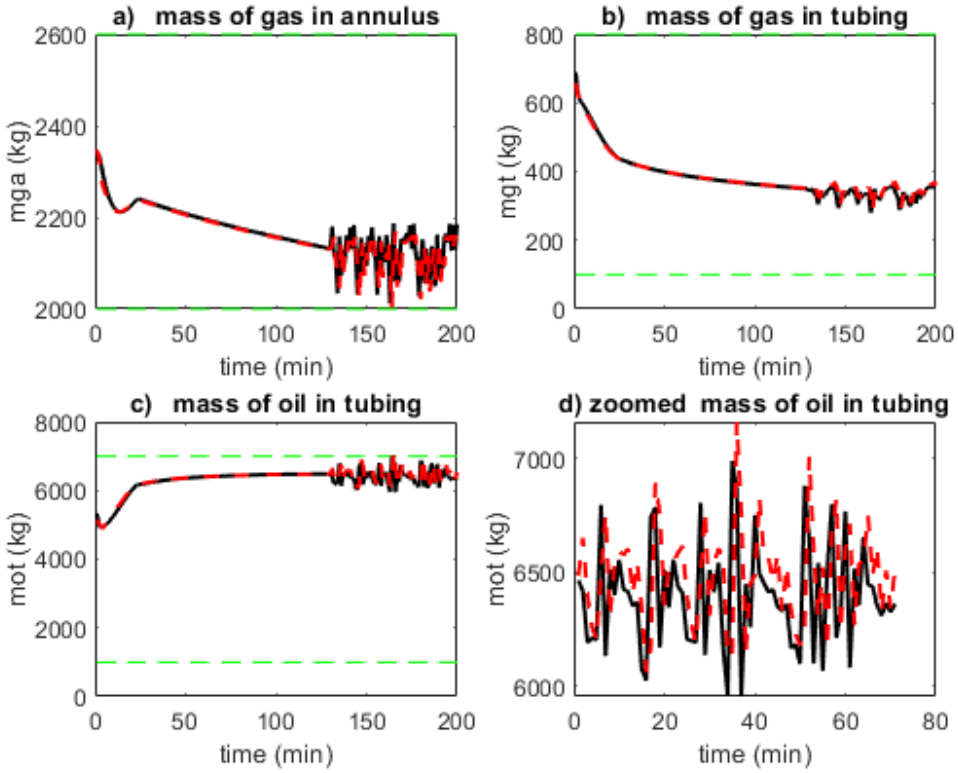

Figure 78: States of gas-lifted system subjected to a fault of 50% increase in C_{pc}. The increased C_{pc}, leads to casing-heading instability.

This is represented in Figure 77 where a = 0.5 and $Ub_n = 1$. A no fault report from the FDI/filter unit implies that the constraints remain unchanged. If there is fault, the constraint decreases linearly with fault until it becomes 0.5 and remains constant

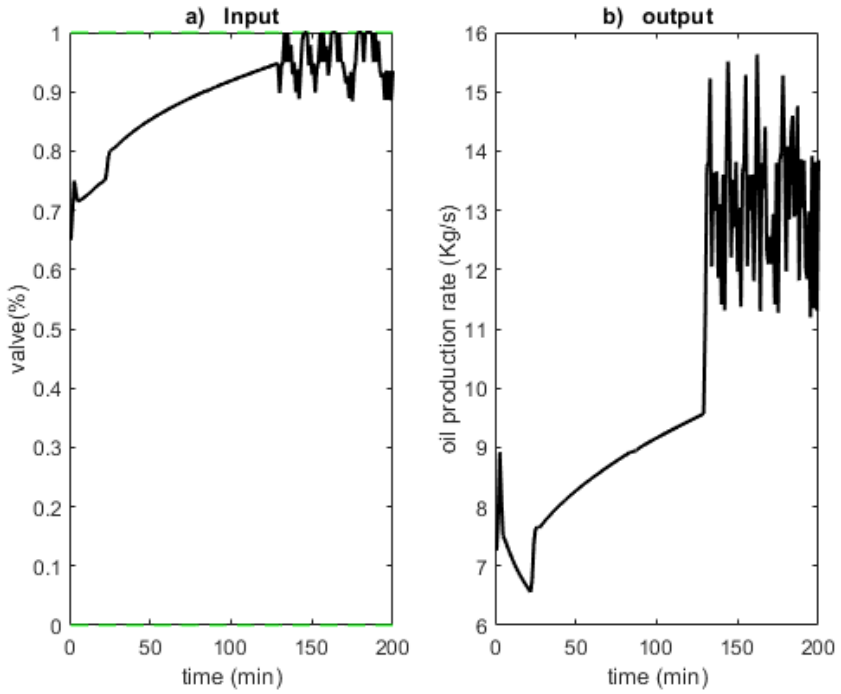

Figure 79: Input and output of gas-lifted system subjected to a fault of 50% increase in C_{pc}. Production increased but instability sets in.

thereafter irrespective of the fault magnitude. By this method, the fault in the production choke valve coefficient is accommodated. If however infeasibility results, or state zones are violated, human operator then decides the course of action as this can become difficult for FTC to handle.

Figure 78 shows the gas-lifted system states with the same controller parameters as in the passive case above except the input target is now $R_u = diag([1]\text{x}10^8)$ as in Figure 76 until a fault of 50% rise in C_{pc} occurs at time t=130 minutes. Figure 79 shows the corresponding input and output. Despite an increase in C_{pc} means higher flow per unit increase in percentage valve opening, the controller tries to maintain high valve opening as shown in 79a. This value of input for the given C_{pc} resulting from fault makes the gas-lifted system go into casing-heading instability as seen in all the states in Figure 78. The zoomed x_3 shown in 78d shows the oscillatory behaviour resulting from the high input for the given C_{pc} more clearly. We avoid this casing-heading instability by replacing the nominal upper bound constraint on the input with (7.12) to prevent the input from reaching the values that lead to infeasibility.

Figure 80 shows the gas-lifted system states after the input constraints is changed due to information from the FDI/filter unit. Figure 81 shows the corresponding input and output after the fault decreased the upper bound sharply to 0.8. The new constraint on

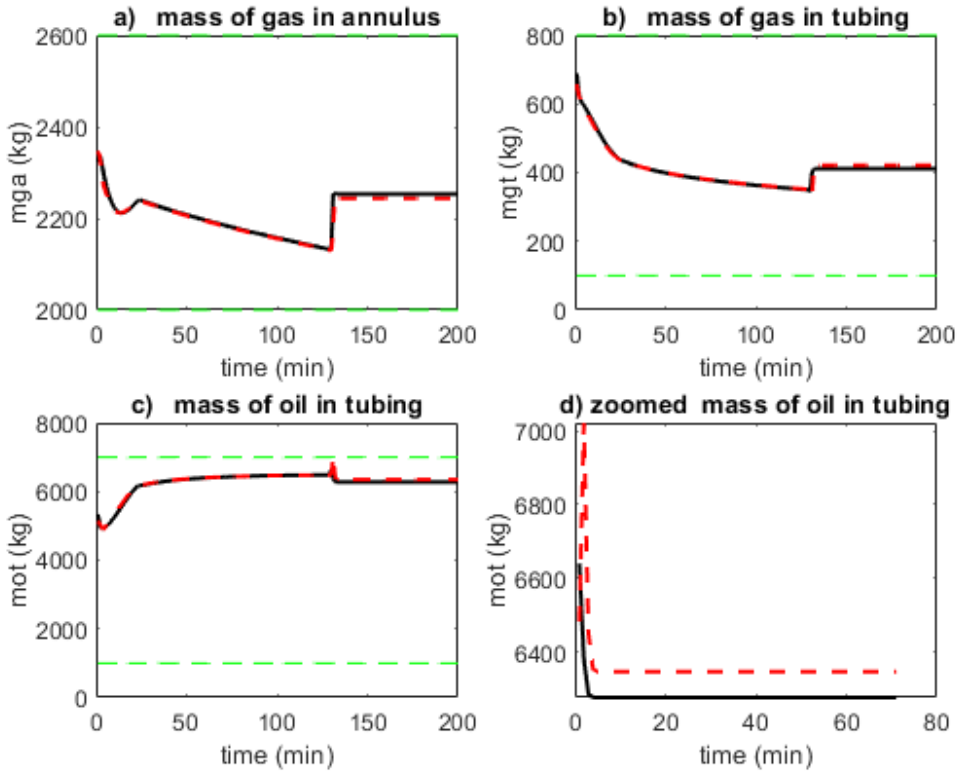

Figure 80: States of gas-lifted system subjected to a fault of 50% decrease in C_{pc} under active FTC. The reduced upper bound of the input stabilised the states.

the upper bound of the input caused the controller to compute an input that converged to the final value of the upper bound on the constraint as shown in Figure 81a. The states in Figure 80 are stable after fault occurrence. The increased value of x_1 helps to increase gas flow from annulus to tubing hence reducing chances of occurrence of casing-heading instability. This could however lead to build up of more gas in the tubing as shown in Figure 80b where x_2 increased after fault.

Due to the increased flow per unit percentage valve change, the production rate increased and saturated at 10.5 kg/s in Figure 81b. In this case the fault leads to an increase in production rate while the active FTC leads to no instability. Note that such increased production has only temporal advantage as the valve might fail completely requiring replacement.

7.5.3 Active Fault-Tolerant Control (AFTC) for Reduced Valve Range Fault

We now considered faults in valve that affects the flow range of the valve. Recall that fault in the valve coefficient modifies the internal control model while the fault in the flow

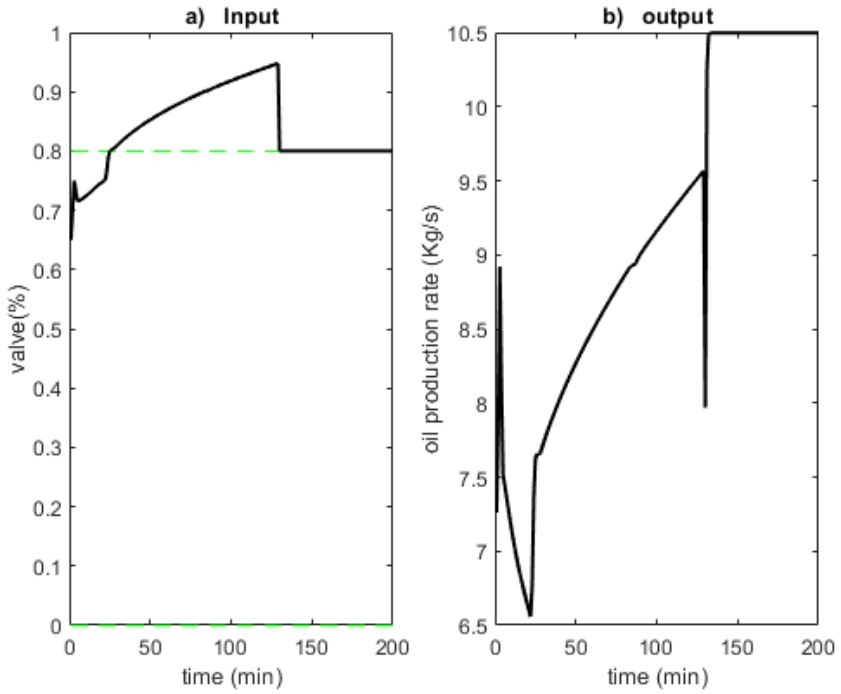

Figure 81: Input and output of gas-lifted system subjected to a fault of 50% increase in C_{pc} under active FTC. The valve constraints stabilises the output.

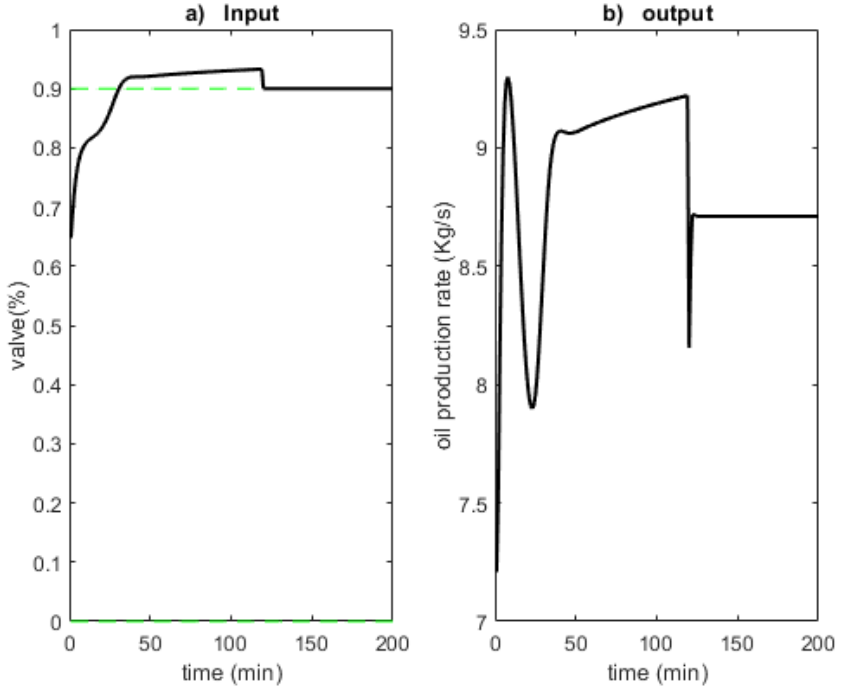

Figure 82: Input and output of gas-lifted system subjected to a fault of 10% decrease in valve range. Change in controller parameter does not alter the behaviour of the output.

range modifies the input constraint in the controller. In the case of a fault limiting the range of the valve, any FTC approach applied did not change the system response as the

output remained constant at 8.7104kg/s as shown in Figure 82. This is because for any FTC approach used here, the input saturates at the upper limit of the input bound. Also the system does not show oscillatory behaviour of casing-heading instability for any FTC approach used.

7.5.4 Comparison of FTC Methods for Various Gas-Lifted System Valve Faults

We compared the performances of various FTC techniques outlined above on the faults discussed. The performance criteria are (a) output change, (b) output and (c) stability. The output change for each FTC technique is the percentage change in output due to the application of a given FTC technique when fault occurs. This is obtained from the difference between the output after fault occurrence but before application of FTC (given in 7.5.1) and the output after application of FTC. The faults considered are 50% decrease in C_{pc}, 50% increase in C_{pc}) and 10% blockage of valve (or 90% upper limit of valve). The FTC techniques used are passive, change in input deviation weight (Q_u) in the controller and decrease in the constraints (Ub_n) on the input for the controller optimisation. The values for (Q_u) and (Ub_n) were chosen from nominal values that do not lead to casing-heading instability.

Table 14: FTC techniques for some valve faults using output deviation from the output without FTC, output after FTC and oscillatory behaviour. A yes under stability implies that there is no casing-heading instability.

fault	**FTC**	**output change (%)**	**output (kg/s)**	**stability**
$0.5C_{pc}$	$Passive$	6.56	5.115	No
	Q_u	16.50	5.5918	No
	Ub_f	-11.61	4.2425	Yes
$1.5C_{pc}$	$Passive$	2.69	10.6425	Yes
	Q_u	16.50	11.0437	Yes
	Ub_f	-6.66	10.6423	Yes
$0.9Ub_n$	$Passive$	0	8.7104	Yes
	Q_u	0	8.7104	Yes
	Ub_f	-	-	Yes

Table 14 compares the performances of some FTC techniques for some valve faults using outpoint change from the output without FTC, output after FTC and oscillatory behaviour. From Table 14, for a 50% decrease in C_{pc}, the passive approach increases the output by 6.56% but there was slight oscillation which damped out after a while. There

was an oscillation when the input deviation weight in the controller was increased but the oil production increased also. Reducing constraints in the input leads to stability for any type of fault. Only in the case of 50% decrease in C_{pc} that instability is witnessed as there is no casing-heading instability when the fault is an increase in C_{pc} nor a 10% decrease in valve range. A fault of reduced control range of valve does not respond to any of the FTC techniques presented above since the change in output remains constant while there is no change in system stability. It however responds to model change involving change in the separator pressure (P_s) but this might not be realistic in practice.

Summarising the table above: Passive FTC provides more robustness but low output change. Reducing the upper control bound ensures stability but production could decline while increasing the controller cost that prioritises the input target increases production but it is prone to casing-heading instability.

7.6 Concluding Remarks

Fault-tolerant control was used for optimal operation of gas-lifted system. Three cases were considered: (a) When a fault was due to a decrease in the production choke coefficient, passive FTC was used to increase production but could not prevent oscillatory behaviour of the system. This passive FTC was accomplished by proper selection of the controller parameters that ensured the NMPC was robust to faults. (b) For the case where the fault was due to increase in the production choke coefficient, active FTC was used to remove casing-heading instability. This involved changing the constraints of the input to reflect the faults thereby preventing the system from sliding into casing-heading instability while increasing oil production. (c) For the fault due to reduction in valve range, active FTC could not alter the output noticeably.

8 CONCLUSION AND FURTHER WORKS

8.1 Conclusion

Gas-lifted system optimisation has been carried out in this thesis using nonlinear model predictive control with input target and control zones. This was done by considering two key factors that affect flow assurance in gas-lifted system namely: (1) casing-heading instability and (2) valve faults.

The model predictive control was first presented. The feasibility and convergence discussion presented. The controller was first tested on a simple CSTR, an ODE system using two nonlinear optimisation approaches: (i) Interior Point OPTimizer (IPOPT) in computer algebra system algorithmic differentiation (CasADi) and (ii) fmincon in MATLAB. Setpoint tracking and zone control were implemented successfully.

Analysis of gas-lifted system was presented. The pressure profile in the annulus and tubing were derived as pressure is the force per sectional area that controls the flow of fluid through the system. Phase portrait at different operating points of the system were examined and they reveal that all trajectories tended towards the centre showing stability. This surprisingly includes the equilibrium point corresponding to the unstable region. Plots of linearised system at different points, bifurcation diagram and the eigenvalue however showed that the gas-lifted system is unstable after the bifurcation point.

Setpoint tracking in the optimisation of gas-lifted system is highly established in literature hence the focus of this work was on the zone control. Finite horizon NMPC was selected and used to optimise the gas-lifted system. The controller stabilised the undisturbed system improving production by 5.63% compared to the open-loop operation when the system was in casing-heading instability. For the disturbed system, the additional degree of freedom from using two inputs attenuated the disturbance quickly compared to one input especially when the desired input was out of input bound. The steady state production, aided by the high input target, reached 12.25kg/s which was far more than 9.57 kg/s for the one input case. This controller showed a 3.76% improvement over PI

controller for the same purpose.

Gas-lifted system are situated in hash or difficult environments that makes state measurements very difficult or unreliable. State estimation using key estimation techniques were then carried out. Linear Kalman filter, Extended Kalman filter, unscented kalman filter and particle filters were examined and the nonlinear filters were used to estimate the system. Based on the noise assumption used, UKF performed slightly better than EKF by examining the RMSE for the residuals, visualising the states and examining the residual using the hypothesis test. This is because the UKF uses three term approximation of Taylor series while EKF uses two term. The additional terms improved the accuracy of the UKF over the EKF for the gas-lifted system. The performance of PF was the least. But with the computational advantage of the EKF, the states of system can be estimated using the EKF since there was just a small difference in performance between using it and UKF.

Fault-tolerant control for the gas-lifted system employing the inherent fault-tolerance capability of the NMPC was implemented. Three cases were considered: (a) When a fault was due to a decrease in the production choke coefficient, passive FTC was used to increase production but could not prevent oscillatory behaviour of the system. This passive FTC was accomplished by proper selection of the controller parameters that ensures the NMPC was robust to faults. (b) For the case where the fault was due to increase in the production choke coefficient, active FTC was used to remove casing-heading instability. This involved changing the constraints of the input to reflect the faults thereby preventing the system from sliding into casing-heading instability while increasing oil production. (c) For the fault due to reduction in valve range, active FTC could not alter the output noticeably.

Casing-heading instability and valve fault both reduce flow assurance in gas-lifted system. They also have interacting influence on each other. The presence of casing-heading instability can lead to early fault in valves while valve faults can lead to casing-heading. Implementing FTC and casing-heading instability therefore leads to optimal operation of the gas-lifted system.

8.2 Further Works

Optimisation in CasADi was used on a simple CSTR system but not extended to gas-lifted system because of difficulties in the solution of the differential equation. The differential equation was solved easily if the gas-lifted system was not in casing-heading

instability region. There was difficulty in obtaining accurate solution of the differential equation which indicates the state trajectory when the system is in casing-heading instability region. The state trajectory remained constant when it reached the first minimum or maximum values hence did not show the oscillation of the system. Further work can look at how to obtain accurate solution of the gas-lifted system differential equation in CasADi to enable the use of IPOPT for optimisation of the system.

The prediction model in the nonlinear MPC was based on the differential algebraic equation presented in chapter 4. This model however does not capture accurately the dynamics of the gas-lifted system compared to the partial differential equation which is difficult for control application. This work can be improved further by using real oil production data that contain the production rate as output with the percentage valve opening and flow rate of gas into the annulus as inputs. A feedforward neural network can be trained to provide a more accurate prediction model for the NMPC based on these data. The result can then be implemented on gas lift experimental apparatus to verify the performance of the controller.

The fault-tolerant control discussed here assumed only one fault at a time and it was due to valve fault. In practice, gas-lifted systems faults are numerous and can occur simultaneously. Valves alone can have different types of fault occurring simultaneously. Further works can look into case of multiple faults in gas-lifted system and apply fault-tolerant control for its optimal operation despite faults presence.

All gas-lifted system parameters are assumed to be known hence there is no uncertainty in the model. Practical gas-lifted system has uncertainties in the model mostly due to the uncertainty in the parameters. Example is discussed in (KRISHNAMOORTHY; FOSS; SKOGESTAD, 2016) where the uncertainty was due to variation in the gas/oil ratio (GOR). Further works can examine the stabilisation of the system under these uncertainties. This is in addition to the robustness of the FTC schemes to the model uncertainty.

REFERENCES

AAMO, O. M.; EIKREM, G.; SIAHAAN, H.; FOSS, B. A. Observer design for multiphase flow in vertical pipes with gas-lift - theory and experiments. *Journal of Process Control*, v. 15, p. 247–257, 2005. ISSN 09591524. Available from: ⟨https://www.sciencedirect.com/science/article/pii/S0959152404000848⟩.

ADUKWU, O.; ODLOAK, D.; JUNIOR, F. K. Stabilization of artificial gas lift system using nonlinear model predictive control with input target and control zones. In: . IEEE, 2020. p. 1–7. ISBN 978-1-7281-5957-7. Available from: ⟨https://ieeexplore.ieee.org/document/9505377/⟩.

ADUKWU, O.; ODLOAK, D.; KASSAB, F. Fault-tolerant control of gas-lifted oil well. *IEEE Access*, IEEE, 2023.

ADUKWU, O.; ODLOAK, D.; KASSAB, F. Optimisation of a gas-lifted system with nonlinear model predictive control. *Energies*, Multidisciplinary Digital Publishing Institute, v. 16, n. 7, p. 3082, 2023.

ADUKWU, O.; ODLOAK, D.; SAAD, A. M.; JUNIOR, F. K. State estimation of gas-lifted oil well using nonlinear filters. *Sensors*, MDPI, v. 22, n. 13, p. 4875, 2022. Available from: ⟨https://www.mdpi.com/1424-8220/22/13/4875⟩.

ALIEV, F. A.; DZHAMALBEKOV, M. A.; IL'YASOV, M. K. Mathematical simulation and control of gas lift. *Journal of Computer and Systems Sciences International*, v. 50, p. 805–814, 2011. ISSN 1064-2307. Not an A paper. Available from: ⟨http://link.springer.com/10.1134/S1064230711030038⟩.

ALLGOWER, F.; FINDEISEN, R.; NAGY, Z. K. Nonlinear model predictive control: From theory to application. *Journal-Chinese Institute Of Chemical Engineers*, CHINESE INST CHEM ENGINEERS, v. 35, n. 3, p. 299–316, 2004.

ARULAMPALAM, M.; MASKELL, S.; GORDON, N.; CLAPP, T. A tutorial on particle filters for online nonlinear/non-gaussian bayesian tracking. *IEEE Transactions on Signal Processing*, v. 50, n. 2, p. 174–188, 2002.

ASHEIM, H. Criteria for gas-lift stability. *Journal of Petroleum Technology*, OnePetro, v. 40, n. 11, p. 1452–1456, 1988.

ATKINSON, T.; RICHTER, A. W.; THROCKMORTON, N. A. The accuracy of linear and nonlinear estimation in the presence of the zero lower bound. *Federal Reserve Bank of Dallas, Working Papers*, v. 2018, 2018. Available from: ⟨https://www.dallasfed.org/-/media/documents/research/papers/2018/wp1804.pdf⟩.

BASSEVILLE, M.; NIKIFOROV, I. V. *Detection of abrupt changes: theory and application*. [S.l.]: prentice Hall Englewood Cliffs, 1993. v. 104.

BIN, H.; GOLAN, M. Gas-lift instability resulted production loss and its remedy by feedback control: dynamical simulation results. In: ONEPETRO. *SPE International Improved Oil Recovery Conference in Asia Pacific*. [S.l.], 2003.

BLANKE, M.; FREI, W. C.; KRAUS, F.; PATTON, J. R.; STAROSWIECKI, M. What is fault-tolerant control? *IFAC Proceedings Volumes*, Elsevier, v. 33, n. 11, p. 41–52, 2000.

BLANKE, M.; KINNAERT, M.; LUNZE, J.; STAROSWIECKI, M.; SCHRÖDER, J. *Diagnosis and fault-tolerant control*. [S.l.]: Springer, 2006. v. 2.

BLICK, E.; BOONE, L. Stabilization of naturally flowing oil wells using feedback control. In: ONEPETRO. *SPE California Regional Meeting*. [S.l.], 1986.

BRADFORD, E.; IMSLAND, L. Stochastic nonlinear model predictive control using gaussian processes. In: IEEE. *2018 European Control Conference (ECC)*. [S.l.], 2018. p. 1027–1034.

BROWN, K. E. Overview of artificial lift systems. *Journal of Petroleum Technology*, OnePetro, v. 34, n. 10, p. 2384–2396, 1982.

CAMACHO, E. F.; ALAMO, T.; PEÑA, D. M. de la. Fault-tolerant model predictive control. In: IEEE. *2010 IEEE 15th Conference on Emerging Technologies & Factory Automation (ETFA 2010)*. [S.l.], 2010. p. 1–8.

CAMACHO, E. F.; ALBA, C. B. *Model predictive control*. [S.l.]: Springer science & business media, 2013.

CAMPOS, M.; GOMES, M.; PEREZ, J.; JOSE, M. Controle avançado e otimização na indústria do petróleo. *Rio de Janeiro: Editora Interciência*, p. 23, 2013.

CAPRON, B. D. O.; ODLOAK, D. A robust lqr-mpc control strategy with input constraints and control zones. *Journal of Process Control*, Elsevier, v. 64, p. 89–99, 2018.

CLARK, R. N. A simplified instrument failure detection scheme. *IEEE Transactions on Aerospace and Electronic Systems*, IEEE, n. 4, p. 558–563, 1978.

CLARK, R. N. The dedicated observer approach to instrument failure detection. In: IEEE. *1979 18th IEEE Conference on Decision and Control including the Symposium on Adaptive Processes*. [S.l.], 1979. v. 2, p. 237–241.

DIEHL, F. C.; ALMEIDA, C. S.; ANZAI, T. K.; GEREVINI, G.; NETO, S. S.; MEIEN, O. F. V.; CAMPOS, M. C.; FARENZENA, M.; TRIERWEILER, J. O. Oil production increase in unstable gas lift systems through nonlinear model predictive control. *Journal of Process Control*, Elsevier, v. 69, p. 58–69, 2018.

EIKREM, G. O.; AAMO, O. M.; FOSS, B. A. On instability in gas lift wells and schemes for stabilization by automatic control. *SPE Production and Operations*, v. 23, p. 268–279, 2008. ISSN 19301855.

EIKREM, G. O.; FOSS, B.; IMSLAND, L.; HU, B.; GOLAN, M. Stabilization of gas lifted wells. *IFAC Proceedings Volumes*, Elsevier, v. 35, n. 1, p. 139–144, 2002.

EIKREM, G. O.; IMSLAND, L.; FOSS, B. Stabilization of gas lifted wells based on state estimation. *IFAC Proceedings Volumes*, Elsevier, v. 37, p. 323–328, 2004. ISSN 14746670. Available from: ⟨http://dx.doi.org/10.1016/S1474-6670(17)38752-9⟩.

EINICKE, G. A. Smoothing, filtering and prediction: Estimating the past, present and future second edition. Prime Publishing - Amazon.com, 2019.

ELFRING, J.; TORTA, E.; MOLENGRAFT, R. van de. Particle filters: A hands-on tutorial. *Sensors (Switzerland)*, MDPI AG, v. 21, p. 1–28, 1 2021. ISSN 14248220.

FANCHI, J. R.; CHRISTIANSEN, R. L. *Introduction to petroleum engineering*. [S.l.]: John Wiley & Sons, 2016.

FRANK, P. System fault diagnosis reliability and related knowledge-based approaches. In: *Fault Diagnostics and Realibility, ch. Fault diagnosis in dynamic systems via state estimation-A Survey*. [S.l.]: D. Reidel Publishing Company, 1987. v. 1, p. 35–98.

GARCIA, A. P. Stability analysis and stabilization of gas lift systems. In: *22nd International Congress of Mechanical Engineering, November*. [S.l.: s.n.], 2013. p. 3–7.

GILBERTSON, E.; HOVER, F.; COLINA, E. Failure mode and sensitivity analysis of gas lift valves. In: *International Conference on Offshore Mechanics and Arctic Engineering*. [S.l.: s.n.], 2010. v. 49101, p. 305–314.

GONZÁLEZ, A. H.; ODLOAK, D. A stable mpc with zone control. *Journal of Process Control*, Elsevier, v. 19, n. 1, p. 110–122, 2009.

HANSEN, H. H. *A Comparative Study of Control Structures Applied in Gas Lift Systems to Prevent Casing Heading*. Dissertação (Mestrado) — Institutt for teknisk kybernetikk, 2012.

HUSSEIN, H.; AL-DURRA, A.; BOIKO, I. Design of gain scheduling control strategy for artificial gas lift in oil production through modified relay feedback test. *Journal of the Franklin Institute*, Elsevier, v. 352, n. 11, p. 5122–5144, 2015.

JAHANSHAHI, E. Control solutions for multiphase flow: Linear and nonlinear approaches to anti-slug control. Norges teknisk-naturvitenskapelige universitet, Fakultet for naturvitenskap . . . , 2013. Available from: ⟨https://brage.bibsys.no/xmlui/handle/11250/248592⟩.

JANSEN, B.; DALSMO, M.; NØKLEBERG, L.; HAVRE, K.; KRISTIANSEN, V.; LEMETAYER, P. Automatic control of unstable gas lifted wells. In: ONEPETRO. *SPE Annual Technical Conference and Exhibition*. [S.l.], 1999.

KALMAN, R. E. A New Approach to Linear Filtering and Prediction Problems. *Journal of Basic Engineering*, v. 82, n. 1, p. 35–45, 03 1960. ISSN 0021-9223. Available from: ⟨https://doi.org/10.1115/1.3662552⟩.

KHAMEHCHI, E.; MAHDIANI, M. R. *Gas allocation optimization methods in artificial gas lift*. [S.l.]: Springer, 2017.

KINDEREN, W. D.; DUNHAM, C.; POULISSE, H. Real-time artificial lift optimization. In: ONEPETRO. *Abu Dhabi International Petroleum Exhibition and Conference*. [S.l.], 1998.

KLAN, P.; GOREZ, R. On aggressiveness of pi control. *IFAC Proceedings Volumes*, Elsevier, v. 38, n. 1, p. 355–360, 2005.

KONATOWSKI, S.; KANIEWSKI, P.; MATUSZEWSKI, J. Comparison of estimation accuracy of ekf, ukf and pf filters. *Annual of Navigation*, Walter de Gruyter GmbH, v. 23, p. 69–87, 4 2017. ISSN 2300-6633.

KRISHNAMOORTHY, D.; FOSS, B.; SKOGESTAD, S. Real-time optimization under uncertainty applied to a gas lifted well network. *Processes*, Multidisciplinary Digital Publishing Institute, v. 4, n. 4, p. 52, 2016.

KRISHNAMOORTHY, D.; FOSS, B.; SKOGESTAD, S. Steady-state real-time optimization using transient measurements. *Computers & Chemical Engineering*, Elsevier, v. 115, p. 34–45, 2018.

LEE, J. H. Model predictive control: Review of the three decades of development. *International Journal of Control, Automation and Systems*, Springer, v. 9, n. 3, p. 415–424, 2011.

MACIEJOWSKI, J. Modelling and predictive control: Enabling technologies for reconfiguration. *IFAC Proceedings Volumes*, Elsevier, v. 30, n. 27, p. 19–29, 1997.

MACIEJOWSKI, J. Reconfiguring control systems by optimization. In: *Proceedings of the European Control Conference*. [S.l.: s.n.], 1997.

MACIEJOWSKI, J. M. Fault-tolerant aspects of mpc. In: IET. *IEE Seminar on Practical Experiences with Predictive Control (Ref. No. 2000/023)*. [S.l.], 2000. p. 3–1.

MACIEJOWSKI, J. M. *Predictive control: with constraints*. [S.l.]: Pearson education, 2002.

MAHMUT, P.; LIN, J.; FU, L. A tutorial on particle filters for fault detection and diagnosis of hybrid systems. *International Journal of Control and Automation*, v. 10, p. 109–120, 04 2017.

MARTIN, P. A.; ODLOAK, D.; KASSAB, F. Robust model predictive control of a pilot plant distillation column. *Control Engineering Practice*, Elsevier, v. 21, n. 3, p. 231–241, 2013.

MAYNE, D. Q. Model predictive control: Recent developments and future promise. *Automatica*, Elsevier, v. 50, n. 12, p. 2967–2986, 2014.

MUNZIR, S.; HALFIANI, V. et al. An optimal control solution using multiple shooting method. *Bulletin of Mathematics*, v. 4, n. 02, p. 143–160, 2012.

NIKOUKHAH, R. A new methodology for observer design and implementation. *IEEE transactions on automatic control*, IEEE, v. 43, n. 2, p. 229–234, 1998.

OCAMPO-MARTINEZ, C. *Model predictive control of complex systems including fault tolerance capabilities: application to sewer networks*. [S.l.]: Universitat Politècnica de Catalunya, 2007.

OCAMPO-MARTÍNEZ, C.; PUIG, V.; QUEVEDO, J.; INGIMUNDARSON, A. Fault tolerant model predictive control applied on the barcelona sewer network. In: IEEE. *Proceedings of the 44th IEEE Conference on Decision and Control*. [S.l.], 2005. p. 1349–1354.

PLUCENIO, A.; PAGANO, D. J.; CAMPONOGARA, E.; TRAPLE, A.; TEIXEIRA, A. Gas-lift optimization and control with nonlinear mpc. *IFAC Proceedings Volumes*, Elsevier, v. 42, n. 11, p. 904–909, 2009.

QIN, S. J.; BADGWELL, T. A. A survey of industrial model predictive control technology. *Control engineering practice*, Elsevier, v. 11, n. 7, p. 733–764, 2003.

RAKOVIĆ, S. V.; LEVINE, W. S. *Handbook of model predictive control*. [S.l.]: Springer, 2018.

RAMESH, K.; GANESAN, R. G.; MAHALAKSHMI, K. Approximation and optimization of discrete systems using order reduction technique. *Energy Procedia*, Elsevier, v. 117, p. 761–768, 2017.

RASHID, K.; BAILEY, W.; COUËT, B. A survey of methods for gas-lift optimization. *Modelling and Simulation in Engineering*, Hindawi, v. 2012, 2012.

RASHID, K.; DEMIREL, S.; COUËT, B. Gas-lift optimization with choke control using a mixed-integer nonlinear formulation. *Industrial & engineering chemistry research*, ACS Publications, v. 50, n. 5, p. 2971–2980, 2011.

ROSICH, A.; PUIG, V.; QUEVEDO, J. Fault-tolerant constrained mpc of pem fuel cells. 2006.

ROSSITER, J. A. *Model-based predictive control: a practical approach*. [S.l.]: CRC press, 2017.

SANTOS, D. *"Fault-control state estimation of linear Gaussian systems subject to additive faults" Ph.D thesis*. [S.l.]: Aeronautic Institute of Technology, Brazil, 2011.

SCHNEIDER, R.; GEORGAKIS, C. How to not make the extended kalman filter fail. *Industrial and Engineering Chemistry Research*, v. 52, p. 3354–3362, 3 2013. ISSN 08885885.

SCIBILIA, F.; HOVD, M.; BITMEAD, R. R. *Stabilization of gas-lift oil wells using topside measurements*. IFAC, 2008. v. 41. 13907–13912 p. ISSN 14746670. ISBN 9783902661005. Available from: ⟨http://dx.doi.org/10.3182/20080706-5-KR-1001.02354⟩.

SHARMA, R.; GLEMMESTAD, B. Optimal distribution of lift gas in gas lifted oil field using mpc and unscented kalman filter. *International Journal of Electrical and Computer Engineering*, v. 6, n. 9, p. 1081–1092, 2012.

SHI, J.; AL-DURRA, A.; ERROUISSI, R.; BOIKO, I. Stabilization of artificial gas-lift process using nonlinear predictive generalized minimum variance control. *Journal of the Franklin Institute*, Elsevier Ltd, v. 356, p. 2031–2059, 2019. ISSN 00160032. Available from: ⟨https://doi.org/10.1016/j.jfranklin.2018.11.032⟩.

SIMON, D. *Optimal state estimation: Kalman, H infinity, and nonlinear approaches*. [S.l.]: John Wiley & Sons, 2006.

SOTOMAYOR, O. A.; ODLOAK, D. Observer-based fault diagnosis in chemical plants. *Chemical Engineering Journal*, Elsevier, v. 112, n. 1-3, p. 93–108, 2005.

THE MATHWORKS, INC. *MATLAB version 9.10.0.1613233 (R2021a)*. Natick, Massachusetts, 2021.

TORRES, L.; JIMÉNEZ-CABAS, J.; GONZÁLEZ, O.; MOLINA, L.; LÓPEZ-ESTRADA, F.-R. Kalman filters for leak diagnosis in pipelines: Brief history and future research. *Journal of Marine Science and Engineering*, Multidisciplinary Digital Publishing Institute, v. 8, n. 3, p. 173, 2020.

ULANICKI, B.; PICINALI, L.; JANUS, T. Measurements and analysis of cavitation in a pressure reducing valve during operation–a case study. *Procedia Engineering*, Elsevier, v. 119, p. 270–279, 2015.

UPPAL, A.; RAY, W.; POORE, A. The classification of the dynamic behavior of continuous stirred tank reactors—influence of reactor residence time. *Chemical Engineering Science*, Elsevier, v. 31, n. 3, p. 205–214, 1976.

VENKATA, S. K.; RAO, S. Fault detection of a flow control valve using vibration analysis and support vector machine. *Electronics*, MDPI, v. 8, n. 10, p. 1062, 2019.

WAN, E. A.; MERWE, R. V. D. The unscented kalman filter for nonlinear estimation. In: IEEE. *Proceedings of the IEEE 2000 Adaptive Systems for Signal Processing, Communications, and Control Symposium (Cat. No. 00EX373)*. [S.l.], 2000. p. 153–158.

WILBERS, D.; MERFELS, C.; STACHNISS, C. A comparison of particle filter and graph-based optimization for localization with landmarks in automated vehicles. In: IEEE. *2019 Third IEEE International Conference on Robotic Computing (IRC)*. [S.l.]: Institute of Electrical and Electronics Engineers Inc., 2019. p. 220–225.

WILLERSRUD, A.; BLANKE, M.; IMSLAND, L.; PAVLOV, A. Fault diagnosis of downhole drilling incidents using adaptive observers and statistical change detection. *Journal of Process Control*, Elsevier, v. 30, p. 90–103, 2015.

WILLERSRUD, A.; IMSLAND, L.; HAUGER, S. O.; KITTILSEN, P. Short-term production optimization of offshore oil and gas production using nonlinear model predictive control. *IFAC Proceedings Volumes*, Elsevier, v. 44, n. 1, p. 10851–10856, 2011.

WILLERSRUD, A.; IMSLAND, L.; HAUGER, S. O.; KITTILSEN, P. Short-term production optimization of offshore oil and gas production using nonlinear model predictive control. *Journal of Process Control*, Elsevier, v. 23, n. 2, p. 215–223, 2013.

WILLERSRUD, A.; IMSLAND, L.; PAVLOV, A.; KAASA, G.-O. A framework for fault diagnosis in managed pressure drilling applied to flow-loop data. *IFAC Proceedings Volumes*, Elsevier, v. 46, n. 32, p. 625–630, 2013.

XU, Z.; GOLAN, M. Criteria for operation stability of gas lift. *SPE paper*, v. 19362, 1989.

ZHANG, X.; DING, F.; XU, L.; YANG, E. Highly computationally efficient state filter based on the delta operator. *International Journal of Adaptive Control and Signal Processing*, Wiley Online Library, v. 33, n. 6, p. 875–889, 2019.

APPENDIX A – GAS LIFT MODEL PRESENTATION

A.0.1 Derivation of Formula

In most gas lift modelling, many assumptions and approximations are made to obtain the model for the particular purpose. The model that more accurately captures the gas-lifted system behavior is the model represented by partial differential equation as presented in (SHI et al., 2019; ALIEV; DZHAMALBEKOV; IL'YASOV, 2011). This model is highly nonlinear and will be very difficult to use in controller design. A simpler model was presented in (JAHANSHAHI, 2013) which is the commonest model (with slight modification in some cases) used for control purposes. In some cases, this model is called a third order model. It uses the mass of gas and oil in the annulus and tubing as the state variables to form the ODE. But the complete model has the algebraic part that covers the density, pressure and flow rates. This gives rise to a differential algebraic equation for the gas-lifted system.

These algebraic variables vary with position. An accurate model considers this variation but controller design involving this can be demanding. Therefore, depending on the need for the models, the algebraic equations can be altered to vary the details. Some assumptions also alter the differential part of the model in very few cases. We derive the case where the pressure profile is more accurately captured while we present also a simplified and less nonlinear algebraic part for ease of controller design. The algebraic variables are usually considered at fixed points of the system and these are the points we will derive them in this chapter except for pressure that we derive the profile.

Variables and constants are defined based on what they refer to at first mention. Thereafter, the variables define themselves based on the subscript where 'at' refers to annulus top, 'a' refers to annulus base, 'tt' refers to tubing top, 'w' refers to well (also/specifically well side of the injection valve), 'o' refers to oil, 'g' refers to gas, 'm' refers to mixture, 'r'

refers to reservoir, 's' refers to separator and 'bh' is bottom hole. Variable definitions are given in table 6 while parameter definitions are given in table 7.

A.0.2 The Differential Equations

The differential equations describing the system mass balance are

The mass balance (differential) equations:

$$\frac{dx_1}{dt} = w_{gl} - w_{iv} \tag{A.1}$$

$$\frac{dx_2}{dt} = w_{iv} + w_{rg} - w_{pg} \tag{A.2}$$

$$\frac{dx_3}{dt} = w_{ro} - w_{po} \tag{A.3}$$

where:

$m_{ga} = x_1 =$ mass of gas in annulus.

$m_{gt} = x_2 =$ mass of gas in tubing.

$m_{ot} = x_3 =$ mass of oil in tubing.

Equation A.1 provides the mass of gas left in the annulus which is dictated by the inflow into the annulus (w_{gl}) and outflow through the injection valve (w_{iv}). The mass of gas in the tubing given in A.2 is contributed by three gas flow rates: flow into the tubing from the annulus (w_{iv}), flow into the tubing from the reservoir (w_{rg}) and the flow out of the tubing through the production choke (w_{pg}). The mass of oil in tubing is given in A.3 which is due to flow rates of oil into the tubing (w_{ro}) and out of the tubing (w_{po}). When it is assumed that the liquid coming from the reservoir is pure oil, then there is no gas flow from the reservoir hence the second term on the right-hand side of (A.2) is ignored.

A.0.3 The Flow Rates

The algebraic equations for the flow rates are derived as follows;

According to Hussein, Al-Durra and Boiko (2015), the volumetric flow rate of oil from the reservoir into the tubing is given by A.4. The mass flow rate relates to volumetric flow rate in A.5.

$$q_{ro} = N_{ro} A_{ro} C_{ro} \sqrt{\frac{(P_r - P_b h)}{g_l}} \tag{A.4}$$

$$w_{ro} = \rho_0 q_{ro} \tag{A.5}$$

The mass flow rate therefore gives:

$$q_{ro} = \rho_0 N_{ro} A_{ro} C_{ro} \sqrt{\frac{(P_r - P_b h)}{g_l}} \tag{A.6}$$

N_{ro}, A_{ro} and C_{ro} are constants and g_l is related to ρ_l by a constant. Lumping the constants together and simplifying.

$$w_{ro} = C_{ro} \sqrt{max(0, \rho_o (P_r - P_{bh}))} \tag{A.7}$$

Cr is a lumped parameter for the flow rate equivalent to the valve characteristics or valve coefficient. The max function in (A.7) is to prevent the flow rate from becoming negative when the pressure downstream gets bigger than upstream. This maintains all the state variables and the algebraic variables positive as the gas-lifted system is a positive system. It means the flow rate returns a zero when the pressure upstream becomes less than the pressure downstream. In general, the gas-lifted system is a positive system implying that the states and variables are non-negative.

But if the productivity index is known, Krishnamoorthy, Foss and Skogestad (2018) gives the w_{ro} as:

$$w_{ro} = PI(P_r - P_{bh}) \tag{A.8}$$

The gas/oil ratio (GOR) for the reservoir is the ratio of gas to oil in the reservoir. It relates the flow rate of oil to the flow rate of gas from the reservoir by:

$$w_{rg} = GOR w_{ro} \tag{A.9}$$

The key thing to note in (A.7) is that the flow rate depends on the valve coefficient, the pressure difference between upstream and downstream and the oil density upstream. Based on this, (A.7) can be extended to obtain the flow rates below:

$$w_{iv} = C_{iv}\sqrt{max(0, \rho_a(P_a - P_w))} \tag{A.10}$$

$$w_{pc} = C_{pc}\sqrt{max(0, \rho_m(P_{wh} - P_s))}f(u) \tag{A.11}$$

Where $f(u)$ is the valve characteristic equation which we choose according to Garcia (2013) as A.12 and u is the input which is the valve opening which is given either in percentage or as a fraction. The input is usually $0 \leq u \leq 1$ or in percentage $0 \leq u \leq 100$.

$$f(u) = 50^{u-1} \tag{A.12}$$

From A.11 produced gas and produced oil through the choke can be obtained as:

$$w_{pg} = \frac{x_2}{x_2 + x_3}w_{pc} \tag{A.13}$$

$$w_{po} = \frac{x_3}{x_2 + x_3}w_{pc} \tag{A.14}$$

The ratio of mass of gas to oil in the tubing mixture is given as λ defined in A.15

$$\lambda = \frac{x_2}{x_3} \tag{A.15}$$

Putting A.15 into A.13 and A.14 and simplifying gives the equation that relates the produced oil and gas with the total flow through the production choke.

$$w_{pg} = \frac{\lambda}{\lambda + 1}w_{pc} \tag{A.16}$$

$$w_{po} = \frac{1}{\lambda + 1}w_{pc} \tag{A.17}$$

Define mass fraction m_f as the ratio of mass of gas in the tubing mixture to the total mass of the tubing mixture, then A.13 and A.14 can further be written as:

$$w_{pg} = m_f w_{pc} \tag{A.18}$$

$$w_{po} = (1 - m_f)w_{pc} \tag{A.19}$$

A.0.4 The Pressures

In the derivation of pressures, various assumptions are made to simplify the mathematical demand for the derivation. These assumptions reduce the chances that the pressures describe exactly the physical behavior of the system which is necessary for accurate controller design. But considering the MPC to be used here has high robustness to model uncertainty, these assumptions do not prevent the model from being adequate for our purpose. We present the simplified pressures at the key parts of the well and tubing.

Pressure at annulus top is contributed by the ideal gas law given as:

$$P_{at}V_a = nRT_a \tag{A.20}$$

From A.20, the pressure at annulus top is given in A.21 while the pressure due to gas column in the annulus is

$$P_{at} = \frac{T_a R}{V_a M_w} M_{ga} \tag{A.21}$$

$$P_g = \frac{m_{ga} g L_a}{V_a} \tag{A.22}$$

The annulus pressure is the combined pressure in A.21 and A.22.

$$P_a = \frac{T_a R}{V_a M_w} M_{ga} + \frac{m_{ga} g L_a}{V_a} \tag{A.23}$$

Similarly, Pressure at tubing top is obtained following A.21 but considering the gas volume is obtained by removing the volume occupied by the oil in the tubing.

$$P_{wh} = \frac{T_t R}{M_w} \left(\frac{m_{gt}}{v_t - \frac{m_{ot}}{\rho_o}} \right) \tag{A.24}$$

The tubing temperature is assumed to be slowly varying hence taken as constant throughout the tubing column.

The pressure at the well side of the injection valve is the pressure at tubing top and pressure due to the liquid column up to the injection point.

$$P_w = P_{wh} + (m_{gt} + m_{ot})\frac{g}{A_t} \tag{A.25}$$

The bottom hole pressure is the well pressure and the pressure due to oil column below the injection point.

$$P_{bh} = P_w + (\rho_o g H_{bh}) \tag{A.26}$$

A.0.5 The Densities

Densities are obtained following the same assumptions above. In the annulus that is purely gas, the density is obtained from 4.17as:

$$\rho_a = \frac{M_w}{T_a R} P \tag{A.27}$$

Based on A.27, the density at any location is obtained by substituting the pressure at the location. P in A.27 is Pa if the density at the annulus side of the injection valve is desired. For the case of the tubing where there is a gas/oil mixture, the density is given as the ratio of the total mass and the total volume of the tubing.

$$\rho_t = \frac{m_{gt} + m_{ot}}{V_t} g \tag{A.28}$$

The density at any point depends on the mass of the mixtures above the given point. Hence in A.28 the mass and volume start from the injection point on the well side.

APPENDIX B – GAS LIFT LINEARISATION PROCESS

This section explains how the elements of the linearised models in (4.49) were obtained before forming the elements of equation (4.51).

The first row depends on (4.49a):

$$\frac{\partial f_1}{\partial x_1} = \frac{\partial w_{gl}}{\partial x_1} - \frac{\partial w_{iv}}{\partial x_1} \tag{B.1}$$

Since w_{gl} is constant, $\frac{\partial w_{gl}}{\partial x_1} = 0$, hence:

$$\frac{\partial f_1}{\partial x_1} = -\frac{\partial w_{iv}}{\partial x_1} \tag{B.2}$$

From (A.10) and noting from (A.27) that ρ_a also depends on x_1,

$$\frac{\partial w_{iv}}{\partial x_1} = \frac{\partial w_{iv}}{\partial \rho_a}.\frac{d\rho_a}{d\boldsymbol{x}_1} + \frac{\partial w_{iv}}{\partial P_a}.\frac{dP_a}{dx_1} \tag{B.3}$$

$$\begin{aligned} &\frac{C_{iv}}{2\sqrt{max(0,\rho_a(P_a-P_w))}}.(P_a-P_w).\frac{Mw}{T_aR}\left(\frac{T_aR}{V_aM_w}+\frac{gL_a}{V_a}\right) \\ &+\frac{C_{iv}}{2\sqrt{max(0,\rho_a(P_a-P_w))}}.\rho_a.\left(\frac{T_aR}{V_aM_w}+\frac{gL_a}{V_a}\right) \end{aligned} \tag{B.4}$$

Hence this simplifies to:

$$\frac{\partial f_1}{\partial x_1} = -\frac{C_{iv}^2}{2w_{iv}}\left(\frac{T_aR}{V_aM_w+\frac{gL_a}{V_a}}\right)\left(2\rho_a - \frac{M_w}{TaR}P_w\right) \tag{B.5}$$

Replacing x_1 with x_2 in (B.1) and noting that ρ_a and P_a are not functions of x_2 implies that:

$$\frac{\partial f_1}{\partial x_2} = \frac{\partial w_{gl}}{\partial x_2} - \frac{\partial w_{iv}}{\partial x_2} \tag{B.6}$$

$$\frac{\partial f_1}{\partial x_2} = -\frac{\partial w_{iv}}{\partial x_2} = -\frac{\partial w_{iv}}{\partial P_w}.\frac{dP_w}{dx_2} \tag{B.7}$$

$$\frac{\partial f_1}{\partial x_2} = -\frac{C_{iv}}{2\sqrt{max(0, \rho_a(P_a - P_w))}}.(-\rho_a).\left(\frac{T_t R}{M_w}\left(\frac{1}{V_t - \frac{x_3}{\rho_0}}\right) + \frac{g}{A_t}\right) \tag{B.8}$$

This simplifies to:

$$\frac{\partial f_1}{\partial x_2} = \frac{\rho_a C_{iv}^2}{2w_{iv}}\left[\frac{T_t R}{M_w}\left(\frac{1}{V_t - \frac{x_3}{\rho_0}}\right) + \frac{g}{A_t}\right] \tag{B.9}$$

Similarly, Replacing x_1 with x_3 in (B.1):

$$\frac{\partial f_1}{\partial x_3} = \frac{\partial w_{gl}}{\partial x_3} - \frac{\partial w_{iv}}{\partial x_3} \tag{B.10}$$

$$\frac{\partial f_1}{\partial x_3} = -\frac{\partial w_{iv}}{\partial x_3} = -\frac{\partial w_{iv}}{\partial P_w}.\frac{dP_w}{dx_3} \tag{B.11}$$

Following similar procedure at (B.8) but noting that the derivative is with respect to x_3:

$$\frac{\partial f_1}{\partial x_3} = \frac{\rho_a C_{iv}^2}{2w_{iv}}\left(\frac{T_t R}{M_w}\frac{x_2}{\rho_o(V_t - \frac{x_3}{\rho_0})^2} + \frac{g}{A_t}\right) \tag{B.12}$$

Simplifying to:

$$\frac{\partial f_1}{\partial x_3} = \frac{\rho_a C_{iv}^2}{2w_{iv}}\left(\frac{T_t R x_2}{\rho_o M_w(V_t - \frac{x_3}{\rho_0})^2} + \frac{g}{A_w}\right) \tag{B.13}$$

We consider the elements of the second row.

$$\frac{\partial f_2}{\partial x_1} = \frac{\partial w_{rg}}{\partial x_1} + \frac{\partial w_{iv}}{\partial x_1} - \frac{\partial w_{pg}}{\partial x_1} \tag{B.14}$$

Note again that w_{rg} and w_{pg} do not depend on x_1, hence:

$$\frac{\partial f_2}{\partial x_1} = \frac{\partial w_{iv}}{\partial x_1} = -\frac{\partial f_1}{\partial x_1} = \frac{C_{iv}^2}{2w_{iv}}\left(\frac{T_a R}{V_a M_w + \frac{gL_a}{V_a}}\right)\left(2\rho_a - \frac{M_w}{TaR}P_w\right) \tag{B.15}$$

Replacing x_1 with x_2 in (B.14) we obtain:

$$\frac{\partial f_2}{\partial x_2} = \frac{\partial w_{rg}}{\partial x_2} + \frac{\partial w_{iv}}{\partial x_2} - \frac{\partial w_{pg}}{\partial x_2} \tag{B.16}$$

All terms in $\frac{\partial f_2}{\partial x_2}$ therefore are functions of x_2. Since $\frac{\partial w_{iv}}{\partial x_2}$ in (B.16) based on (B.8) is known, we find $\frac{\partial w_{rg}}{\partial x_2}$ and $\frac{\partial w_{pg}}{\partial x_2}$ as follows:

Based on (A.7) and (A.9):

$$\frac{\partial w_{rg}}{\partial x_2} = GOR\frac{\partial}{\partial x_2}C_r\sqrt{max(0, \rho_o(P_r - P_{bh}))} \tag{B.17}$$

Following similar procedure that results in (B.9) and replacing C_{iv} with C_r, P_a with P_r, P_w with P_{bh}, and ρ_a with ρ_0, we obtain:

$$\frac{\partial w_{rg}}{\partial x_2} = GOR.\frac{-\rho_o C_r}{2\sqrt{max(0, \rho_o(P_r - P_{bh}))}}\left(\frac{T_t R}{M_w}\left(\frac{1}{V_t - \frac{x_3}{\rho_0}}\right) + \frac{g}{A_t}\right) \tag{B.18}$$

Note that $\frac{\partial P_{bh}}{\partial x_2} = \frac{\partial P_w}{\partial x_2}$ in this case.

Further simplification gives:

$$\frac{\partial w_{rg}}{\partial x_2} = -\frac{\rho_o C_r^2 GOR}{2w_{ro}}\left(\frac{\rho_o T_t R}{M_w(V_t\rho_o - x_3)} + \frac{g}{A_t}\right) \tag{B.19}$$

Note that:

$$\frac{\partial w_{iv}}{\partial x_2} = -\frac{\rho_a C_{iv}^2}{2w_{iv}}\left[\frac{T_t R}{M_w}\left(\frac{1}{V_t - \frac{x_3}{\rho_0}}\right) + \frac{g}{A_t}\right] \tag{B.20}$$

Noting that w_{pc} also depends on x_2.

$$\frac{\partial w_{pg}}{\partial x_2} = w_{pc}.\frac{\partial}{\partial x_2}(\frac{x_2}{x_2 + x_3}) + (\frac{x_2}{x_2 + x_3}).\frac{\partial w_{pc}}{\partial x_2} \tag{B.21}$$

$$\frac{\partial w_{pg}}{\partial x_2} = w_{pc}.(\frac{x_3}{(x_2+x_3)^2}) + \frac{x_2}{x_2+x_3} \left\{ \frac{C_{pc}50^{u-1}}{2\sqrt{max(0,\rho_m(P_{wh}-P_s))}}.(P_{wh}-P_s).\frac{1}{v_t} + \frac{C_{pc}}{2\sqrt{max(0,\rho_o(P_{wh}-P_s))}}.\rho_m.\frac{T_tR}{M_w}\frac{1}{V_t-\frac{x_3}{\rho_o}} \right\} \tag{B.22}$$

This simplifies to:

$$\frac{\partial w_{pg}}{\partial x_2} = w_{pc}.(\frac{x_3}{(x_2+x_3)^2}) + \frac{x_2}{x_2+x_3} \left\{ \frac{(C_{pc}50^{u-1})^2(P_{wh}-P_s)}{2w_{pc}v_t} + \frac{(C_{pc}50^{u-1})^2\rho_m T_tR}{2w_{pc}M_w(V_t-\frac{x_3}{\rho_o})} \right\} \tag{B.23}$$

$$\frac{\partial w_{pg}}{\partial x_2} = w_{pc}.(\frac{x_3}{(x_2+x_3)^2}) + \frac{x_2}{x_2+x_3}\frac{(C_{pc}50^{u-1})^2}{2w_{pc}v_t} \left\{ (P_{wh}-P_s) + \frac{\rho_m T_tR}{M_w(V_t-\frac{x_3}{\rho_o})} \right\} \tag{B.24}$$

Equation (B.16) is therefore obtained from (B.19), (B.20) and (B.24).

Replacing x_1 with x_3 in (B.16) we obtain:

$$\frac{\partial f_2}{\partial x_3} = \frac{\partial w_{rg}}{\partial x_3} + \frac{\partial w_{iv}}{\partial x_3} - \frac{\partial w_{pg}}{\partial x_3} \tag{B.25}$$

Similarly, all terms in $\frac{\partial f_2}{\partial x_3}$ obtained by replacing x_1 with x_3 in (B.25) are functions of x_3.

Since $\frac{\partial w_{iv}}{\partial x_3}$ in (B.25) based on (B.10) is known, we find $\frac{\partial w_{rg}}{\partial x_3}$ and $\frac{\partial w_{pg}}{\partial x_3}$ as follows:

$$\frac{\partial w_{rg}}{\partial x_3} = GOR\frac{-\rho_o C_r}{2\sqrt{max(0,\rho_o(P_r-P_{bh}))}}\left(\frac{T_tR}{M_w}\left(\frac{-x2}{-\rho_o(V_t-\frac{x_3}{\rho_0})^2}\right)+\frac{g}{A_t}\right) \tag{B.26}$$

Which simplifies to:

$$\frac{\partial w_{rg}}{\partial x_3} = -\frac{\rho_o C_r^2 GOR}{2w_{ro}}\left(\frac{T_tRx_2}{M_w(V_t-\frac{x_3}{\rho_0})^2}+\frac{g}{A_t}\right) \tag{B.27}$$

Note that:

$$\frac{\partial w_{iv}}{\partial x_3} = \frac{\rho_a C_{iv}^2}{2w_{iv}}\left(\frac{T_t R x_2}{\rho_o M_w (V_t - \frac{x_3}{\rho_0})^2} + \frac{g}{A_w}\right) \tag{B.28}$$

And:

$$\frac{\partial w_{pg}}{\partial x_2} = w_{pc}.\frac{\partial}{\partial x_2}(\frac{x_2}{x_2 + x_3}) + (\frac{x_2}{x_2 + x_3}).\frac{\partial w_{pc}}{\partial x_2} \tag{B.29}$$

Following from (B.20) and (B.21) and noting that the derivative here is with respect to x_3:

$$\begin{aligned} \frac{\partial w_{pg}}{\partial x_3} &= w_{pc}.\frac{-x_2}{(x_2 + x_3)^2} + \frac{x_2}{x_2 + x_3} \\ \left\{\frac{(C_{pc}50^{u-1})^2}{2w_{pc}}\left[\frac{(P_{wh} - P_s)}{v_t} + \frac{\rho_m T_t R}{\rho_0 M_w (V_t - \frac{x_3}{\rho_0})^2}\right]\right\} \end{aligned} \tag{B.30}$$

Equation (B.25) is therefore obtained from (B.27), (B.28) and (B.30).

We consider the elements of the last row.

$$\frac{\partial f_3}{\partial x_1} = \frac{\partial w_{ro}}{\partial x_1} - \frac{\partial w_{po}}{\partial x_1} \tag{B.31}$$

From (A.8) and following from (A.26), (A.25) and (A.24), it is seen that w_{ro} is independent of x_1. Also, from (A.14) and (A.11), w_{po} is independent of x_1, hence:

$$\frac{\partial f_3}{\partial x_1} = 0 \tag{B.32}$$

We replace x_1 in (B.31) with x_2 to obtain the equation:

$$\frac{\partial f_3}{\partial x_2} = \frac{\partial w_{ro}}{\partial x_2} - \frac{\partial w_{po}}{\partial x_2} \tag{B.33}$$

Then:

$$\frac{\partial w_{ro}}{\partial x_2} = -\frac{\rho_o C_r^2}{2w_{ro}}\left(\frac{\rho_o T_t R}{M_w(V_t \rho_o - x_3)} + \frac{g}{A_t}\right) \tag{B.34}$$

From (A.6) we follow similar procedure as in (B.19).

$$\frac{\partial w_{po}}{\partial x_2} = w_{pc}.(\frac{-x_3}{(x_2+x_3)^2}) + \frac{x_3}{x_2+x_3}$$
$$.\left\{\frac{C_{pc}50^{u-1}}{2\sqrt{max(0,\rho_o(P_{wh}-P_s))}}.(P_{wh}-P_s).\frac{1}{v_t}\right.$$
$$\left. + \frac{C_{pc}50^{u-1}}{2\sqrt{max(0,\rho_o(P_{wh}-P_s))}}.\rho_m.\frac{T_tR}{M_w}\frac{x_2}{(V_t-\frac{x_3}{\rho_o})^2\rho_0}\right\} \tag{B.35}$$

Which simplifies to:

$$\frac{\partial w_{po}}{\partial x_2} = w_{pc}.\frac{-x_3}{(x_2+x_3)^2} + \frac{x_3}{x_2+x_3}$$
$$\left\{\frac{(C_{pc}50^{u-1})^2}{2w_{pc}}\left[\frac{(P_{wh}-P_s)}{v_t} + \frac{-\rho_m T_t R}{\rho_0 M_w (V_t-\frac{x_3}{\rho_0})^2}\right]\right\} \tag{B.36}$$

Equation (B.33) is therefore obtained from (B.34) and (B.36).

Similarly, $\frac{\partial f_3}{\partial x_3}$ is obtained from (B.31) by replacing x_1 with x_3.

$$\frac{\partial f_3}{\partial x_3} = \frac{\partial w_{ro}}{\partial x_3} - \frac{\partial w_{po}}{\partial x_3} \tag{B.37}$$

From (A.9), w_{ro} is obtained straightforwardly from (B.27) as:

$$\frac{\partial w_{ro}}{\partial x_3} = -\frac{\rho_o C_r^2}{2w_{ro}}\left(\frac{T_tRx_2}{M_w(V_t-\frac{x_3}{\rho_0})^2} + \frac{g}{A_t}\right) \tag{B.38}$$

And:

$$\frac{\partial w_{po}}{\partial x_3} = w_{pc}.\frac{x_2}{(x_2+x_3)^2} + \frac{x_2}{x_2+x_3}$$
$$\left\{\frac{(C_{pc}50^{u-1})^2}{2w_{pc}}\left[\frac{(P_{wh}-P_s)}{v_t} + \frac{\rho_m T_t R x_2}{\rho_0 M_w (V_t-\frac{x_3}{\rho_0})^2}\right]\right\} \tag{B.39}$$

Equation (B.37) is therefore obtained from (B.38) and (B.39).

Next, we obtain the elements of matrix B.

$$\frac{\partial f_1}{\partial u} = \frac{\partial w_{gl}}{\partial u} - \frac{\partial w_{iv}}{\partial u} \tag{B.40}$$

The input is only introduced through w_{pc} in (A.11) hence any algebraic variable that does not depend on w_{pc} is independent of u. Consequently:

$$\frac{\partial f_1}{\partial u} = 0 \tag{B.41}$$

Next:

$$\frac{\partial f_2}{\partial u} = \frac{\partial w_{rg}}{\partial u} + \frac{\partial w_{iv}}{\partial u} - \frac{\partial w_{pg}}{\partial u} \tag{B.42}$$

Neither w_{rg} nor w_{iv} depends on u, hence:

$$\frac{\partial f_2}{\partial u} = -\frac{\partial w_{pg}}{\partial u} \tag{B.43}$$

$$\frac{\partial f_2}{\partial u} = -\frac{x_2}{x_2 + x_3} C_{pc} \sqrt{max(0, \rho_m(P_{wh} - P_s))} 50^{u-1} \ln(50) \tag{B.44}$$

Next:

$$\frac{\partial f_3}{\partial u} = \frac{\partial w_{ro}}{\partial u} - \frac{\partial w_{po}}{\partial u} \tag{B.45}$$

Also, w_{ro} does not depend on u, hence:

$$\frac{\partial f_3}{\partial u} = -\frac{\partial w_{po}}{\partial u} \tag{B.46}$$

$$\frac{\partial f_2}{\partial u} = -\frac{x_3}{x_2 + x_3} C_{pc} \sqrt{max(0, \rho_m(P_{wh} - P_s))} 50^{u-1} \ln(50) \tag{B.47}$$

Next, we obtain the elements of matrix C.

Matrix C is obtained from output which here is the produced oil in (A.14).

$$\frac{\partial y}{\partial x_1} = \frac{\partial w_{po}}{\partial x_1} \tag{B.48}$$

$$\frac{\partial y}{\partial x_1} = 0 \tag{B.49}$$

Also:

$$\frac{\partial y}{\partial x_2} = \frac{\partial w_{po}}{\partial x_2} \tag{B.50}$$

This is obtained from (B.36) as:

$$\frac{\partial y}{\partial x_2} = w_{pc}.\frac{x_2}{(x_2+x_3)^2} + \frac{x_2}{x_2+x_3} \left\{ \frac{(C_{pc}50^{u-1})^2}{2w_{pc}} \left[\frac{(P_{wh}-P_s)}{v_t} + \frac{\rho_m T_t R x_2}{\rho_0 M_w (V_t - \frac{x_3}{\rho_0})^2} \right] \right\} \tag{B.51}$$

$$\frac{\partial y}{\partial x_3} = \frac{\partial w_{po}}{\partial x_3} \tag{B.52}$$

This is obtained from (B.39) as:

$$\frac{\partial y}{\partial x_3} = w_{pc}.\frac{-x_3}{(x_2+x_3)^2} + \frac{x_3}{x_2+x_3} \left\{ \frac{(C_{pc}50^{u-1})^2}{2w_{pc}} \left[\frac{(P_{wh}-P_s)}{v_t} + \frac{-\rho_m T_t R}{\rho_0 M_w (V_t - \frac{x_3}{\rho_0})^2} \right] \right\} \tag{B.53}$$

For the D matrix,

$$\frac{\partial y}{\partial u} = \frac{\partial w_{po}}{\partial u} \tag{B.54}$$

$$\frac{\partial y}{\partial u} = \frac{x_3}{x_2+x_3} w_{pc} \ln 50 \tag{B.55}$$